Error Performance Analysis of GSM and GCQSM using Golden Codewords, H-QAM and Labelling Diversity

Nathael Sibanda

A thesis submitted in fulfilment of the requirement for the degree of

Doctor of Philosophy in Engineering
(ELECTRONIC ENGINEERING)

School of Engineering
The University of KwaZulu-Natal,
Durban, South Africa

April 5, 2024

Error Performance Analysis of GSM and GCQSM using Golden Codewords, H-QAM and Labelling Diversity

Nathael Sibanda

Supervisor: Prof. Hongjun Xu

Co-Supervisor: Prof. Narushan Pillay

A thesis submitted in fulfilment of the requirement for the degree of

Doctor of Philosophy in Engineering
(ELECTRONIC ENGINEERING)

School of Engineering
The University of KwaZulu-Natal
South Africa

April 5, 2024

Certification

As the candidate's supervisor, I have approved this thesis for submission.

Signature:.....Date.....**April 5, 2024**.....

Signed: **Prof. Hongjun Xu**

As the candidate's co-supervisor, I have approved this thesis for submission.

Signature:.....Date.....**April 5, 2024**.....

Signed: **Prof. Narushan Pillay**

Declaration 1 - Plagiarism

I, **Nathael Sibanda**, declare that;

1. The research reported in this thesis, except where otherwise indicated, is my original research.
2. This thesis has not been submitted for any degree or examination at any other university.
3. This thesis does not contain other persons' data, pictures, graphs or other information unless specifically acknowledged as being sourced from other persons.
4. This thesis does not contain other persons' writing unless specifically acknowledged as being sourced from other researchers. Where other written sources have been quoted, then:
   (a) Their words have been re-written but the general information attributed to them has been referenced,
   (b) Where their exact words have been used, then their writing has been placed in italics and inside quotation marks and referenced.
5. This thesis does not contain text, graphics or tables copied and pasted from the Internet, unless specifically acknowledged, and the source is detailed in the thesis and in the references sections.

Signed.....Date.....**April 5, 2024**.....

Declaration 2 - Publication

Details of contribution to publications that form part and/or include research presented in this thesis (include publications in preparation, submitted, in the press and published and give details of the contributions of each author to the experimental work and writing of each publication):

1. N. Sibanda, H. Xu, and N. Pillay, "Golden codeword-based generalised spatial modulation," International Journal of Communication Systems, vol. 35, no. 10, p. e5144, Jul. 2022.

2. N. Sibanda, H. Xu, and N. Pillay, "Error performance analysis of generalised quadrature spatial modulation using H-8QAM," Scientific Reports, vol. 12, no. 1, pp. 1–13, Nov. 2022.

3. N. Sibanda, H. Xu, and N. Pillay, "Error performance analysis of multiple active antennas GSM and GCQSM with labelling diversity," [*Under review with Wiley International Journal of Communication Systems*]

Signature:.....Date.....**April 5, 2024**.....

Signed: **Nathael Sibanda**

Dedication

... in loving memory of my late **Mother** and **Father**.You are loved and missed!...

...Glory be to God!...

Acknowledgements

With immense pleasure and a deep sense of gratitude, I wish to express my sincere thanks to my supervisor **Prof. Hongjun Xu**, without his motivation and continuous encouragement, this research would not have been completed.

I am also grateful to my co-supervisor **Prof. Narushan Pillay**, without his motivation and continuous encouragement, this research would not have been completed.

I wish to extend my profound gratitude to **my family** for all the sacrifices they made during my research and also for providing me with moral support and encouragement whenever required.

... "I THANK YOU ALL FOR YOUR PART IN MY JOURNEY"....

... "GLORY BE TO GOD!"....

Place: Durban

Date: **April 5, 2024** **Nathael Sibanda**

Abstract

Conventional generalised spatial modulation (C-GSM) is a multiple-input multiple-output (MIMO) technique in which information is transmitted using a spatial constellation. This constellation consists of active transmit antennas grouped together, along with a conventional *M*-ary quadrature amplitude modulation (C-*M*-QAM) or *M*-ary phase shift keying (C-*M*-PSK) signal constellation. In contrast, generalised quadrature spatial modulation (GQSM) is an enhanced version of GSM where the complex data symbol's real and imaginary components are concurrently but separately conveyed through two or more antennas, contingent upon the spatial symbols.

The first objective of this work is seen in Part (II) and it entails the proposal of a bit error rate (BER) improvement technique for GSM called Golden codeword-based generalised spatial modulation (GCW-GSM). GCW-GSM uses the principles of C-GSM together with golden codewords (GCWs). A framework for designing GCW-GSM systems is presented in Part (II), and an analytical bound on the average bit error rate (ABER) of GCW-GSM over independent and identically distributed (i.i.d.) Rayleigh frequency-flat fading channels is derived. Monte Carlo simulation results are used to validate the accuracy of this bound. In addition, simulation results show that GCW-GSM achieves significant gains of $6.0\ dB$ and $2.9\ dB$, for a BER of 1×10^{-5}, compared to 4×4 C-256QAM conventional spatial modulation (C-SM) and 4×4 C-64QAM conventional quadrature spatial modulation (C-QSM), respectively, for a transmission rate of $10\ bits/s/Hz$.

The GCW-GSM scheme uses a maximum likelihood detector (MLD) with poor BER performance and high computational complexity (CC) due to the presence of GCWs, especially when using high-order digital modulation schemes. Therefore, the second objective of this work is seen in Part (III) and it entails the proposal of a new scheme that integrates GQSM and hexagonal quadrature amplitude modulation (H-*M*QAM) to improve the error performance, increase the spectral efficiency (SE), and minimise the CC introduced by GCWs in high-order modulation scenarios of C-GSM

systems. Therefore, the proposed scheme is called GQSM using H-8QAM (GQSM-H-8QAM). This study, investigates the error performance of the proposed GQSM-H-8QAM scheme over Rayleigh frequency-flat fading channels in the presence of additive white Gaussian noise (AWGN). Moreover, a theoretical expression for the average bit error probability (ABEP) of the GQSM-H-8QAM scheme is formulated and validated by Monte Carlo simulations. The ABEP agrees closely with the simulation results, especially at high signal-to-noise ratios (SNR)s. The results of the simulation demonstrate an enhancement in the error performance of the GQSM-H-8QAM scheme compared to different spatial modulation (SM) schemes such as GCW-GSM, conventional quadrature spatial modulation (C-QSM), C-GSM at the same SE. The proposed scheme outperformed various schemes superior to the GCW-GSM scheme, in particular, an error performance improvement of $0.61\ dB$ at an SE of $8\ bits/s/Hz$ for the 4×4 GQSM-H-8QAM scheme was observed over 4×4 generalised complex quadrature spatial modulation (GCQSM) scheme using C-8QAM. Also, an improvement of $2.58\ dB$ was seen over 4×4 C-QSM-C-64QAM, and a gain of $4.85\ dB$ was seen over 4×4 C-GSM-C-64QAM.

To further improve the error performance of MIMO-SM schemes, in Part (IV), this study builds on C-GSM by fusing it with multiple active antennas and optimised constellation maps (labelling diversity(LD)). Two methods are proposed: Generalised spatial modulation with multiple active antennas and labelling diversity (MAA-GSM-LD) and Generalised complex quadrature spatial modulation with labelling diversity (GCQSM-LD). The first method in Part (IV) is MAA-GSM-LD, which builds on C-GSM by incorporating multiple active antennas and optimised labelling maps with a maximised minimum product distance (MMPD) between constellations. This MMPD contributes to better detection and thus improves the error performance of MIMO-SM schemes. In MAA-GSM-LD, four C-*M*-QAM symbols are sent simultaneously per time slot, over Rayleigh frequency-flat fading channels.

The second scheme in Part (IV), builds on MAA-GSM by splitting the four symbols generated in MAA-GSM-LD into the quadrature and in-phase dimensions, thus avoiding inter-antenna synchronisation and consequently improving the error performance of MIMO-SM schemes. This method is herein named GCQSM-LD. Moreover, the upper bounds of the ABER expressions for the proposed MAA-GSM-LD and GCQSM-LD schemes are derived over i.i.d Rayleigh frequency-flat fading channels. Monte Carlo simulations validate the ABER expressions. When contrasted with the simulation outcome, the ABEP is found to become progressively stringent at high SNR ratios.

Furthermore, the simulation outcomes reveal an enhancement in the error performance of both MAA-GSM-LD and GCQSM-LD over various MIMO-SM schemes such as GCQSM and GSM multiplexing two symbols (MIMO-GSM), at the same SE. For MAA-GSM-LD, an improvement in error performance of $1.0\ dB$ with an SE of $11\ bits/s/Hz$ is observed in 6×4 MAA-GSM-LD C-16QAM versus 6×4 GQSM C-16QAM and $4.3\ dB$ versus 6×4 GCW-GSM-C-16QAM. For GCQSM-LD, an improvement in the error performance of $4.7\ dB$ with an SE of $14\ bits/s/Hz$ is seen in 8×4 GCQSM-LD C-16QAM over 4×4 GCQSM-C-64QAM and $3.6\ dB$ over 4×4 GQSM-AG-C-32QAM.

***Index Terms*—-Error performance; golden codewords; hexagonal-quadrature amplitude modulation; labelling diversity; multiple-input multiple-output.**

Contents

List of Figures

List of Figures

List of Tables

List of Tables

List of Acronyms

ABEP	Average bit error probability
ABER	Average bit error rate
AWGN	Additive white Gaussian noise
BER	Bit error rate
BPSK	Binary Phase Shift Keying
C-GSM	Conventional-generalised spatial modulation
C-QSM	Conventional-quadrature spatial modulation
C-SM	Conventional-spatial modulation
C-SMux	Spatial multiplexing
CCA	Computational complexity analysis
CR	Constellation rearrangement
CSI	Channel state information
ESE-GSM	Enhanced spectral efficiency generalised spatial modulation
GC	Golden code
GCQSM	Generalised complex quadrature spatial modulation
GCW	Golden codeword
GCW-GSM	Golden codeword-based generalised spatial modulation
GQSM	Generalised quadrature spatial modulation
GQSM-AG	Generalised quadrature spatial modulation using antenna grouping

GRV	Gaussian random variable
GSM-CR	Generalised spatial modulation with constellation reassignment
H-QAM	Hexagonal quadrature amplitude modulation
IAS	Inter-antenna synchronisation
i.i.d	Independent and identically distributed
ICI	Inter-channel interference
IEEE	Institute of Electrical and Electronics Engineers
ISI	Inter-symbol interference
LOS	Line-of-sight
M-MED	Maximised-minimum Euclidean distance
MED	Minimum Euclidean distance
M-MPD	Maximised-minimum product distance
MIMO	Multiple-input multiple-output
MIMO-GSM	C-GSM spatial multiplexing two different symbols from two different transmit antennas
MLD	Maximum-likelihood detection
PA	Peak-to-average
PEP	Pairwise error probability
PSK	Phase shift keying
QAM	Quadrature spatial modulation
SE	Spectral efficiency
SIMO	Single-input multiple-output
SNR	Signal-to-noise-ratio
STBC	Space time block code
STLD	Space time labelling diversity
V-BLAST	Vertical Bell Labs Layered Space-time Architecture

WiMAX Worldwide interoperability for microwave access

X-QAM Cross quadrature amplitude modulation

Preface

The research discussed in this thesis was carried out in the College of Agriculture, Engineering and Science (School of Electrical, Electronic and Computer Engineering) of The University of Kwa-Zulu Natal, Durban, from June 2019 until September 2023 by Nathael Sibanda under the supervision of **Prof. Hongjun Xu** and co-supervised by **Prof. Narushan Pillay**.

As the candidate's Supervisor, I, **Prof. Hongjun Xu**, agree to the submission of this thesis.

Signed:.....Date:.....**April 5, 2024**.....

As the candidate's Co-Supervisor, I, **Prof. Narushan Pillay**, agree to the submission of this thesis.

Signed:.....Date:.....**April 5, 2024**.....

I, **Nathael Sibanda**, hereby declare that all the material incorporated in this thesis is my own original work, except where acknowledgement is made by name or in the form of a reference. The work contained herein has not been submitted in any form for any degree or diploma to any other institution.

Signed:.....Date:.....**April 5, 2024**.....

The University of KwaZulu-Natal, April 5, 2024

Part I

Introduction

1 Introduction

In the last decade, the need for communication systems with elevated data transmission rates has increased as a result of the rapid development of wireless communication technology [1]. Nowadays the pressure for wireless communication networks with a robust link margin and elevated data rates has been intensified by COVID-19. This in turn has forced mankind to work indoors and thus depend heavily on wireless communications with high bandwidth efficiency and link reliability.

Recent research has shown that the deployment of multiple antennas at both the transmitting and receiving terminals of wireless communication systems increases the throughput and reliability of wireless communication channels [2]. Hence, this technique is referred to as multiple-input multiple-output (MIMO) wireless communications [3]. The appeal of MIMO systems is the ability to increase throughput through spatial multiplexing and enhance the error performance of wireless communication links using spatial diversity [2].

In spatial multiplexing, streams are generated from input signals or data bits. These streams are transmitted in the same frequency channel via different transmit antennas. This allows payload data and messages to be sent to multiple receivers simultaneously, improving throughput/spectral efficiency (SE) [4]. An example of a multiplexing scheme is the Vertical Bell labs layered space-time (V-BLAST) scheme [5], whose architecture improves SE by transmitting N_T (number of transmit antennas) signals in each time slot [5]. However, the multiple active transmit antennas in the V-BLAST architecture require N_T high-frequency chains, which are associated with the disadvantage of synchronisation between antennas [6].

Also, MIMO systems enhance link robustness by transmitting multiple duplicate data copies to a receiver across separate channels to curb fading [7]. An example of such a MIMO system is the Alamouti space-time block code (STBC) [8]. Despite their advantages, MIMO schemes have the disadvantages of inter-channel interference (ICI), inter-antenna synchronisation (IAS) and high power consumption due to multiple-active transmit antennas, which in turn leads to degradation of the error performance and poor improvement of the SE [6, 9, 10]. Hence, to mitigate the aforementioned drawbacks of MIMO schemes, research led to the discovery of STBCs such as the golden code (GC) [11], conventional spatial modulation (C-SM) techniques [12], uncoded space-time labelling diversity (USTLD) techniques and energy efficient hexagonal quadrature amplitude

techniques (H-*M*QAM) [13, 14].

In this thesis, in an effort to improve the error performance of MIMO-SM systems, this study extends the original MIMO-SM systems to conventional generalised spatial modulation (C-GSM) with golden codewords (GCW). To also improve on the error performance and/ SE of MIMO-SM systems, this study extends the conventional generalised quadrature spatial modulation (C-GQSM) with conventional quadrature amplitude modulation (C-QAM) to C-GQSM with hexagonal quadrature amplitude (H-QAM) systems. Moreover, this work also partly investigates C-GSM with GC over Rician fading channels. Finally, to further improve the error performance of MIMO-SM systems, C-GSM is extended by incorporating it with multiple active transmitters, optimised labelling maps and attributes of conventional quadrature spatial modulation (C-QSM). Following in Section 2 of Part (I), is the review of various fading channel environments, followed by Section 3 which is an example of a MIMO scheme over Rayleigh frequency-flat fading channels. Next, in Subsection 3.1 is the discussion of techniques that have and/or can be used to enhance the error performance and/or SE of MIMO-SM systems.

2 Review of various fading channels

The physical medium separating the transmit and receive antennas is known as the propagation environment [3, 15]. It is made of all the components that influence how the sent signal travels between the transmitter and the receiver. The capacity of the MIMO channel is influenced by the propagation environment [3, 15]. Various models are available in wireless communication networks to depict the characteristics of the MIMO channel, which can vary depending on the propagation environment. In this thesis, Rayleigh frequency-flat fading channels with a transfer function $\mathbf{H} \in \mathbb{C}^{N_R \times N_T}$ are considered; where N_R is the number of the receiver antennas and N_T is the number of transmit antennas.

2.1 Rayleigh Fading

The Rayleigh fading channel is primarily employed to characterise the propagation scenario when a direct line of sight (LOS) connection between the transmitter and receiver is weak or absent [3, 15]. This statistical distribution is mostly used to mimic multi-path fading in metropolitan settings with a high density of reflectors lacking a clear LOS component. Thus, the entries of $\mathbf{H} \in \mathbb{C}^{N_R \times N_T}$ are

independent and identically distributed (i.i.d) Gaussian random variables (GRVs) with zero mean and unit variance. Thus, based on the central limit theorem [7, 9, 15], the fading coefficient of the in-phase (I) and quadrature-phase (Q) components of i.i.d GRVs can be expressed as:

$$\alpha = \alpha^I + j\alpha^Q, \tag{1}$$

where the in-phase component is α^I and the quadrature component is α^Q. Both α^I and α^Q are modelled as GRVs with zero mean and a variance of $\frac{1}{2}$. The fading amplitude is expressed following the formulation in [16] as follows:

$$A = \sqrt{|\alpha^I|^2 + |\alpha^Q|^2}. \tag{2}$$

Thus, the amplitude of fading, denoted as A, follows a Rayleigh distribution with a probability density function (PDF) given by [16] as

$$f(A) = \frac{A}{\sigma^2} \exp(\frac{-A}{2\sigma^2}), \tag{3}$$

where σ^2 is the variance of A.

2.2 Rician Fading

The Rician distribution is commonly used to describe multipath fading channels with a clear LOS. The PDF of Rician fading is given in [15, 17], as

$$p(A) = 2(K+1)A \exp(-K - A^2(1+K)) I_o(2\sqrt{K(K+1)A}), \tag{4}$$

where I_o refers to the modified Bessel function of the first kind with order zero, K is the Rician factor and A is the amplitude of the channel [15, 17]. Finally, the entries of $\mathbf{H} \in \mathbb{C}^{N_R \times N_T}$ are modelled as [18],

$$\mathbf{H} = \sqrt{\frac{K}{1+K}} + \sqrt{\frac{1}{1+k}}\mathbf{H}', \tag{5}$$

where the fraction $\frac{K}{1+K}$ represents the average power of the LOS component, whereas $\frac{1}{1+K}$ signifies the average power of the random component. Furthermore, the matrix $\mathbf{H}' \in \mathbb{C}^{N_R \times N_T}$ is characterised by entries that are i.i.d GRVs with zero mean and unit variance.

2.3 Nakagami-*m* Fading

Channels with severe to moderate fading are frequently described using the Nakagami-*m* distribution [19, 20]. The Nakagami-*m* model is employed primarily because it fits empirical fading data well and characterises the channel effectively when maximum ratio combining is used at the receiver [20, 21]. According to [22, 23], the Nakagami-*m* entries of $\mathbf{H}$ for the N_T-th transmit antenna and the N_R-th receive antenna, respectively, are modelled as

$$h_{N_R,N_T} = \sqrt{\sum_{i=1}^{m} |z_i^R|^2} + j\sqrt{\sum_{i=1}^{m} |z_i^I|^2}, \tag{6}$$

where z_i^R and z_i^I are i.i.d GRVs with distribution $CN(0,(2m)^{-1})$. The envelope of the Nakagami-*m* fading channel is distributed according to [22, 24],

$$p(A) = \frac{2m^m A^{2m-1}}{\Gamma(m)} \exp\left(-mA^2\right), \tag{7}$$

where $\Gamma(.)$ is the gamma function. Thus, the PDF of the phase is given in [22], as

$$p(\theta) = \frac{\Gamma(m)|\sin(2\theta)|^{m-1}}{2^m \Gamma^2(\frac{m}{2})}. \tag{8}$$

The Nakagami-*m* distribution is not uniform [22], except for the special case of $m = 1$, which corresponds to a Rayleigh fading.

3 MIMO system model and various methods for improving the error performance and/ or SE.

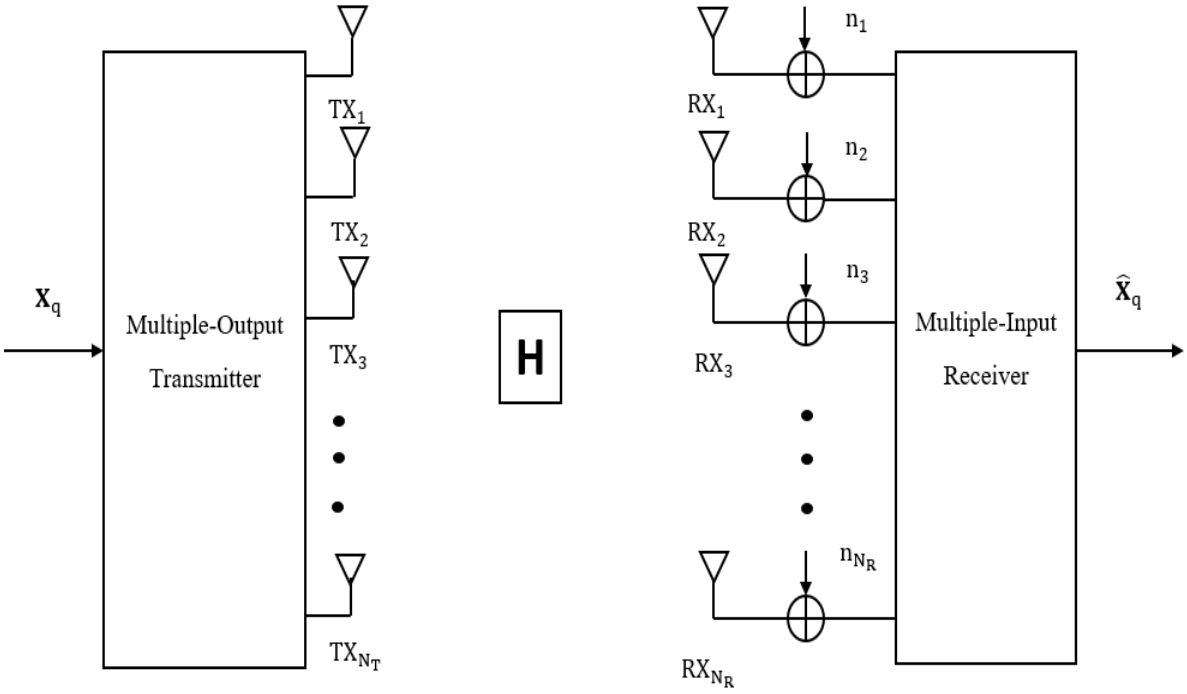

Fig. 1: MIMO system model over Rayleigh frequency-flat fading channels.

Fig. 1 provides an illustration of a MIMO system model which employs a Rayleigh frequency-flat fading channel, denoted as $\mathbf{H}$ and having dimensions of $\mathbb{C}^{N_R \times N_T}$. Within this setup, $\mathbf{h}_{k_l}$, where $1 \leq l \leq N_T$, signifies the lth column vector in the channel gain matrix $\mathbf{H}$, which is structured as $\mathbf{H} = \begin{bmatrix} \mathbf{h}_{k_1} & \mathbf{h}_{k_2} & \mathbf{h}_{k_3} & ... & \mathbf{h}_{kN_T} \end{bmatrix}$. Each $\mathbf{h}_{k_l}$ is itself a column vector, comprising elements like h_{1k_l}, h_{2k_l}, h_{3k_l}, and so forth, up to $h_{N_R k_l}$.

In Fig. 1, we also encounter $\mathbf{n}$, a vector with dimensions of $\mathbb{C}^{N_R \times 1}$, representing the additive white Gaussian noise (AWGN) vector. This vector can be expressed as $\begin{bmatrix} n_1 & n_2 & n_3 & ... & n_{N_R} \end{bmatrix}^T$. It is important to assume that the elements of both $\mathbf{n}$ and $\mathbf{H}$ are i.i.d GRVs with distribution $CN(0, 1)$, respectively.

To illustrate, symbols or data are transmitted through multiple transmit antennas in the form of an $N_T \times 1$ transmit vector, denoted as $\mathbf{x}_q$. These symbols or data are received as $\mathbf{y}$, which is a complex vector with dimensions $\mathbb{C}^{N_R \times 1}$ representing the signal vector at the receiver. The received vector $\mathbf{y}$ can be expressed as shown in (9). Finally, ρ denotes the average signal-to-noise ratio (SNR).

$$\mathbf{y} = \sqrt{\frac{\rho}{N_T}}\mathbf{H}\mathbf{x}_q + \mathbf{n}. \tag{9}$$

Following in subsections 3.1 to 3.3, is the discussion of various methods that have been and/ or can be used to improve the error performance and/ SE of MIMO wireless communication networks.

3.1 Spatial Modulation Techniques of Improving the *SE* and/or error performance of MIMO wireless communication networks

3.1.1 Conventional Spatial Modulation

To address the challenges associated with ICI and IAS in MIMO systems, Jeganathan *et al.* [12], presented a solution known as conventional spatial modulation (C-SM). C-SM represents a transmission technique that provides an SE gain equal to the base-two logarithm of the number of transmit antennas, as explained in [25]. Under the C-SM scheme, only one transmit antenna is active during each time slot. This approach leads to an enhancement in the average bit error rate (ABER) because ICI is mitigated. Simultaneously, it contributes to a reduction in hardware complexity, algorithmic complexity, and power consumption, as outlined in [12] and [25].

Figs. 3 and 4 illustrate a model of an $N_T \times N_R$ M-ary quadrature amplitude modulation (M-QAM) C-SM system, where M signifies the modulation order of the QAM system. In C-SM, binary information, $r = \log_2(MN_T)$ bits, are allocated to a spatial/transmit antenna index k and an M-QAM symbol x_q. The assignment of values to k and x_q is determined by the C-SM mapping table, which is accessible to both the transmitter and the receiver. An example of a C-SM mapping table for a transmission rate of 3 $bits/s/Hz$ is provided in Fig. 2 of [26]. The output vector of the C-SM mapper, denoted as $\mathbf{x}_{kq}$, can be expressed as shown in Fig. 2 [12]. This $\mathbf{x}_{kq}$ represents an $N_T \times 1$ signal vector, with x_q representing the qth M-QAM symbol, where $E|x_q|^2 = 1$, and q belongs to the range $[1 : M]$. The modulated symbol x_q is transmitted through a single active transmit antenna corresponding to the index k. Consequently, the signal vector $\mathbf{x}_{kq}$ features a single non-zero entry, which is x_q, associated with the kth active transmit antenna. The transmitted signal is then propagated over a Rayleigh frequency-flat fading channel $\mathbf{H} \in \mathbb{C}^{N_R \times N_T}$ and is subjected to AWGN, represented by $\mathbf{n} \in \mathbb{C}^{N_R \times 1}$. Both the entries of $\mathbf{H}$ and $\mathbf{n}$ are modelled as i.i.d GRVs with distribution $CN(0, 1)$. Finally, ρ stands for the average SNR.

The received signal $\mathbf{y} \in \mathbb{C}^{N_R \times 1}$ is given by (10) as

$$\mathbf{y} = \sqrt{\frac{\rho}{N_T}}\mathbf{H}\mathbf{x}_{kq} + \mathbf{n}, \tag{10}$$

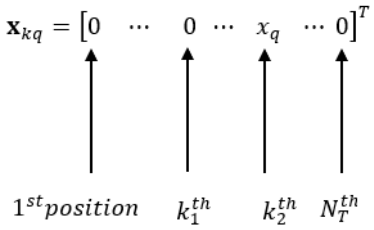

Fig. 2: Transmitted vector $\mathbf{x}_{iq}$ for the C-SM scheme.

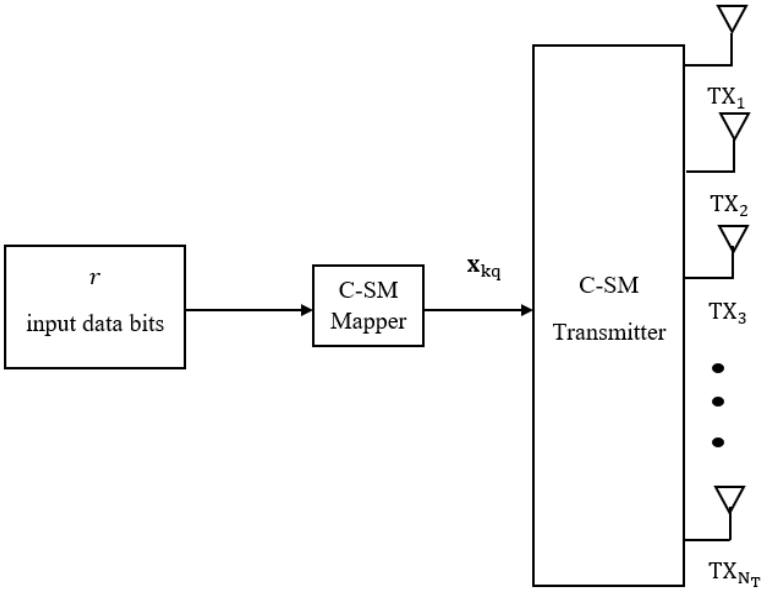

Fig. 3: C-SM Transmission side system model over Rayleigh frequency-flat fading channels.

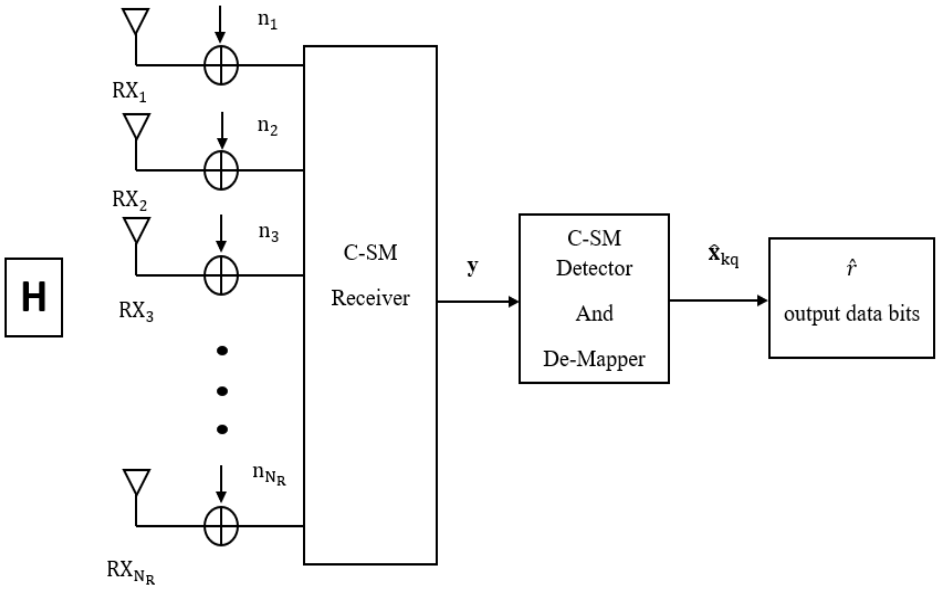

Fig. 4: C-SM Receiver side system model over Rayleigh frequency-flat fading channels.

Despite the benefits it offers, research efforts, as demonstrated in [27] and [28], have uncovered certain limitations of C-SM. One of those limitations associated with the configuration utilising a single active transmit antenna in C-SM is its restriction on the number of information bits that can be spatially encoded. This limitation, in turn, has a direct impact on the achievable SE of the system, as discussed in [25] and [27]. In response to these constraints observed in C-SM, Younis *et al.* [24], proposed a solution known as conventional generalised spatial modulation (C-GSM), which is further explored in the subsequent sub-subsection 3.1.2.

3.1.2 C-GSM

In an effort to curb/improve on the setbacks of C-SM, Younis *et al.* [24], proposed C-GSM scheme, which is an extension of the C-SM scheme that permits the transmission of the same data symbol from multiple active transmit antennas [24, 29]. C-GSM systems can be divided into two categories: single-symbol transmission and multiple-symbol transmission [4, 29]. The first category is the single-symbol transmission, which is also mainly known as C-GSM. C-GSM sends out the same modulated symbol using two active transmit antennas. The second approach uses numerous active transmit antennas to communicate various complex signals [4, 29]. GSM architecture of being able to enable the activation of more than two transmit antennas during each transmission instance contributes to mitigating the hardware complexity constraints typically encountered in C-SM and index modulation schemes [4, 29]. As a result, C-GSM enhances the total SE by a factor equivalent to the binary logarithm of the available antenna combinations, as indicated in [4].

An instance of a C-GSM system model can be described as an $N_T \times N_R$ M-QAM system, which offers a total of $n = \binom{N_T}{N_A}$ potential transmit antenna pairs. However, only $N_c = \left\lfloor \log_2 \binom{N_T}{N_A} \right\rfloor_{2^p}$ pairs are eligible for transmission, with the condition that N_c must be less than or equal to n. It is worth noting that N_A has been previously discussed in [24], and typically, a value of 2 is used unless specified otherwise. The SE for C-GSM is provided in [4] and [29] as

$$\mathfrak{m} = \log_2(M) + \left\lfloor \log_2 \binom{N_T}{N_A} \right\rfloor_{2^p}, \tag{11}$$

In C-GSM, the modulated symbol is concurrently transmitted by two active transmit antennas during each time slot, structured as an $N_T \times 1$ transmit vector denoted as $\mathbf{x}$. This vector $\mathbf{x}$ consists of two non-zero elements, both representing the same modulated symbol, thus indicating that it is transmitted twice in C-GSM. The positions of these two non-zero elements correspond to the indices of the selected active transmit antennas, as illustrated in Fig. 5. Comprehensive details about the potential antenna combinations and mapping tables for C-GSM can be found in [30] and [31].

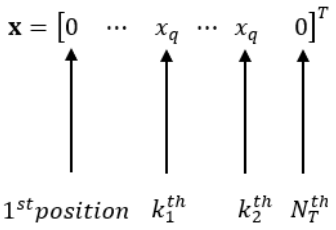

Fig. 5: C-GSM transmitted vector $\mathbf{x}$.

The received signal in C-GSM is given by (12) as

$$\mathbf{y} = \sqrt{\frac{\rho}{2}}\mathbf{H}\mathbf{x} + \mathbf{n}, \tag{12}$$

where the received signal vector is represented by $\mathbf{y}$ and is a complex vector with dimensions of $N_R \times 1$. The matrix $\mathbf{H}$ signifies the Rayleigh frequency-flat channel fading characteristics and has dimensions of $N_R \times N_T$. The received AWGN vector is denoted as $\mathbf{n}$ and also has dimensions of $N_R \times 1$. The vector $\mathbf{h}_l$, where $1 \leq l \leq N_T$, corresponds to the lth column of the channel gain matrix $\mathbf{H}$, which can be constructed as $\mathbf{H} = \begin{bmatrix} \mathbf{h}_{k_1} & \mathbf{h}_{k_2} & \mathbf{h}_{k_3} & \dots & \mathbf{h}_{k_{N_T}} \end{bmatrix}$. Each $\mathbf{h}_{k_l}$ is a column vector comprising elements h_{1k_l}, h_{2k_l}, h_{3k_l}, and so forth, up to $h_{N_R k_l}$. It is noteworthy that the elements of

both $\mathbf{n}$ and $\mathbf{H}$ are assumed to be i.i.d complex GRVs with a distribution having a mean of zero and unity variance, denoted as $CN(0,1)$. Lastly, ρ represents the average (SNR).

3.1.3 MIMO-GSM

Despite the advancements in reducing hardware complexity achieved in C-GSM, when considering identical system configurations, it is observed that the bit error rate (BER) performance of C-GSM is limited and deteriorates compared to that of C-SM, as discussed in [4] and [24]. Consequently, Wang *et al.* [4] introduced a multiple active antenna or MIMO spatial multiplexing GSM (MIMO-GSM) system, which allows for the simultaneous transmission of two or more distinct symbols within a single time slot. The key distinction between C-GSM and MIMO-GSM lies in their ability to transmit symbols per time slot—C-GSM sends only one symbol, whereas MIMO-GSM can send multiple symbols per time slot [4]. As a result, MIMO-GSM exhibits improved error performance, SE, and reduced hardware complexity when compared to C-GSM. The SE of MIMO-GSM is detailed in [4] as

$$\mathfrak{m} = N_A \log_2(M) + \left\lfloor \log_2 \binom{N_T}{N_A} \right\rfloor_{2^p} \tag{13}$$

MIMO-GSM adopts a configuration similar to that of C-GSM, utilising an $N_T \times N_R$ M-QAM system under comparable fading channel and AWGN noise conditions. Like C-GSM, MIMO-GSM's input information is divided into two categories: spatial input bits (antenna pair index), akin to C-GSM, and symbol bits. However, in MIMO-GSM, these symbol bits represent two or more distinct symbols, contrasting with C-GSM, where they correspond to a single symbol's data bits. For instance, in a scenario where a MIMO-GSM system transmits two distinct M-QAM symbols, with spatial information involving $N_T = 4$, possible antenna pairs could be $\Big[(1,3);(1,4);(2,3);(2,4)\Big]$ paired with bit indices $\Big[00;01;10;11\Big]$, respectively. Additional antenna combinations and mapping tables can be found in [30] for reference. Just like C-GSM, these two distinct symbols in MIMO-GSM are transmitted through two separate transmitting antennas, forming an $N_T \times 1$ transmit vector $\mathbf{x}$, as shown in Fig. 6.

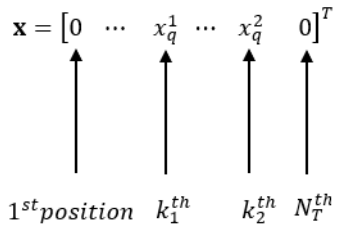

Fig. 6: MIMO-GSM transmitted vector $\mathbf{x}$.

3.1.4 Quadrature Spatial Modulation

An alternative technique explored for improving the error performance and/or SE of MIMO-SM systems is referred to as Conventional-quadrature spatial modulation (C-QSM), as detailed in [32]. C-QSM expands the spatial constellation of SM systems into a two-dimensional space, specifically the in-phase (*I*) and quadrature (*Q*) dimensions. In this configuration, the *I* dimension is utilised for transmitting the real part of a single amplitude/phase modulated symbol, while the *Q* dimension is allocated for transmitting the imaginary part of the same amplitude/phase modulated symbol, as elaborated in [32] and [33]. Notably, the *I* components are modulated onto cosine carriers, and the *Q* components are modulated onto sine carriers. This design effectively mitigates ICI, leading to improved error performance compared to C-SM systems, as discussed in [34].

Moreover, C-QSM enhances the Spectral Efficiency ($\mathfrak{m}$) by $\log_2(N_T)$ bits/s/Hz when contrasted with the C-SM scheme, as reported in [32]. It is essential to highlight that C-QSM surpasses C-SM regarding error performance and outperforms GSM systems in terms of SE, as demonstrated in [32], [35], and [36].

In the context of a C-QSM system, consider an $N_T \times N_R$ M-QAM system model, as illustrated in Figs. 8 and 9. The input information for this system is categorised into two parts, similar to C-GSM and MIMO-GSM: spatial input bits (representing antenna pair indices) and symbol bits.

The first category, involves (b) information bits, where $b = \log_2(M)$ bits are mapped onto an amplitude/phase-modulated symbol (x_q). This symbol is then divided into its real and imaginary components. These distinct real and imaginary components of the symbol x_q are transmitted concurrently by two transmitting antennas within the same time slot, structured as an $N_T \times 1$ transmit vector $\mathbf{x}$, depicted in Fig. 7. This vector $\mathbf{x}$ comprises two non-zero elements, representing the real part (x_q^I) and the imaginary part (x_q^Q) of the symbol. Additionally, the positions of these two

non-zero elements correspond to the indices of the two chosen active transmit antennas.

The second part of the input information relates to spatial details and pertains to the two selected active transmit antennas. Specifically, $\mathfrak{D} = \log_2 N_c$ bits are allocated to a distinct generalised antenna labelled as k_1, responsible for the *I* dimension of the system. These same $\mathfrak{D}$ bits are also assigned to another separate generalised antenna, designated as k_2, responsible for the *Q* dimension of the system.

Tables 1 and 2 provide an example illustrating the mapping process for C-QSM, demonstrating how this spatial information is assigned. Furthermore, the SE of C-QSM is given in [32] as

$$\mathfrak{m} = \log_2(M) + 2\log_2(N_T) bits/s/Hz. \tag{14}$$

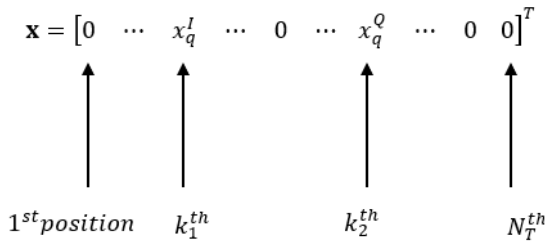

Fig. 7: Transmitted vector $\mathbf{x}$ for the C-QSM scheme.

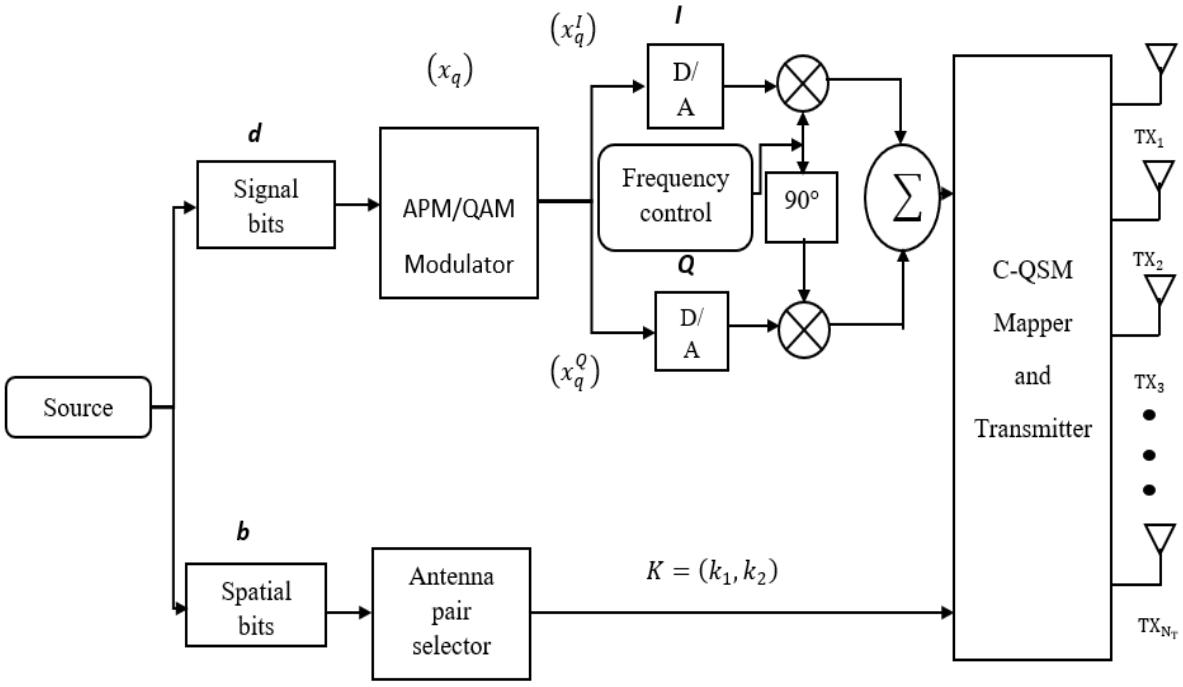

Fig. 8: C-QSM Transmission side system model over Rayleigh frequency-flat channels.

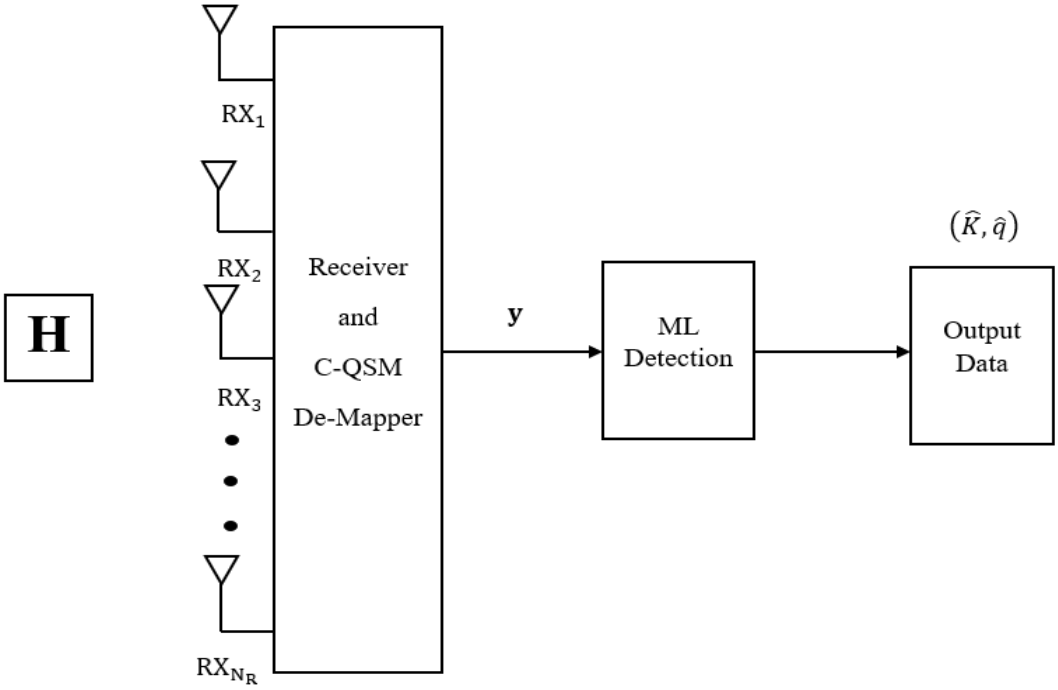

Fig. 9: C-QSM Receiver side system model over Rayleigh frequency-flat channels.

Table 1: Example of the mapping process for C-QSM ($M = 4$, $N_T = 2$ and $N_R = 4$).

Input bits $\log_2(MN_T^2)$	First $\log_2(M)$ bits (symbol bits)	Second $\log_2(N_T)$ bits (I-dimension antenna)	Third $\log_2(N_T)$ bits (Q-dimension antenna)
0001	$[00]$ $x_q = -1 + j1$ $x_q^I = -1$ $x_q^Q = +1$	$[0] = T_{X1}$	$[1] = T_{X2}$

Table 2: Example of the mapping process for C-QSM ($M = 16$, $N_T = 4$ and $N_R = 4$).

Input bits $\log_2(MN_T^2)$	First $\log_2(M)$ bits (symbol bits)	Second $\log_2(N_T)$ bits (*I*-dimension antenna)	Third $\log_2(N_T)$ bits (*Q*-dimension antenna)
10011101	$[1001]$ $x_q = +3 + j1$ $x_q^I = +3$ $x_q^Q = +1$	$[11] = T_{X4}$	$[01] = T_{X2}$

The received signal in C-QSM ($\mathbf{y} \in \mathbb{C}^{N_R \times 1}$) is given in (15), as

$$\begin{aligned} \mathbf{y} &= \sqrt{\frac{\rho}{2}}\mathbf{H}\mathbf{x} + \mathbf{n}, \\ &= \sqrt{\frac{\rho}{2}}\left(\mathbf{h}_{k_1} x_q^I + j\mathbf{h}_{k_2} x_q^Q\right) + \mathbf{n}, \end{aligned} \tag{15}$$

where the Rayleigh frequency-flat fading channel matrix, is denoted as $\mathbf{H}$, with dimensions of $\mathbb{C}^{N_R \times N_T}$. Additionally, the AWGN vector is represented as $\mathbf{n}$, with dimensions $\mathbb{C}^{N_R \times 1}$.

The vector $\mathbf{h}_{k_l}$, where $1 \leq l \leq N_T$, signifies the lth column vector in the channel gain matrix $\mathbf{H}$, which can be structured as $\mathbf{H} = \begin{bmatrix} \mathbf{h}_{k_1} & \mathbf{h}_{k_2} & \mathbf{h}_{k_3} & ... & \mathbf{h}_{kN_T} \end{bmatrix}$. Each $\mathbf{h}_{k_l}$ is itself a column vector, comprising elements such as h_{1k_l}, h_{2k_l}, h_{3k_l}, and so forth, up to $h_{N_R k_l}$. It is important to note that the elements of both $\mathbf{n}$ and $\mathbf{H}$ are presumed to be i.i.d GRVs with a mean of zero and a variance of 1, denoted as $CN(0, 1)$. Lastly, ρ stands for the average SNR.

Although C-QSM has the potential to enhance the error performance and SE of C-SM wireless communication networks, it comes with the drawback of requiring a larger number of transmit antennas compared to conventional spatial multiplexing (C-SMux) techniques. This limitation affects the extent to which SM systems can improve their error performance, as outlined in [37]. To address these limitations, researchers have proposed a solution known as generalised quadrature spatial modulation (C-GQSM) [37], which is discussed in the subsequent Section 3.1.5.

3.1.5 Generalised Quadrature Spatial Modulation

To achieve a high SE, Castillo *et. al.* [37], proposed a generalised quadrature spatial modulation scheme using antenna grouping (GQSM-AG). GQSM-AG is a scheme that divides the total number

of transmit antennas into distinct groups, each with two transmit antennas [37, 38]. However, this concept can be expanded to form groups with more than two transmit antennas. Each group transmits a unique *M*-QAM /phase-shift keying (*M*-PSK) signal at each period using the C-QSM technique's approach. The outcome is an enhancement in SE with a decrease in the overall number of needed transmit antennas [37, 38].

The GQSM-AG system consists of $n_b = \frac{N_T}{2}$ blocks or groups of transmit antennas, where each group employs the C-QSM approach to send a unique symbol per time slot. Each group can transmit a bit stream $\boldsymbol{b}$ which is equivalent to $\mathfrak{m} = 2 + \log_2(M)\ bits/s/Hz$ per time slot using just two transmit antennas [37] as seen in the GQSM-AG system model in Fig.10. The first two bits are modulated using a spatial constellation and the second $\log_2(M)$ bits are for the *M*-QAM modulated symbol to be transmitted. The first step is to split the *M*-QAM symbol (x_q) into its real and imaginary components like in C-QSM. The spatial constellation in the *K*-th group is then used to transmit the real part of the symbol (x_q) using one transmit antenna, and the imaginary part is transmitted using a different transmit antenna within the same group [37]. The symbol components are transmitted in the form of a vector $\mathbf{x}$, which has two non-zero elements and the position of those two elements corresponds to the indices of the two chosen active transmit antennas per *K*-th group. A detailed mapping example is provided in [37] and the SE of GQSM-AG is given in [37] as

$$\mathfrak{m} = \mathfrak{n}_b\big[\log_2(M) + 2\log_2(N_T)\big] bits/s/Hz. \tag{16}$$

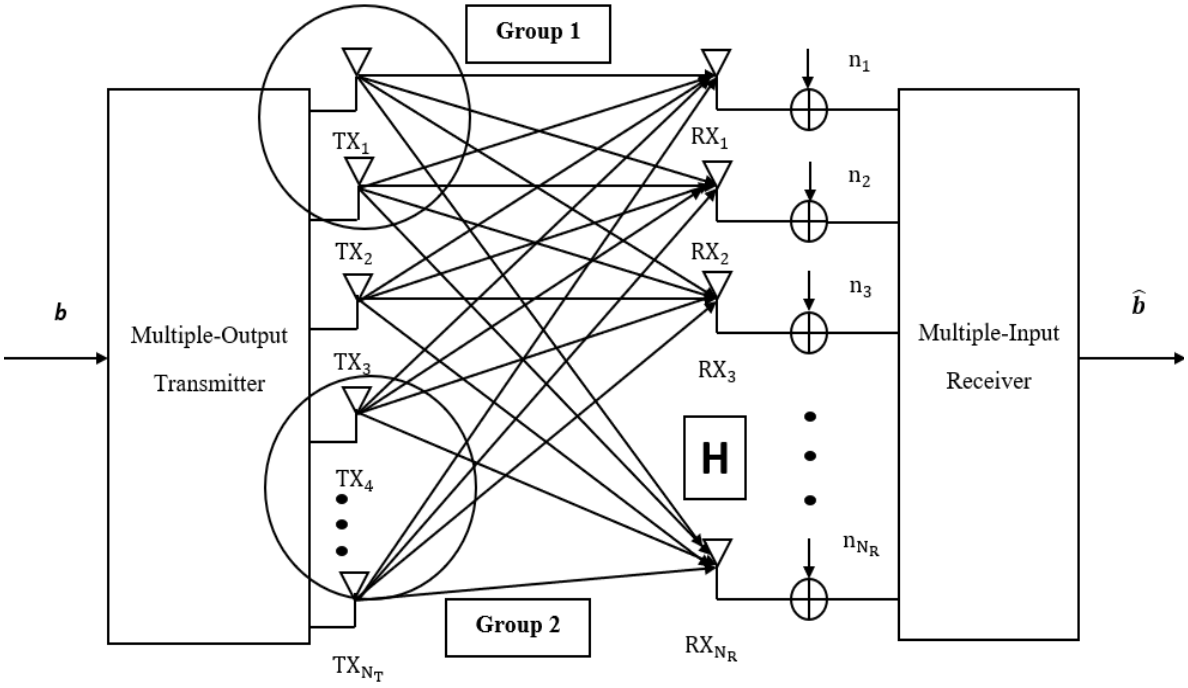

Fig. 10: GQSM-AG system model over Rayleigh frequency-flat channels.

The received GQSM-AG signal ($\mathbf{y} \in \mathbb{C}^{N_R \times 1}$) is given in (17) [37], as

$$\begin{aligned} \mathbf{y} &= \sqrt{\frac{\rho}{n_b}}\mathbf{H}\mathbf{x} + \mathbf{n}, \\ &= \sqrt{\frac{\rho}{n_b}}\left(\mathbf{h}_{k_1} x_q^I + j\mathbf{h}_{k_2} x_q^Q\right) + \mathbf{n}, \end{aligned} \tag{17}$$

where the Rayleigh frequency-flat fading channel matrix is symbolised as $\mathbf{H}$, featuring dimensions of $\mathbb{C}^{N_R \times N_T}$. Simultaneously, $\mathbf{n}$, a vector with dimensions of $\mathbb{C}^{N_R \times 1}$, represents the AWGN vector. The vector $\mathbf{h}_{k_l}$, where $1 \leq l \leq N_T$, signifies the lth column vector within the channel gain matrix $\mathbf{H}$, which is organised as $\mathbf{H} = \left[\mathbf{h}_{k_1} \quad \mathbf{h}_{k_2} \quad \mathbf{h}_{k_3} \quad ... \quad \mathbf{h}_{kN_T}\right]$. Each $\mathbf{h}_{k_l}$ is itself a column vector, comprising elements like h_{1k_l}, h_{2k_l}, h_{3k_l}, and so forth, up to $h_{N_R k_l}$. It is assumed that the elements of both $\mathbf{n}$ and $\mathbf{H}$ are i.i.d GRVs with distribution $CN(0, 1)$. Finally, ρ denotes the average SNR.

3.2 Space-Time Coding Techniques for Improving the SE and/or error performance of MIMO wireless communication networks.

In 1998, Tarokh *et al.*, introduced space-time codes (STC)s as an innovative approach for providing transmit diversity in MIMO fading channels, as documented in [39] and [40]. Before this groundbreaking study, diverse strategies such as temporal diversity, frequency diversity, and receive

antenna diversity were primarily employed to combat multi-path fading in MIMO wireless communication systems. Among these strategies, receive antenna diversity was the most prevalent choice. However, due to its associated hardware complexity, which remained relatively simple, cost-effective, and compact, effectively implementing receive antenna diversity at remote units posed significant challenges.

Consequently, in pursuit of enabling high-data-rate transmission over wireless fading channels, transmit diversity techniques like STCs were subsequently proposed for commercial deployment at base stations, as elaborated in [39–42]. The STC architecture essentially represents a holistic approach that encompasses the joint design of coding, modulation, transmission, and reception diversity, as highlighted in [39] and [40].

Space-time codes (STCs) fall into two primary categories: Space-time block codes (STBCs) and Space-time trellis codes (STTCs), as extensively explained in [39] and [40]. STBCs operate on blocks of input symbols, resulting in a matrix output where columns signify different time instances and rows correspond to individual antennas. Unlike single-antenna block codes tailored for the AWGN channel, STBCs, as a general rule, do not inherently yield coding gain unless they are paired with an external coding scheme. The distinctive characteristic of STBCs lies in their capability to provide full diversity while maintaining a notably straightforward decoding process, as delineated in [39–42].

In contrast, STTCs operate on one input symbol at a time, generating a sequence of vector symbols with a length corresponding to the number of antennas. Similar to conventional trellis-coded modulation for single-antenna channels, STTCs yield coding gain, as discussed in [39–42]. While both STTCs and STBCs provide full diversity gain, the primary advantage of STTCs over STBCs is their ability to deliver coding gain. However, it is important to note that STTCs come with the drawback of being challenging to design and typically necessitate highly complex encoders and decoders.

For a brief survey of STBCs under i.i.d Rayleigh frequency-flat fading channels, the subsequent sub-subsections (3.2.1-3.2.2) provide an extensive review of the literature in this field.

3.2.1 Alamouti Scheme

STBCs effectively harness redundancy for multiple transmissions between the transmitter and receiver by transmitting various versions of information signals. This approach significantly enhances the probability that some of these signals will experience less attenuation than others, as elucidated in [8]. Consequently, the system offers a substantially improved likelihood of using one or more copies of the received signals, thereby augmenting data rates and enhancing link reliability. An illustrative example of such a system is the Alamouti scheme, as introduced in [8].

The conventional Alamouti scheme, depicted in the system model in Figs. 11 and 12, typically involves two transmit antennas and one or more receive antennas. The codewords employed in the Alamouti scheme are orthogonal and have the unique capability of achieving full transmit diversity, a characteristic that is inherently linked to the number of transmitting and receiving antennas. Notably, this full diversity is achieved while still adhering to the requirement of maintaining a straightforward linear decoding algorithm, a feature outlined in [8, 39, 43–45].

Furthermore, the Alamouti scheme can be readily extended to encompass a system featuring two transmit antennas and N_R receive antennas (referred to as a $2 \times N_R$ system). In this extended configuration, the scheme offers an impressive diversity order of $2N_R$, as detailed in [8, 39, 43–45]. This advancement significantly enhances the system's ability to harness diversity gains.

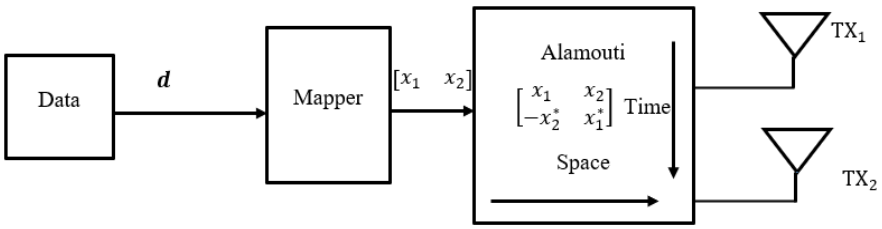

Fig. 11: Alamouti transmission side system model over Rayleigh frequency-flat fading channels.

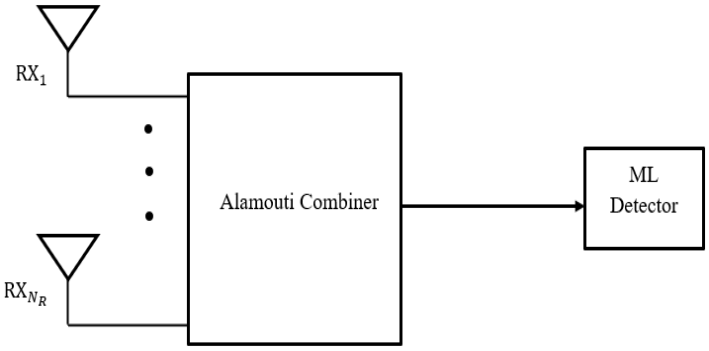

Fig. 12: Alamouti receiver side system model over Rayleigh frequency-flat fading channels.

Within the Alamouti scheme, it is important to note that the transmitter does not possess access to channel state information (CSI), whereas the receiver is assumed to have perfect CSI. The mathematical representation of the Alamouti STBC transmission matrix is formally presented as equation (18), consistent with the description found in [8].

$$\mathbf{X} = \begin{pmatrix} x_1 & x_2 \\ -x_2^* & x_1^* \end{pmatrix}, \tag{18}$$

where x_1 and x_2 correspond to symbols originating from either an *M*-QAM or PSK constellation. These symbol pairs signify that the STBC system simultaneously transmits symbols in both space, referring to transmission across two antennas, and time, representing two successive transmission intervals. During the first time slot, antenna one transmits the symbol (x_1), while antenna two conveys the symbol (x_2). In the subsequent time slot, the roles reverse, with antenna one transmitting ($-x_2^*$) and antenna two sending (x_1^*), as outlined in [8]. The resulting received signals can be expressed as follows:

$$\begin{aligned} \mathbf{y}_1 &= \sqrt{\frac{\rho}{2}}\left(\mathbf{h}_1 x_1 + \mathbf{h}_2 x_2\right) + \mathbf{n}_1, \\ \mathbf{y}_2 &= \sqrt{\frac{\rho}{2}}\Big(\mathbf{h}_3(-x_2^*) + \mathbf{h}_4(x_1^*)\Big) + \mathbf{n}_2, \end{aligned} \tag{19}$$

where $\mathbf{y}_i$, $i \in [1:2]$ represents the received signal vector for the i^{th} instance. Each $\mathbf{y}_i$ is a complex vector in $\mathbb{C}^{N_R \times 1}$. Similarly, $\mathbf{h}_l$, $l \in [1:4]$, represents the channel gain vector and these channels are assumed to be characterised by Rayleigh fast fading. This means that the channels remain constant

within a single time slot but can take on independent values in subsequent time slots.

Additionally, $\mathbf{n}_i$, $i \in [1;2]$, denotes the AWGN vector, which is a complex vector in $\mathbb{C}^{N_R \times 1}$. The individual entries of both $\mathbf{h}_l$ and $\mathbf{n}_i$ are i.i.d GRVs with a distribution $CN(0,1)$, respectively. Lastly, ρ represents the average SNR.

Even though the Alamouti scheme incorporates spatial diversity, it does not realise the multiplexing gain, as elucidated in [8]. To be more precise, the Alamouti scheme operates as a half-rate STBC, with the code rate being defined as the number of transmitted symbols per transmission time slot, as stated in [8]. Consequently, ongoing research efforts have led to the development of an enhanced scheme known as the golden code (GC), which is explored in the subsequent subsection 3.2.2.

3.2.2 Golden Code

The Golden Code (GC) is a noteworthy development in wireless communication systems. It is a 2×2 linear dispersion STBC that provides both full rate and full diversity. GC's construction relies on cyclic division algebras, a significant advancement detailed in academic works such as [46–49].

A distinctive feature of GC is its unique cubic shaping and the presence of a non-vanishing minimum determinant algebraic structure, well-documented in [46, 50]. Unlike the orthogonal nature of the Alamouti codeword matrix, GC's codeword matrix is non-orthogonal. The encoding of GC is a process that involves creating two pairs of GC codewords. Each GC codeword represents a combination of two complex input symbols, and a noteworthy characteristic is that the two codewords within a pair are transmitted in separate time slots, as expounded in [46, 48]. In comparison with the Alamouti STBC scheme, GC not only attains full multiplexing gain, allowing for higher data rates but also excels in achieving full diversity, which significantly enhances link reliability [46, 50].

GC's merit is further evident in its widespread adoption across various applications, such as the IEEE 802.16 standard. GC's unique capabilities strike an exceptional balance between data rate and reliability, reinforcing its status as a preferred choice in advanced wireless communication systems, as underscored in [50].

The GC encoding process involves taking a set of four complex-valued symbols and producing four specific super-symbols, referred to as golden codewords (GCWs). The resulting matrix of GCWs can be represented using the expression provided in (20), a concept extensively discussed in [11, 46, 48, 49].

$$\boldsymbol{G} = \frac{1}{\sqrt{5}} \begin{pmatrix} \alpha(x_1 + x_2\theta) & \bar{\alpha}\gamma(x_3 + x_4\bar{\theta}) \\ \alpha(x_3 + x_4\theta) & \bar{\alpha}(x_1 + x_2\bar{\theta}) \end{pmatrix}, \tag{20}$$

where x_i belongs to the *M*-QAM signal set χ_M, and $i \in [1:4]$. The signal set χ_M is assumed to have a power normalization such that $E|x_i|^2 = 1$. Several constants in (20) are defined as, $\theta = \frac{1+\sqrt{5}}{2}$, $\bar{\theta} = (1-\theta)$, $\alpha = (1 + j\bar{\theta})$, $\bar{\alpha} = (1 + j\theta)$, and $\gamma = j$. The expression in (20) encompasses four super-symbols: $S^1 = \frac{1}{\sqrt{5}}\alpha(x_1 + x_2\theta)$, $S^2 = \frac{1}{\sqrt{5}}\bar{\alpha}(x_1 + x_2\bar{\theta})$, $S^3 = \frac{1}{\sqrt{5}}\alpha(x_3 + x_4\theta)$, and $S^4 = \frac{1}{\sqrt{5}}\bar{\alpha}\gamma(x_3 + x_4\bar{\theta})$. As each x_i has unit power, these super-symbols also satisfy $E|S^i|^2 = 1$ for $i \in [1:4]$. These super-symbols are grouped into pairs, namely $\{S^1, S^2\}$ and $\{S^3, S^4\}$. The GC scheme utilises two time slots to transmit these four pairs of GCWs. The received signal may be given as

$$\begin{aligned} \mathbf{y}_1 &= \mathbf{h}_1 S^1 + \mathbf{h}_2 S^2 + \mathbf{n}_1, \\ \mathbf{y}_2 &= \mathbf{h}_3 S^3 + \mathbf{h}_4 S^4 + \mathbf{n}_2, \end{aligned} \tag{21}$$

where $\mathbf{y}_i$ represents the received signal vector for the i^{th} time slot, and $\mathbf{y}_i$ is a complex vector in $\mathbb{C}^{N_R \times 1}$. The channel gain vector $\mathbf{h}_i$, $i \in [1:4]$, characterises the channel response between the transmitter and receiver. The channels $\mathbf{h}_i$ are considered as Rayleigh frequency-flat fast-fading channels, implying that the channels remain constant during a given time slot and take on independent values in subsequent time slots. Additionally, $\mathbf{n}_l$, $l \in [1:2]$ denotes the AWGN vector for the l^{th} time slot, also residing in $\mathbb{C}^{N_R \times 1}$. The elements of the channel gain vectors $\mathbf{h}_i$ and noise vectors $\mathbf{n}_l$, are assumed to be i.i.d GRVs with distribution $CN(0,1)$ for $\mathbf{h}_i$ and $CN(0, \frac{\rho}{2})$ for $\mathbf{n}_l$, respectively. ρ represents the average SNR.

3.3 Space time Labeling diversity (STLD) methods for improving the error performance and/ SE of MIMO wireless communication networks

Space-time labelling diversity (STLD) has emerged as a novel paradigm widely adopted within wireless communication systems, driven by the amplified SE and heightened link robustness afforded by MIMO methodologies [51–54]. The investigation of STLD spans both encoded and unencoded communication systems, underscoring its comprehensive analytical scope.

3.3.1 Coded STLD

In MIMO wireless communication networks, substantial scholarly attention has been drawn towards the pursuit of optimising the asymptotic coding gain, as evidenced by a body of work encompassing references [51, 53, 55–57]. Huang *et al.* [51], put forth an optimal strategy for constellation diversity in $N_R \times N_T$ bit-interleaved space-time coded modulation (BI-STCM). Additionally, their exploration extended to the formulation of a labelling criterion tailored for BI-STCM. Within this context, Huang *et al.* [55], introduced an elevated 16-QAM labelling diversity (LD) scheme, specifically designed for BI-STCM iterative decoding utilising Alamouti STBC. Also, the application of STLD manifested in 2×2 wireless local area networks (WLAN)s, as documented in Ejaz *et al.* [56]. An improved LD paradigm, optimising for asymptotic coding gain, was introduced by Krasicki and Szulakiewicz in [52, 53, 57]. However, it is important to note that the utilisation of a coded modulation scheme mandates the incorporation of identification (ID) for channel modelling, thereby incurring heightened system intricacies leading to escalated energy consumption and elevated latencies. Hence, this motivated the need for LD applications in uncoded modulation schemes [54, 58].

3.3.2 Uncoded STLD

In [53], the strategy of employing labelling mapping through constellation rearrangement has been harnessed to bolster the BER of STLD configurations. This involves mapping identical information bits into distinct signal constellations for subsequent transmission [53, 54]. This technique has found application across diverse frameworks including multi-packet transmission systems [58]. In a more contemporary context, the work presented in Xu *et al.* [54], details the LD principles to STBC systems, resulting in an innovation termed uncoded space-time labeling diversity (USTLD). USTLD manifests a noteworthy enhancement in the error performance improvement as compared to conventional STBC schemes. Figs.13 and 14 show an example of USTLD system model.

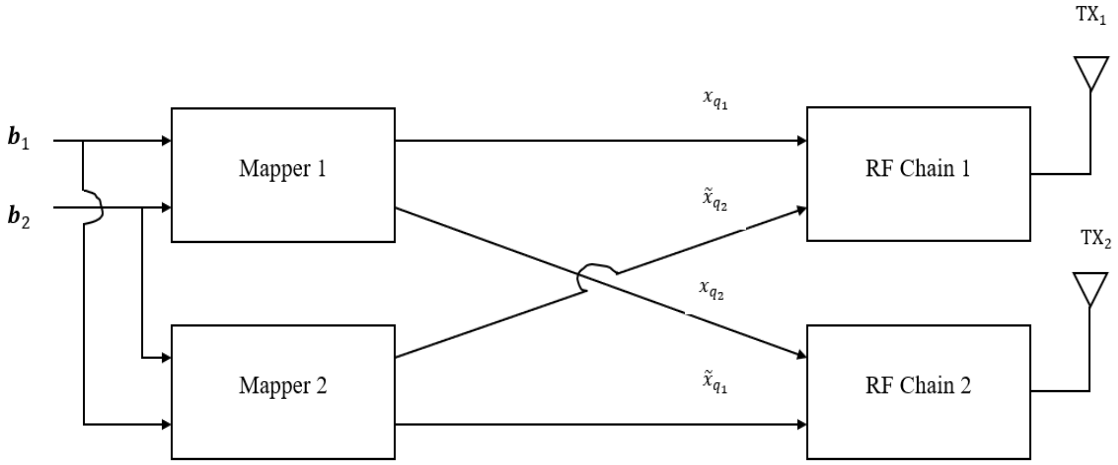

Fig. 13: USTLD transmitter side system model over Rayleigh frequency-flat fading channels.

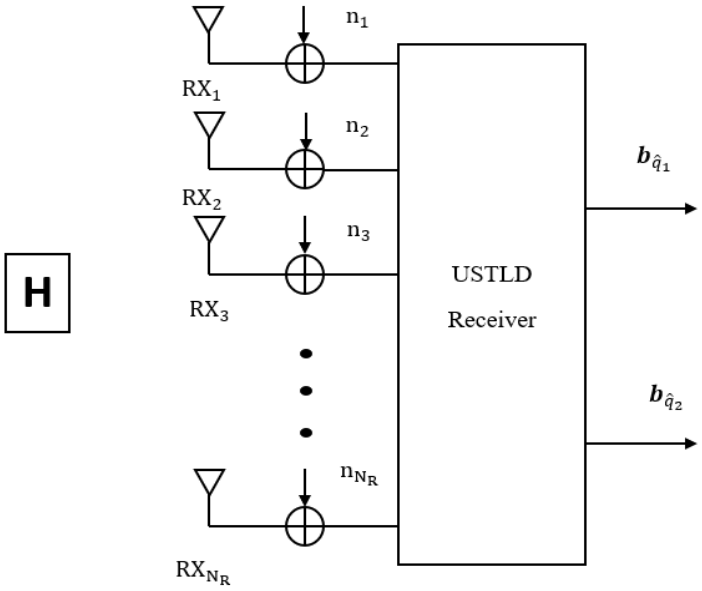

Fig. 14: USTLD receiver side system model over Rayleigh frequency-flat fading channels.

Consider a USTLD MIMO system shown in Figs. 13 and 14, with $N_T = 2$ transmit antennas and N_R receive antennas. The message bits are divided into two separate bit streams: $\boldsymbol{b_1} = \left[b_{1,1}b_{1,2}\cdots b_{1,r}\right]$ and $\boldsymbol{b_2} = \left[b_{2,1}b_{2,2}\cdots b_{2,r}\right]$, where $r = \log_2 M$. These bit streams are then processed by two distinct mappers known as mapper one ($\mathfrak{S}_1$) and mapper two ($\mathfrak{S}_2$), respectively. Mapper ($\mathfrak{S}_1$) assigns the input bits to Gray-coded M-QAM or M-PSK constellation points in the Argand plane, resulting in two symbols, S_q^1 and S_q^2, with $q \in [1 : M]$.

Mapper ($\mathfrak{S}_2$) performs a similar operation by mapping the identical input bits onto an M-QAM or M-PSK constellation points in the Argand plane. This process results in the symbols $\tilde{S}_q^1$ and $\tilde{S}_q^2$. It is

assumed that the expected squared magnitude of these symbols, $E\{|S_q^i|^2\} = 1$, $i \in [1:2]$ and $E\{|\tilde{S}_q^i|^2\} = 1$.

While mapper ($\mathfrak{S}_1$) follows the conventional Gray-coded approach, mapper ($\mathfrak{S}_2$)'s design, is aimed at ensuring LD [53, 54]. Detailed information regarding the design of mapper 2 has been discussed in [53, 54]. Subsequently, in the first time slot, antenna 1 and antenna 2 simultaneously transmit S_q^1 and S_q^2, respectively, and in the second time slot, they transmit $\tilde{S}_q^2$ and $\tilde{S}_q^1$, respectively.

The channel connecting the transmitter and receiver is considered a Rayleigh frequency-flat fast-fading channel, which signifies that the channel's characteristics remain fixed within each time slot but take on independent values between time slot 1 (denoted as $\mathbf{H}_1$) and time slot 2 (denoted as $\mathbf{H}_2$) [53, 54]. In this context, the received signal vector is represented by an $N_R \times 1$ vector and can be described as follows in time slot l, $l \in [1:2]$ [54]:

$$\mathbf{y}_l = \sqrt{\frac{\rho}{2}}\mathbf{H}_l\mathbf{x}_l + \mathbf{n}_l, \tag{22}$$

where $\mathbf{y}_l$ represents an $N_R \times 1$ vector with elements denoted as $y_{1,l}$, $y_{2,l}$, $y_{3,l}$, and so forth, up to $y_{N_R,l}$. The vector $\mathbf{n}_l \in \mathbb{C}^{N_R \times 1}$ stands for the AWGN vector, while $\mathbf{H}_l \in \mathbb{C}^{N_R \times 2}$ is the channel matrix [54]. The elements of both $\mathbf{n}_l$ and $\mathbf{H}_l$ are considered to be i.i.d GRVs with distributions: $\mathit{CN}(0, \sigma^2)$ for the noise vector and $\mathit{CN}(0, 1)$ for the channel matrix [54]. It is important to note that $\frac{\rho}{2}$ denotes the average SNR associated with the transmission antenna [54].

4 Research Motivation and contributions

4.1 Research Motivation

C-SM is a MIMO technique utilising spatial and signal constellations, requiring only one transmit antenna per channel use [59]. C-SM outperforms schemes like Alamouti STBC and V-BLAST due to reduced ICI and IAS, resulting in enhanced error performance [12]. Additionally, C-SM demonstrates improved bandwidth efficiency over single-antenna conventional modulation [60]. However, the SE of C-SM is restricted by the number of physical antennas, leading to the introduction of C-GSM to mitigate this limitation [24].

C-GSM addresses the limitation of the number of transmit antennas being a power of two in C-SM setups, allowing non-power-of-two antenna configurations [24]. In C-GSM, data bits are categorised as symbol signal bits and spatial constellation bits, with unique antenna groupings represented by indices. This scheme boosts SE by accommodating multiple active transmission antennas [24]. However, C-GSM's ABER is limited and degraded compared to C-SM under identical setups [24]. Moreover, the C-GSM approach can be combined with various digital modulation techniques. SE improvements are achievable by expanding the spatial domain or enhancing signal modulation. A fully generalised spatial modulation system that varies active antennas, achieving high SEs but at the cost of heightened receiver complexity was proposed in Hussein *et al.* [61]. This scheme can achieve high SE, however, increasing signal constellation size, as shown in [30], decreases minimum Euclidean distance (ED), thus degrading the ABER performance. Hence, a need to devise C-GSM systems that balance SE, reliability, and receiver complexity. An example of such systems will be incorporating C-GSM systems with GC.

The optimality of the GC has been examined in [62], and it has been explored in the context of media-based modulations in [63]. Furthermore, Liu *et al.*, have demonstrated in [64] that the GC can deliver coding gain within MIMO systems, thereby enhancing the ABER performance in MIMO wireless links, including those utilising C-GSM schemes. Despite its numerous advantages and broad applications, the GC is encumbered by high complexity when it comes to maximum-likelihood detection (MLD). Therefore, drawing from insights presented in [62], [63], and [64], the need to improve the BER performance and SE of MIMO C-GSM systems has become apparent. This need serves as the driving force behind the creation of a BER performance-enhanced C-GSM approach, which leverages M-QAM signal constellations and GCWs, as elaborated in Part (II). The proposed scheme is called Golden Codeword-based generalised spatial modulation (GCW-GSM).

Over the past decade, efforts have been made to enhance the error performance and SE of both SM and GSM systems. One notable outcome of these endeavours is the development of C-QSM by Mesleh *et al.* [32]. C-QSM introduces a novel approach by extending the spatial constellation into two dimensions, namely the (I) and (Q) dimensions. This effectively eliminates ICI, consequently leading to the enhancement of the error performance of SM systems [34]. However, it is essential to acknowledge that, despite its potential to elevate the error performance and SE of SM wireless communication networks, C-QSM does possess certain limitations. Notably, it necessitates the utilisation of a substantial number of transmit antennas compared to C-SMux techniques. This

characteristic imposes restrictions on the degree to which the error performance can be improved within SM systems [37].

In an effort to address the limitations of C-QSM, a study conducted by Mohaisen *et al.* [31] introduced a novel scheme known as generalised complex quadrature spatial modulation (GCQSM). GCQSM leverages the foundation of C-QSM and integrates the characteristics of C-GSM into the scheme. This enhancement focuses on boosting SE by transmitting two amplitude/phase modulated symbols from two distinct constellation sets in each channel utilisation. This process involves unique combinations of antennas in both the I and Q domains. However, a key consideration arises when comparing GCQSM to C-SM, C-GSM, and C-QSM. This expansion of the modulation set results in a reduction in the minimum distance between transmitted symbols at the transmitter of GCQSM systems. As a consequence, the error performance of the GCQSM scheme experiences a noticeable degradation, largely due to its dependency on the minimum Euclidean distance (MED) between the transmitted vector symbols, as highlighted in [30]. This diminished performance is a direct result of a larger modulation set and reduced minimum symbol distance.

To further enhance the error performance of GSM systems, an innovative approach is introduced by building upon GCQSM. This proposed scheme incorporates hexagonal quadrature amplitude modulation (H-QAM) constellations. H-QAM systems offer the advantage of a maximised MED (M-MED) while maintaining a relatively low peak-to-average power ratio (PA) [13]. These constellations are structured in a hexagonal layout, which was found in [13], to surpass the performance of conventional-QAM (C-QAM) systems. This preference is attributed to the M-MED between neighbouring constellation points and the average symbol energy, as established in both Naidoo *et al.* [30] and Singya *et al.* [13].

As a result, the proposed approach in Part (III) is motivated by the goal of elevating the error performance and/or SE of GSM systems. This is achieved by extending GCQSM through a fusion with rotated H-8QAM systems, as observed in the work of Cogen *et al.* [65]. This new scheme harnesses the potential of rotated H-8QAM and incorporates general combinations of antennas in both the I and Q domains. This novel system is called generalised quadrature spatial modulation using H-8QAM (GQSM-H8QAM).

Thus, motivated to further improve the error performance of GSM and GQSM systems, we propose

to incorporate optimised labelling maps with C-GSM systems and GQSM systems. Optimised labelling maps were found to maximise the minimum product distance (MPD) of STBCs in [66, 67] and in turn, this led to an improvement in the error performance of STBCs [54, 66, 68]. Hence, in order to further improve the error performance of GSM and GQSM systems, it was proposed to add labelling diversity (LD) to C-GSM and GQSM systems by fusing them with optimised labelling maps [53, 54, 66, 68]. This entails the proposal of two techniques in Part (IV), called multiple active antenna generalised spatial modulation with labelling diversity (MAA-GSM-LD) and generalised complex spatial modulation with labelling diversity (GCQSM-LD).

MAA-GSM-LD builds on C-GSM and optimised labelling maps, by fusing the attributes of C-GSM with those of LD [54]. In Wang *et al.* [4], a multiple active antenna GSM (MIMO-GSM) scheme was proposed and it exhibited improved error performance as compared to C-GSM and C-SM systems. Thus, in [4], it was shown that multiple active transmit antennas increase spatial diversity thereby improving robustness against fading. Hence, in order to improve the error performance of MIMO GSM systems, a scheme that extends MIMO-GSM into transmitting four symbols simultaneously, from Gray-coded QAM constellations and optimised labelling QAM maps was proposed. It was proposed to fuse MIMO-GSM with optimised labelling maps because it was shown in [66] and [68], that optimised labelling maps increase the robustness of SM systems against fading, hence improving the error performance of SM systems.

Also, to further improve on the error performance of MIMO-GQSM schemes, it was proposed to extend the MAA-GSM-LD scheme with C-QSM attributes of expanding the spatial domain into the I-phase and Q phase dimensions. This proposed scheme is herein named generalised complex quadrature spatial modulation with LD (GCQSM-LD). This proposed scheme builds on MAA-GSM-LD and instead of sending four symbols from C-QAM constellations, it draws four symbols, (two from conventional Gray-coded QAM constellations and two from optimised labelling QAM maps) in the same way as in MAA-GSM-LD. The four symbols are then split into imaginary and real parts of the signal, which are then sent by the I-phase and Q-phase dimensions, respectively [32, 34]. This further improves the robustness of the proposed schemes as the I and Q spatial domains are designed to reduce IAS, thereby improving robustness against channel fading.

Finally, the major contributions of this research are either published or submitted for review as journal papers. The details are as follows:

4.2 Research Contributions

Paper A

N. Sibanda, H. Xu, and N. Pillay, "Golden codeword-based generalised spatial modulation," International Journal of Communication Systems, vol. 35, no. 10, p. e5144, Jul. 2022.

In summary, the main contributions of Paper A are:

1. Proposal of a new C-GSM scheme that improves the error performance of C-GSM systems by equipping them with GCWs. Hence the name, GCW-GSM.
2. Derivation of a closed form ABER expression for the proposed scheme over i.i.d Rayleigh frequency-flat fading channels. Using Monte Carlo simulation results, this expression is shown to confirm the accuracy of the simulation.
3. Comparison of the performance of the proposed scheme in Rayleigh frequency-flat fading channels and the Rician channel.

Paper B

N. Sibanda, H. Xu, and N. Pillay, "Error performance analysis of generalised quadrature spatial modulation using H-8QAM," Scientific Reports, vol. 12, no. 1, pp.1–13, Nov. 2022.

In summary, the main contributions of Paper B are:

1. Proposal of a new GQSM scheme called GSM with H-QAM (GQSM-H-8QAM), that improves the error performance of GCQSM systems by equipping them with rotated H-8QAM. The H-8QAM systems have a lattice structure that has an M-MED and relatively low PA compared to C-QAM. This helps improve the error performance of SM schemes.
2. Derivation of an upper bound ABER expression for the GQSM-H-8QAM scheme over i.i.d Rayleigh frequency-flat fading channels.
3. Validation of the derived analytical bound using Monte Carlo simulation results.

Paper C

N. Sibanda, H. Xu, and N. Pillay, "Error performance analysis of multiple active antennas GSM and GCQSM with labelling diversity," [*Under review with Wiley International Journal of Communication Systems*]

Thus, the main contributions of Paper C are:

1. Proposal of a new GSM scheme called MAA-GSM-LD which incorporates MIMO-GSM and optimised LD maps that maximise the MPD of STBCs, which in turn improves the error performance of the STBCs.
2. Derivation of a union-bound ABER expression for the MAA-GSM-LD scheme over i.i.d Rayleigh frequency-flat fading channels.
3. Validation of the derived analytical union-bound for the MAA-GSM-LD scheme using Monte Carlo simulation results.
4. Proposal of a scheme called GCQSM that extends the MAA-GSM-LD scheme into the QSM domain by using optimised LD maps with GCQSM.
5. Derivation of an upper bound ABER expression for the GCQSM-LD scheme over i.i.d Rayleigh frequency-flat fading channels.
6. Validation of the derived analytical bound for the GCQSM-LD scheme using Monte Carlo simulation results.

4.3 Structure of Thesis

Finally, the work covered in this thesis has been detailed in Parts, with Part (II) covering Paper A, Part (III) covering Paper B in detail, Part (IV) covering Paper C in detail and finally the conclusion and suggestions for possible future research work are covered in Part (V).

References

[1] M. R. Bhalla and A. V. Bhalla, "Generations of mobile wireless technology: A survey," *International Journal of Computer Application*, vol. 5, no. 4, pp. 26–32, Aug. 2010.

[2] D. J. Love and R. W. Heath, "Equal gain transmission in multiple-input multiple-output wireless systems," *IEEE Transactions on Communications*, vol. 51, no. 7, pp. 1102–1110, Jul. 2003.

[3] A. Goldsmith, *Wireless Communications,*. New York: Cambridge University Press, 2005.

[4] J. Wang, S. Jia, and J. Song, "Generalised spatial modulation system with multiple active transmit antennas and low complexity detection scheme," *IEEE Transactions on Wireless Communications*, vol. 11, no. 4, pp. 1605–1615, Mar. 2012.

[5] P. W. Wolniansky, G. J. Foschini, G. D. Golden, and R. A. Valenzuela, "V-blast: an architecture for realizing very high data rates over the rich-scattering wireless channel," in *1998 URSI International Symposium on Signals, Systems, and Electronics. Conference Proceedings (Cat. No.98EX167)*. IEEE, Oct. 1998, pp. 295–300.

[6] T. Svantesson and A. Ranheim, "Mutual coupling effects on the capacity of multielement antenna systems," in *2001 IEEE International Conference on Acoustics, Speech, and Signal Processing. Proceedings (Cat. No.01CH37221)*. IEEE, May. 2001, pp. 2485–2488.

[7] C. K. Agubor, F. K. Opara, and G. N. Eze, "A Review of Diversity Techniques for Wireless Communications," *Academic Research International (ARInt.)*, vol. 4, no. 2, pp. 157–167, Mar. 2013.

[8] S. M. Alamouti, "A simple transmit diversity technique for wireless communications," *IEEE Journal on selected areas in communications*, vol. 16, no. 8, pp. 1451–1458, Oct. 1998.

[9] A. Goldsmith, N. Jindal, and S. Vishwanath, "Capacity limits of mimo channels," *IEEE Journal on Selected Areas in Communications*, vol. 21, no. 5, pp. 684–702, Jun. 2003.

[10] R. Y. Mesleh, H. Hass, L. Yenwoo, and Y. Sangboh, "Interchannel interference avoidance in mimo transmission by exploiting spatial information," in *2005 IEEE 16th International Symposium on Personal, Indoor and Mobile Radio Communications*. IEEE, Sep. 2005, pp. 141–145.

[11] H. Xu and N. Pillay, "Golden codeword-based modulation schemes for single-input multiple-output systems," *International Journal of Communication Systems*, vol. 32, no. 10, p. e3963, Jul. 2019.

[12] J. Jeganathan, A. Ghrayeb, and L. Szczecinski, "Spatial modulation: Optimal detection and performance analysis," *IEEE Communications Letters*, vol. 12, no. 8, pp. 545–547, Aug. 2008.

[13] K. P. Singya, N. Kumar, V. Bhatia, and M. Alouini, "On the performance of hexagonal, cross, and rectangular qam for multi-relay systems," *IEEE Access*, vol. 7, no. 1, pp. 60 602–60 616, May. 2019.

[14] P. K. Singya, P. Shaik, N. Kumar, V. Bhatia, and M. Alouini, "A survey on design and performance of higher-order qam constellations," *arXiv preprint arXiv:2004.14708*, Apr. 2020.

[15] M. K. Simon and M. S. Alouini, *Digital communication over generalized fading channels: a unified approach to performance analysis*. New York: Wiley-Interscience Publication, 2000.

[16] E. G. Larsson, P. Stoica, and G. Ganesan, *Space-time block coding for wireless communications*. Cambridge university press, 2003.

[17] S. O. Rice, "Mathematical analysis of random noise," *The Bell System Technical Journal*, vol. 23, no. 3, pp. 282–332, Jul. 1944.

[18] R. Mesleh, M. Di-Renzo, H. Haas, and P. M. Grant, "Trellis coded spatial modulation," *IEEE Transactions on Wireless Communications*, vol. 9, no. 7, pp. 2349–2361, Jul. 2010.

[19] M. Nakagami, "The m-distribution—a general formula of intensity distribution of rapid fading," in *Statistical Methods in Radio Wave Propagation*. ScienceDirect, Jun. 1960, pp. 3–6.

[20] N. C. Beaulieu and C. Cheng, "Efficient nakagami-m fading channel simulation," *IEEE Transactions on Vehicular Technology*, vol. 54, no. 2, pp. 413–424, Mar. 2005.

[21] U. Charash, "Reception through nakagami fading multipath channels with random delays," *IEEE Transactions on Communications*, vol. 27, no. 4, pp. 657–670, Apr. 1979.

[22] M. D. Yacoub, "Nakagami-m phase-envelope joint distribution: An improved model," in *2009 SBMO/IEEE MTT-S International Microwave and Optoelectronics Conference (IMOC)*. IEEE, Nov. 2009, pp. 335–339.

[23] ——, "Nakagami- m phase–envelope joint distribution: A new model," *IEEE Transactions on Vehicular Technology*, vol. 59, no. 3, pp. 1552–1557, Mar. 2010.

[24] A. Younis, N. Serafimovski, R. Mesleh, and H. Haas, "Generalised spatial modulation," in *2010 conference record of the forty fourth Asilomar conference on signals, systems and computers*. IEEE, Nov. 2010, pp. 1498–1502.

[25] A. Younis, "Spatial modulation: Theory to practice," Ph.D. dissertation, The University of Edinburgh, 2014.

[26] R. Mesleh, H. Haas, C. W. Ahn, and S. Yun, "Spatial modulation - a new low complexity spectral efficiency enhancing technique," in *2006 First International Conference on Communications and Networking in China*. IEEE, Oct. 2006, pp. 1–5.

[27] M. Di-Renzo, H. Haas, A. Ghrayeb, S. Sugiura, and L. Hanzo, "Spatial modulation for generalized mimo: Challenges, opportunities, and implementation," *Proceedings of the IEEE*, vol. 102, no. 1, pp. 56–103, Jan. 2014.

[28] P. Yang, M. Di-Renzo, Y. Xiao, S. Li, and L. Hanzo, "Design guidelines for spatial modulation," *IEEE Communications Surveys & Tutorials*, vol. 17, no. 1, pp. 6–26, May. 2014.

[29] R. Pillay, N. Pillay, and H. Xu, "Improved error performance for generalised spatial modulation with enhanced spectral efficiency," *International Journal of Communication Systems*, vol. 33, no. 2, p. e4176, Jan. 2020.

[30] N. R. Naidoo, "Enhanced performance and efficiency schemes for generalised spatial modulation," Ph.D. dissertation, University of KwaZulu-Natal, 2017.

[31] M. Mohaisen, "Generalised complex quadrature spatial modulation," *Wireless Communications and Mobile Computing*, vol. 2019, no. 1, p. 3137927, Apr. 2019.

[32] R. Y. Mesleh, S. S. Ikki, and H. M. Aggoune, "Quadrature spatial modulation," *IEEE Transactions on Vehicular Technology*, vol. 64, no. 6, pp. 2738–2742, Jul. 2014.

[33] V. V. Gudla and V. B. Kumaravelu, "Permutation index-quadrature spatial modulation: A spectral efficient spatial modulation for next generation networks," *AEU-International Journal of Electronics and Communications*, vol. 111, no. 1, p. 152917, Nov. 2019.

[34] S. Oladoyinbo, N. Pillay, and H. Xu, "Adaptive quadrature spatial modulation," *IETE Technical Review*, vol. 37, no. 6, pp. 579–590, Nov. 2020.

[35] R. Mesleh and S. S. Ikki, "A high spectral efficiency spatial modulation technique," in *2014 IEEE 80th Vehicular Technology Conference (VTC2014-Fall)*. IEEE, Sep. 2014, pp. 1–5.

[36] S. Naidu, N. Pillay, and H. Xu, "A study of quadrature spatial modulation," in *2015 Southern Africa Telecommunication Networks and Applications Conference (SATNAC)*. SATNAC, Sep. 2015, pp. 3–8.

[37] F. Castillo-Soria, J. Cortez-González, R. Ramirez-Gutierrez, M. M.-B. Fermín, and L. Soriano-Equigua, "Generalized quadrature spatial modulation scheme using antenna grouping," *ETRI Journal*, vol. 39, no. 5, pp. 707–717, Oct. 2017.

[38] L. Xiao, P. Xiao, Y. Xiao, H. Haas, A. Mohamed, and L. Hanzo, "Compressive sensing assisted generalized quadrature spatial modulation for massive mimo systems," *IEEE Transactions on Communications*, vol. 67, no. 7, pp. 4795–4810, Jul. 2019.

[39] V. Tarokh, N. Seshadri, and A. R. Calderbank, "Space-time codes for high data rate wireless communication: performance criterion and code construction," *IEEE Transactions on Information Theory*, vol. 44, no. 2, pp. 744–765, Mar. 1998.

[40] V. Tarokh, H. Jafarkhani, and A. R. Calderbank, "Space-time block codes from orthogonal designs," *IEEE Transactions on Information Theory*, vol. 45, no. 5, pp. 1456–1467, Jul. 1999.

[41] ——, "Space-time block coding for wireless communications: performance results," *IEEE Journal on Selected Areas in Communications*, vol. 17, no. 3, pp. 451–460, Mar. 1999.

[42] V. Tarokh, N. S. A. Naguib, and A. R. Calderbank, "Space-time codes for high data rate wireless communication: performance criteria in the presence of channel estimation errors, mobility, and multiple paths," *IEEE Transactions on Communications*, vol. 47, no. 2, pp. 199–207, Feb. 1999.

[43] A. saeed, H. Xu, and T. Quazi, "Alamouti space-time block coded hierarchical modulation with signal space diversity and mrc reception in nakagami-m fading channel," *IET Communications*, vol. 8, no. 4, pp. 516–524, Mar. 2014.

[44] T. Jung and K. Cheun, "Design of concatenated space-time block codes using signal space diversity and the alamouti scheme," *IEEE Communications Letters*, vol. 7, no. 7, pp. 329–331, Jul. 2003.

[45] S. Jeony, J. Lee, I. Kyung, and M. S. Kim, "Component-interleaved alamouti coding with rotated constellations for signal space diversity," in *2010 IEEE International Symposium on Broadband Multimedia Systems and Broadcasting (BMSB)*. IEEE, Mar. 2010, pp. 1–6.

[46] J. C. Belfiore, G. Rekaya, and E. Viterbo, "The golden code: a 2×2 full-rate space-time code with nonvanishing determinants," *IEEE Transactions on Information Theory*, vol. 51, no. 4, pp. 1432–1436, Apr. 2005.

[47] ——, "Space Time Block Codes," *IEEE Transactions on information theory*, vol. 51, no. 4, pp. 1432–1436, Jul. 2005.

[48] S. Sirinaunpiboon, A. R. Calderbank, and S. D. Howard, "Fast essentially maximum likelihood decoding of the golden code," *IEEE Transactions on Information Theory*, vol. 57, no. 6, pp. 3537–3541, Jun. 2011.

[49] M. O. Sinnokrot and J. R. Barry, "Fast maximum-likelihood decoding of the golden code," *IEEE Transactions on Wireless Communications*, vol. 1, no. 9, pp. 26–31, Jan. 2010.

[50] L. Zheng and D. Tse, "Diversity and multiplexing: A fundamental tradeoff in multiple-antenna channels," *IEEE Transactions on information theory,*, vol. 49, no. 5, pp. 1073–1096, May. 2003.

[51] Y. Huang and J. A. Ritcey, "Optimal constellation labelling for iteratively decoded bit-interleaved spacetime coded modulation," *IEEE Transactions on Information Theory*, vol. 51, no. 5, pp. 1865–1871, May. 2005.

[52] M. Krasicki, "Improved labelling diversity for iteratively-decoded multi-antenna systems," in *2011 7th International Wireless Communications and Mobile Computing Conference*. IEEE, Aug. 2011, pp. 359–364.

[53] ——, "Essence of 16-qam labelling diversity," *Electronics letters*, vol. 49, no. 8, pp. 567–569, Apr. 2013.

[54] H. Xu, K. Govindasamy, and N. Pillay, "Uncoded space-time labeling diversity," *IEEE Communications Letters*, vol. 20, no. 8, pp. 1511–1514, Aug. 2016.

[55] Y. Huang and J. A. Ritcey, "Improved 16-qam constellation labeling for bi-stcm-id with the alamouti scheme," *IEEE Communications Letters*, vol. 9, no. 2, pp. 157–159, Jan. 2005.

[56] S. Ejaz, Y. FengFan, and H. Xu, "Labeling diversity for 2×2 wlan coded-cooperative networks," *Radioengineering*, vol. 24, no. 9, pp. 470–480, Jun. 2015.

[57] M. K. 1 and P. Szulakiewicz, "Boosted space-time diversity scheme for wireless communications," *Electronics letters*, vol. 45, no. 16, pp. 843–845, Jul. 2009.

[58] H. Samra and Z. Ding, "Symbol mapping diversity design for multiple packet transmission," *IEEE Transactions on Wireless Communications*, vol. 53, no. 5, pp. 810–817, May. 2005.

[59] R. Y. Mesleh, H. Haas, S. Sinanovic, C. W. Ahn, and S. Yun, "Spatial modulation," *IEEE Transactions on Vehicular Technology*, vol. 57, no. 4, pp. 2228–2241, Jul. 2008.

[60] N. R. Naidoo, H. Xu, and T. A. Quazi, "Spatial modulation: optimal detector asymptotic performance and multiple-stage detection," *IET communications*, vol. 5, no. 10, pp. 1368–1376, Jul. 2011.

[61] H. S. Hussein, H. Esmaiel, and D. Jiang, "Fully generalised spatial modulation technique for underwater communication," *Electronics Letters*, vol. 54, no. 14, pp. 907–909, Jul. 2018.

[62] F. Oggier, "On the Optimality of the golden code," in *2006 IEEE Information Theory Workshop - ITW '06 Chengdu*. IEEE, Oct. 2006, pp. 468–472.

[63] N. Pillay and H. Xu, "RF mirror media-based modulation for Golden codes," *Journal of Telecommunication, Electronic and Computer Engineering (JTEC)*, vol. 10, no. 3, pp. 21–24, Aug. 2018.

[64] M. Liu, M. Helard, J. F. Helard, and M. Crussiere, "A fast decodable full-rate STBC with high coding gain for 4$\times$ 2 MIMO systems," in *2013 IEEE 24th Annual International Symposium on Personal, Indoor, and Mobile Radio Communications (PIMRC)*. IEEE, Sep. 2013, pp. 677–681.

[65] F. Cogen and E. Aydin, "Performance analysis of hexagonal qam constellations on quadrature spatial modulation with perfect and imperfect channel estimation," *Physical Communication*, vol. 47, no. 1, p. 101379, May. 2021.

[66] K. Govindasamy, H. Xu, and N. Pillay, "Space-time block coded spatial modulation with labelling diversity," *International Journal of Communication Systems*, vol. 31, no. 1, p. e3395, Jan. 2018.

[67] S. E. Krouk, *Modulation and Coding Techniques in Wireless Communications*. New Jersey: John Wiley & Sons Ltd,, 2011.

[68] B. S. Adejumobi and T. Shongwe, "Labeling diversity for media-based space-time block coded spatial modulation," *IEEE Access*, vol. 8, no. 1, pp. 99 870–99 879, May. 2020.

Part II

Paper A

Paper A

Golden Codeword-based Generalised Spatial Modulation

1 Abstract

Conventional-generalised spatial modulation (C-GSM) is an $N_T \times N_R$ multiple-input multiple-output (MIMO) spatial modulation (SM) scheme that transmits the same complex amplitude/phase modulation symbol from multiple active transmit antennas. By using two active transmit antennas during a transmission interval, C-GSM is capable of achieving high spectral efficiencies (SE)s but however, as the size of the signal constellation/domain increases, the minimum Euclidean distances (ED) between the symbols decreases. Hence, this leads to a degradation of the average bit error rate (ABER) performance of the scheme. Hence motivated to improve the error performance of the C-GSM scheme, firstly, this study proposes a new scheme called Golden codeword-based generalised spatial modulation (GCW-GSM), which combines C-GSM and the golden code (GC) to take advantage of the benefits of both with a good trade-off for positive error performance improvement to the limitations of the two schemes (C-GSM and GC). The proposed scheme uses conventional quadrature amplitude modulation (C-QAM) and it is investigated over Rayleigh frequency-flat fading channels with additive white Gaussian noise. Secondly, a closed-form expression of the theoretical average bit error probability of the proposed GCW-GSM scheme is formulated. Compared to simulation results, it is increasingly tight at high signal-to-noise ratio values. Finally, the proposed scheme performance over the Rayleigh frequency-flat fading channel is compared to that over the Rician channel. An improvement in the error performance of $6\ dB$ with an SE of $10\ bits/s/Hz$ is seen in 4×4 C-16QAM GCW-GSM over 4×4 C-256QAM conventional-spatial modulation and 4×4 C-256QAM C-GSM schemes at a bit error rate (BER) of 1×10^{-5}. Also, the 4×4 C-16QAM GCW-GSM scheme exhibits an improvement in the error performance of $2.9\ dB$ with an SE of $10\ bits/s/Hz$ over the 4×4 C-64QAM conventional quadrature spatial modulation scheme at a BER of 1×10^{-5}. Finally, the 4×4 16-QAM GCW-GSM under Rayleigh frequency-flat fading channel has a performance gain of $5\ dB$ over 4×4 16-QAM GCW-GSM under Rician fading with a Rician K factor of 3.

***Index Terms*—Error performance; generalised spatial modulation; golden code; multiple-input multiple-output; space-time block codes.**

2 Introduction

In the past decade, there has been an explosive increase in the demand for wireless communication networks with high data rates and reliable link margins. In Love *et al.* [1], it has been shown that multiple-input multiple-output (MIMO) systems can be used to enhance spectral efficiency (SE) and/or increase link quality of wireless communication networks against multipath fading. MIMO systems are defined as the use of multiple antennas at both the transmitting and receiving ends of a wireless communication link. The concept of MIMO systems is based on improving the overall error performance of wireless communication links through spatial diversity and/or improving SE through spatial multiplexing [1].

Diversity is a technique for improving the reliability of wireless communication links by using two or more communication channels with different characteristics [2]. It is a method that may be used to combat fading and co-channel interference using multiple replicas of the same signal transmitted and/or received on multiple independent individual channels with different levels of fading and interference [2]. Alternatively, a redundant forward error correction code may be added, and different parts of the message transmitted over different channels to avoid error bursts [2]. Two techniques that may be used to enhance diversity and/or coding gain in MIMO systems are the Golden code (GC) and Conventional-generalised spatial modulation (C-GSM).

The GC is regarded as a 2×2 algebraic perfect space-time block code (STBC) with unprecedented performance and an SE of $2\log_2(M)\ bits/s/Hz$, where M is the amplitude/phase modulation order [3]. GC is a full-rate, full-diversity STBC with two transmit antennas for a coherent MIMO channel [3]. Full rate because four symbols are transmitted in two-time slots by two transmit antennas. It also has cubic shaping and a non-vanishing minimum determinant due to its algebraic structure [3]. The GC can be regarded as one type of space-time labelling diversity (STLD) since two of its super symbols in each pair, convey the same information [4, 5]. The STLD properties of the GC also enhance coding gain in MIMO wireless links and thus significantly improve wireless links' reliability [6]. The GC was proposed for MIMO systems, and it has been applied in the IEEE 802.16e WiMAX standard [5].

Conventional spatial modulation (C-SM) is a technique that can improve SE by mapping information bits to both the spatial constellation (transmit antenna indices) and signal constellation [7]. In

Jeganathan *et al.* [8], C-SM was compared with other MIMO transmission schemes (vertical Bell Labs layered space-time scheme and Alamouti STBC scheme), and it was found to be advantageous as it avoids inter-channel interference (ICI) and inter-antenna synchronisation (IAS) [9]. However, C-SM SE is governed by the practical number of transmit antennas that can be used, and thus, C-GSM was proposed to help lessen this limitation [10]. C-GSM lessens the limitation in C-SM by overcoming the constraint that transmission antennas must be a power of two in C-SM [10]. Thus, in C-GSM, a block of information bits is mapped into a constellation symbol and transmit antennas index. The antennas index is a combination of transmit antennas activated per time slot. This combination depends on the random incoming data stream [10]. This is different from C-SM where only a single transmit antenna is activated at each instance. Thus, C-GSM increases the overall SE by the base-two logarithm of the number of antenna combinations and this reduces the number of transmit antennas needed for the same SE [10].

2.1 Motivation

C-GSM overcomes the SE limitation of C-SM schemes by permitting the use of multiple active transmission antennas [10]. However, for identical configurations, the average bit error rate (ABER) of C-GSM is limited and degraded as compared to C-SM [10]. Moreover, the C-GSM scheme may be utilised in conjunction with any digital modulation technique. The SE of C-GSM may be improved by either expanding the size of the spatial domain or by enhancing the signal modulation domain. In Hussein *et al.* [11], a fully generalised spatial modulation system enhances the spatial constellation by varying the number of active transmit antennas during a transmission interval. This system can achieve high SEs. However, it results in high receiver complexity and as seen in [12], as the size of the signal constellation increases, the minimum Euclidean distance (ED) between the symbols decreases, thereby degrading the ABER performance. Thus, the need for the development of a system that can be both spectrally efficient and reliable with a suitable receiver computational complexity (CC) trade-off.

The GC optimality was studied in [13] and the GC has been considered for media-based modulations in [14]. Liu *et al.* [6], shows that the GC can achieve high coding gain in MIMO systems and thus improve the ABER performance on MIMO wireless links. Despite its advantages and extensive application, the GC is limited due to the extremely high complexity imposed by maximum-likelihood detection (MLD). Hence, based on [6, 13] and [14], combined with the necessity to improve ABER performance and SE of MIMO C-GSM systems, this motivates the development of a BER

performance-enhanced C-GSM technique that utilises M-QAM signal constellations and GC codewords (GCWs). C-GSM is chosen because it offers spatial diversity gain and increases MIMO wireless communication network links' reliability, by providing replicas of the transmitted signal to the receiver while retaining the achieved SE like in [10]. The fusion of GC and C-GSM is proposed because it has STLD properties that can enhance coding gain and hence lead to an improvement in the ABER of MIMO wireless network links [6]. Specifically, for this proposed GCW-based GSM scheme, a single pair of GCWs is chosen to be the transmitted data. This is because GCWs can enhance performance gain, which in turn enhances link reliability [5]. Hence this scheme adopts spatial multiplexing of approximately the same GC symbols as the method adopted in [10]. Thus, the proposed scheme is called Golden codeword-based generalised spatial modulation (GCW-GSM).

In summary, the main contributions of this paper are:

1. Proposal of a new C-GSM scheme that improves the error performance of C-GSM systems by equipping them with GCWs. Hence the name, GCW-GSM.
2. Derivation of a closed form ABER expression for the proposed scheme over independent and identically distributed (i.i.d) Rayleigh frequency-flat fading channels. Using Monte Carlo simulation results, this expression is shown to confirm the accuracy of the simulation.
3. Comparison of the performance of the proposed scheme in Rayleigh frequency-flat fading channels and the Rician channel.

The remainder of this paper is structured as follows: Section 3 presents the system model of the proposed scheme. Section 4 entails the MLD CC analysis of the proposed scheme. Section 5 entails the theoretical analysis of the ABER performance of the system over i.i.d Rayleigh frequency-flat fading channels with additive white Gaussian noise (AWGN). Section 6 presents simulations, numerical results, and discussion. Finally, the paper is concluded in Section 7.

2.2 Notation

This paper employs distinct formatting for vectors and matrices, employing bold lowercase and uppercase letters, respectively. Scalar quantities are denoted using regular letters. The set $\mathbb{C}^{Q\times R}$ comprises complex-valued matrices with dimensions $Q \times R$. This paper also employs use of various mathematical operators: $[\cdot]^T$ signifies matrix transposition, $(\cdot)^H$ indicates Hermitian conjugation, $(\cdot)^*$

represents complex conjugation, $|\cdot|$ denotes the Euclidean norm, and $\|\cdot\|_F$ stands for the Frobenius norm. The notation $\lfloor\cdot\rfloor_{2^p}$ denotes the largest integer less than or equal to the argument, which is a positive integer power of 2. The Gaussian Q-function is introduced as $Q(\cdot)$ and the expectation operator is denoted as $E\{\cdot\}$. For optimisation purposes, this paper employs $\underset{w}{\text{argmin}}\{\cdot\}$ and $\underset{w}{\text{argmax}}\{\cdot\}$ to find the minimum or maximum value of a given argument with respect to the variable w. Additionally, the real and imaginary parts of a complex argument are denoted as $\Re(\cdot)$ and $j(\cdot)$, respectively. Finally, the binomial coefficient is expressed using the notation $\binom{\cdot}{\cdot}$.

3 System Model

The main component of the proposed GCW-GSM scheme is the GCWs. This section, briefly presents the concept of the GC and then describes the proposed GCW-GSM scheme.

3.1 The Golden code

The Golden encoder takes four complex-valued symbols and generates four super-symbols (GCWs). The generated GCW matrix is given on (1) in [5] as:

$$\boldsymbol{G} = \frac{1}{\sqrt{5}} \begin{pmatrix} \alpha(x_1 + x_2\theta) & \bar{\alpha}\gamma(x_3 + x_4\bar{\theta}) \\ \alpha(x_3 + x_4\theta) & \bar{\alpha}(x_1 + x_2\bar{\theta}) \end{pmatrix} \tag{A.1}$$

where $x_i \in \chi_M$, $i \in [1:4]$, χ_M is the M-QAM signal set, and it is assumed that $E\{|x_i|^2\} = 1$. $\theta = \frac{1+\sqrt{5}}{2}$ is the golden number, $\bar{\theta} = (1-\theta)$, $\alpha = (1 + j\bar{\theta})$, $\bar{\alpha} = (1 + j\theta)$ and $\gamma = j$. In (A.1), there are four super symbols, $S^1 = \frac{1}{\sqrt{5}}\alpha(x_1 + x_2\theta)$, $S^2 = \frac{1}{\sqrt{5}}\bar{\alpha}(x_1 + x_2\bar{\theta})$, $S^3 = \frac{1}{\sqrt{5}}\alpha(x_3 + x_4\theta)$ and $S^4 = \frac{1}{\sqrt{5}}\bar{\alpha}\gamma(x_3 + x_4\bar{\theta})$. Since $E\{|x_i|^2\} = 1$, it also that implies that $E\{|S^i|^2\} = 1$, $i \in [1:4]$. These super symbols form pairs of GCWs, and those pairs are $\{S^1, S^2\}$ and $\{S^3, S^4\}$. The GCWs pair $\{S^1, S^2\}$ is the only one used in this paper for the GCW-GSM scheme.

3.2 Proposed GCW-GSM system model

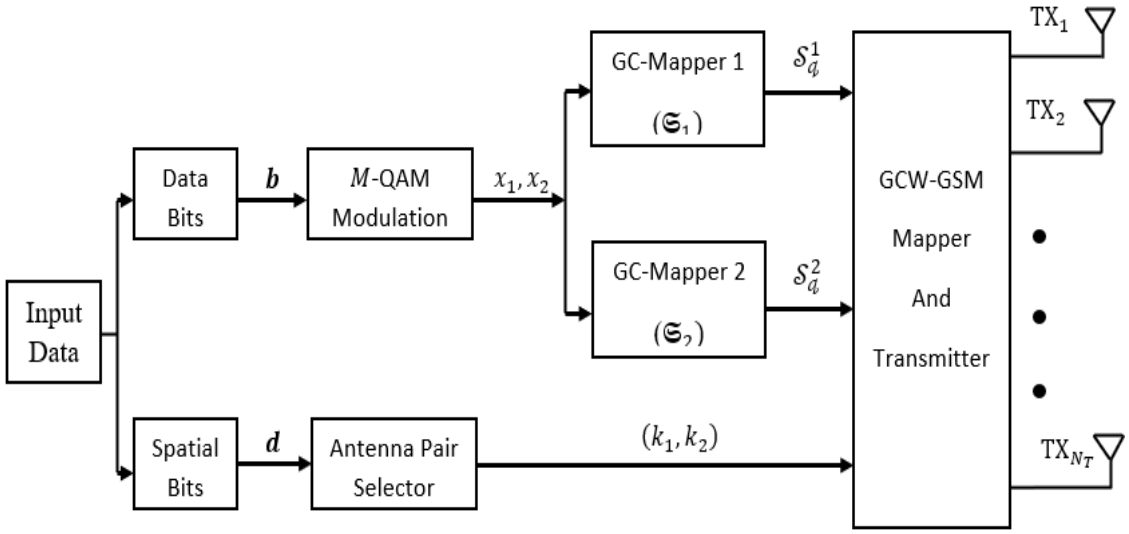

Fig. A.1: Transmission side of the proposed GCW-GSM system model.

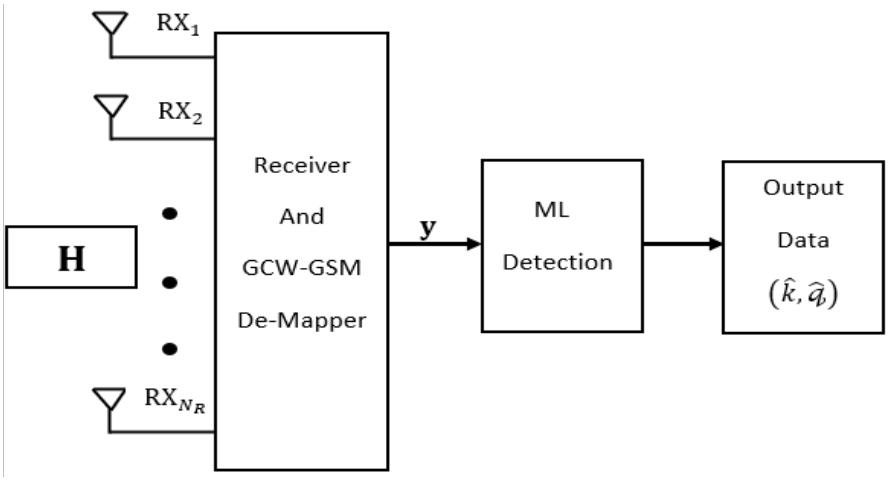

Fig. A.2: Receiver side of the proposed GCW-GSM system model.

Consider a MIMO $N_T \times N_R$ M-QAM system shown in Figs. A.1 and A.2, where N_T denotes the total number of transmit antennas, of which N_A are simultaneously active and N_R denotes the total number of receiver antennas, respectively. For this MIMO communication system, there exists $n = \binom{N_T}{N_A}$ possible transmit antenna pairs of which only $N_c = \lfloor \log_2 \binom{N_T}{N_A} \rfloor_{2^p}$ pairs are permissible for transmission, with $N_c \leq n$. Note that the choice of N_A has been discussed in [10], and the customarily chosen value for C-GSM systems and this paper is 2.

Let the input information consist of two categories, the spatial input bits (antenna pair index) and two GC super symbols bits. The first input information category is the spatial information, where

$\mathfrak{D} = \log_2 N_c$ bits are assigned to the K^{th} antenna pair of transmit antennas (k_1 and k_2). An example is where, $N_T = 4$, possible antenna pairs $\Big[(1,3);(1,4);(2,3);(2,4)\Big]$ are assigned bit indices $\Big[00;01;10;11\Big]$, respectively. A mapping table of grouped bits and antenna combinations is given in Tables A.1 and A.2 [15, 16].

Table A.1: Unique antenna mapping pairs used for $N_T = 4$ and $N_c = 4$.

Data bits	Antenna bits	Transmit-antenna pairs
$\boldsymbol{b}$	00	T_{X1}, T_{X3}
$\boldsymbol{b}$	01	T_{X1}, T_{X4}
$\boldsymbol{b}$	10	T_{X2}, T_{X3}
$\boldsymbol{b}$	00	T_{X2}, T_{X4}

Table A.2: Unique antenna mapping pairs used for $N_T = 6$ and $N_c = 8$.

Data bits	Antenna bits	Transmit-antenna pairs
$\boldsymbol{b}$	000	T_{X1}, T_{X2}
$\boldsymbol{b}$	001	T_{X1}, T_{X3}
$\boldsymbol{b}$	010	T_{X1}, T_{X4}
$\boldsymbol{b}$	011	T_{X1}, T_{X5}
$\boldsymbol{b}$	100	T_{X1}, T_{X6}
$\boldsymbol{b}$	101	T_{X2}, T_{X3}
$\boldsymbol{b}$	110	T_{X2}, T_{X4}
$\boldsymbol{b}$	111	T_{X2}, T_{X5}

The second input information category is the symbols bit-stream. A bit-stream $\boldsymbol{b} = \Big[b_1 b_2 \cdots b_{2r}\Big]$, where $r = \log_2 M$ is fed into two mappers ($\mathfrak{S}_1$) and ($\mathfrak{S}_2$). In mappers one ($\mathfrak{S}_1$) and two ($\mathfrak{S}_2$), the $2r$ input bits are mapped onto constellation points from the signal sets of the GC ($\{\frac{1}{\sqrt{5}}\alpha(x_1 + x_2\theta)\}$ and $\{\frac{1}{\sqrt{5}}\bar{\alpha}(x_1 + x_2\bar{\theta})\}$) in the Argand plane and yield two super symbols, $S_q^1 = \mathfrak{S}_1(q)$ and $S_q^2 = \mathfrak{S}_2(q)$, where $S_q^1 = \frac{1}{\sqrt{5}}\alpha(x_1 + x_2\theta)$, $S_q^2 = \frac{1}{\sqrt{5}}\bar{\alpha}(x_1 + x_2\bar{\theta})$ and $q = 1 + \sum_{k=1}^{2r} 2^{2r-k}$, $q \in [1 : M^2]$. The SE of the proposed GCW-GSM scheme is given as

$$\mathfrak{m} = 2\log_2(M) + \lfloor \log_2 \binom{N_T}{N_A} \rfloor_{2^p}. \tag{A.2}$$

The modulated GC super symbols S_q^1 and S_q^2, are transmitted by two activated transmit antennas simultaneously per time slot, in the form of an $N_T \times 1$ transmit vector $\mathbf{x}$. The vector $\mathbf{x}$ has two non-zero elements, which are the two transmitted GC symbols S_q^1 and S_q^2, respectively. Moreover, the positions of these two non-zero elements correspond to the indices of the chosen active transmit antennas, as shown in Fig. A.3.

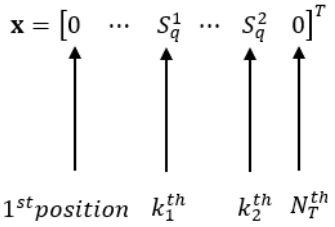

Fig. A.3: GCW-GSM transmitted vector $\mathbf{x}$.

The received signal is given by (A.3) as

$$\mathbf{y} = \sqrt{\frac{\rho}{2}}\mathbf{H}\mathbf{x} + \mathbf{n}, \tag{A.3}$$

where $\mathbf{y} \in \mathbb{C}^{N_R \times 1}$ is the received signal vector, $\mathbf{H} \in \mathbb{C}^{N_R \times N_T}$ is the channel fading matrix, and $\mathbf{n} \in \mathbb{C}^{N_R \times 1}$ is the received AWGN noise vector. $\mathbf{h}_l (1 \leq l \leq N_T)$ is the lth column of the vector channel gain matrix $\mathbf{H} = \begin{bmatrix} \mathbf{h}_1 & \mathbf{h}_2 & \mathbf{h}_3 & ... & \mathbf{h}_{N_T} \end{bmatrix}$ and $\mathbf{h}_l = \begin{bmatrix} h_{1l} & h_{2l} & h_{3l} & ... & h_{N_R l} \end{bmatrix}^T$. The elements of both $\mathbf{n}$ and $\mathbf{H}$ are assumed to be i.i.d Gaussian random variables (GRVs) with distribution $CN(0, 1)$, respectively. ρ is the average signal-to-noise ratio (SNR).

3.3 GCW-GSM MLD

At the receiver, the antenna pair index and the data symbols are jointly decoded using the MLD principle [17], as follows,

$$\begin{aligned} \left[\hat{K}, \hat{q}\right] &= \underset{\substack{q \in 1:M^2 \\ K \in 1:N_c}}{\operatorname{argmin}} \left\{ \left\| \mathbf{y} - \sqrt{\frac{\rho}{2}}\mathbf{H}\hat{\mathbf{x}} \right\|_F^2 \right\}, \\ &= \underset{\substack{q \in 1:M^2 \\ K \in 1:N_c}}{\operatorname{argmin}} \left\{ \|\mathfrak{g}\|_F^2 - 2Re\left\{ \mathbf{y}^H \mathfrak{g} \right\} \right\}, \end{aligned} \tag{A.4}$$

where $(\hat{K})$ is the estimated transmit antenna pair index, $\hat{q}$ is the index of the estimated transmitted

GC super symbols, $\mathfrak{g} = \sqrt{\frac{\rho}{2}}\left(\mathbf{h}_{k_1} S_{\hat{q}}^{1} + \mathbf{h}_{k_2} S_{\hat{q}}^{2}\right)$ and $\hat{\mathbf{x}}$ is the estimated received vector shown in Fig. A.4, respectively.

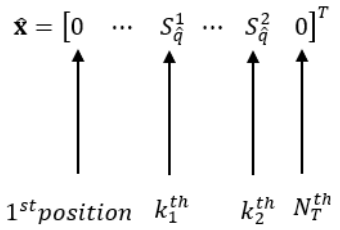

Fig. A.4: GCW-GSM estimated received signal vector $\hat{\mathbf{x}}$.

4 MLD CC analysis of the proposed GCW-GSM scheme

C-SM, C-GSM, (C-GSM spatial multiplexing two different symbols from two different transmit antennas) MIMO-GSM, conventional-quadrature spatial modulation (C-QSM), generalised quadrature spatial modulation using antenna grouping (GQSM-AG) and generalised spatial modulation with constellation reassignment (GSM-CR) MLD CCs have been studied before in [9], [18] and [19]. GCW-GSM is like C-GSM with the major difference being that in GCW-GSM there is twice the search space in the MLD as compared to C-GSM because of the GC-symbols used. Hence, the MLD CC of GCW-GSM is similar to that of C-GSM. Table A.3 shows the MLD CC formulae of the aforementioned systems used in this paper together with the calculated MLD CC under the same conditions ($N_T = 4$, $N_R = 4$ and $\mathfrak{m} = 10\ bits/s/Hz$). In addition, Table A.4 gives the calculated CC ratios between the proposed scheme (GCW-GSM) to the various schemes incorporated in this paper. Hence as seen from Tables A.3 and A.4, the proposed scheme has an MLD CC equal to that of C-GSM, MIMO-GSM and GSM-CR. Table A.3 shows that the proposed scheme has an acceptable MLD CC compared to the existing SM schemes. A lower-than-discussed complexity detection results in a poor error performance of the proposed scheme, hence for now, in this paper, a simple complexity detection is proposed, and it is based on reducing the detection subset as outlined by definition 1 in Appendix A of Part (II). This reduces the MLD CC as the cardinality of GC super symbols set is reduced as outlined by definition 1 in Appendix A of Part (II). In future, the author would like to propose low-complexity detection algorithms for the proposed scheme to lower the CC.

Table A.3: MLD CC analysis under similar parameter settings ($N_T = 4$, $N_R = 4$ and $\mathfrak{m} = 10$ $bits/s/Hz$).

Scheme	Complexity Formulae	Simulation parameters	CC
GCW-GSM	$N_R N_c M^2 (N_A + 2)$	$M = 16, N_c = 4, N_A = 2$	$16,384$
C-SM	$N_T M(3N_R + 1)$	$M = 256$	$13,312$
C-QSM	$2^{\mathfrak{m}}(8N_R)$	$M = 64$	$32,768$
C-GSM	$N_R M(N_A + 2)N_c$	$M = 256, N_c = 4, N_A = 2$	$16,384$
GSM-CR	$N_R M(N_A + 2)N_c$	$M = 256, N_c = 4, N_A = 2$	$16,384$
MIMO-GSM	$N_R M^{N_A}(N_A + 2)N_c$	$M = 16, N_c = 4, N_A = 2$	$16,384$
GQSM-AG	$(3 + \frac{N_T}{2})2^{\mathfrak{m}} N_R$	$M = 8$	$20,480$

Table A.4: MLD CC ratios analysis under under similar parameter settings ($N_T = 4$, $N_R = 4$ and $\mathfrak{m} = 10\, bits/s/Hz$).

Ratios ($\mathfrak{r}$)	Ratios scheme	Ratio Formulae	CC ratio
$\mathfrak{r}_1$	$\frac{GCW-GSM}{C-SM}$	$\frac{N_R N_c M^2 (N_A+2)}{N_T M(3N_R+1)}$	1.23
$\mathfrak{r}_2$	$\frac{GCW-GSM}{C-GSM}$	$\frac{N_R N_c M^2 (N_A+2)}{N_c M(N_A+2)}$	1.00
$\mathfrak{r}_3$	$\frac{GCW-GSM}{GSM-CR}$	$\frac{N_R N_c M^2 (N_A+2)}{N_c M(N_A+2)}$	1.00
$\mathfrak{r}_4$	$\frac{GCW-GSM}{MIMO-GSM}$	$\frac{N_R N_c M^2 (N_A+2)}{N_c M^{N_a}(N_A+2)}$	1.00
$\mathfrak{r}_5$	$\frac{GCW-GSM}{C-QSM}$	$\frac{N_R N_c M^2 (N_A+2)}{8N_R}$	0.50
$\mathfrak{r}_6$	$\frac{GCW-GSM}{GQSM-AG}$	$\frac{N_R N_c M^2 (N_A+2)}{N_R 2^{\mathfrak{m}}(3+\frac{N_T}{2})}$	0.80

5 Error performance analysis of the GCW-GSM scheme

The detection discussed in Section 3.3 is a joint detection. It follows the same approach as [17] and [16], where independent GC super symbols and transmit antenna pair index processes are assumed. There are two types of errors in the detection in Section 3.3. One is the error of estimating the average bit error probability (ABEP) of the transmit antenna pair index (P_a) given that the GC super symbols are perfectly detected, while the other one is the error in estimating GC super symbols (P_d) given that the transmit antenna pair index is perfectly detected. The overall ABEP is then union-bounded by

$$P_e = 1 - P_c = P_a + P_d - P_a P_d, \tag{A.5}$$

where $P_c = (1 - P_a)(1 - P_d)$ is the correct probability for both transmitted GC symbols and the

transmit antenna pair index. However, it is incorrect to assume independent estimation processes, since the optimal ML detector performs a joint detection of the GC symbols and the transmit antenna pair index. The assumption of independent estimation processes represents an ideal scenario [17]. Following in Subsections 5.2 and 5.1 is the ABEP of each estimation process considered separately.

5.1 Analytical ABEP of transmit antenna pair index estimation

The ABEP of the transmit antenna pair index (P_a) is formulated using the same approach as [17] and [16]. Unlike C-SM, GCW-GSM employs two active transmit antennas per transmission interval like C-GSM and (P_a) for C-GSM has been determined before in [10] and [16]. Hence, given that the GC super symbols are perfectly detected, the (P_a) expression is given in [16] and then modified accordingly to suit a larger search space. (P_a) is then given in (A.6) as

$$P_a \leq \sum_{K=1}^{2N_c} \sum_{q=1}^{M^2} \sum_{\hat{K}=1}^{2N_c} \frac{N(K,\hat{K})\mu_\alpha^{N_R} \sum_{\omega=0}^{N_R-1} \binom{N_R-1+\omega}{\omega} \left(1-\mu_\alpha\right)^\omega}{M^2 N_c} \tag{A.6}$$

where $N(k,\hat{k})$ is the number of bits in error between the transmit antenna pair index K and the estimated transmit antenna pair index $\hat{K}$. $\mu_\alpha = \frac{1}{2}\left(1-\sqrt{\frac{\sigma_{\alpha^2}}{1+\sigma_{\alpha^2}}}\right)$ and $\sigma_{\alpha^2} = \frac{\rho}{2}|S_q^1|^2$ as described in [17] and [16].

5.2 Analytical ABEP of GC symbols estimation

In this subsection, the ABEP of GC symbols estimation (P_d), is formulated. Assuming perfect transmit antenna pair index detection and based on the equivalent system model in (A.3), the union bound is employed to formulate (P_d) [5]. (P_d) may be defined as

$$P_d(\rho) \leq \frac{1}{M^2 N_c} \sum_{q=1}^{M^2} \sum_{\hat{q}\neq q}^{M^2} \frac{N(q,\hat{q}) P(\mathbf{x}\rightarrow\hat{\mathbf{x}})}{\log_2(M^2 N_c)}, \tag{A.7}$$

where $N(q,\hat{q})$ is the number of bit errors for the associated pairwise error probability (PEP) event $P(\mathbf{x}\rightarrow\hat{\mathbf{x}})$ between the transmitted vector $\mathbf{x}$ and the received vector $\hat{\mathbf{x}}$. The conditional PEP, $P(\mathbf{x}\rightarrow\hat{\mathbf{x}})$ can be formulated as

$$P(\mathbf{x} \to \hat{\mathbf{x}}|\mathbf{H}) = P\left(\left\|\mathbf{y} - \sqrt{\frac{\rho}{2}}\mathbf{H}\mathbf{x}\right\|_F^2 > \left\|\mathbf{y} - \sqrt{\frac{\rho}{2}}\mathbf{H}\hat{\mathbf{x}}\right\|_F^2\right). \tag{A.8}$$

Then, $(A.8)$ leads to $(A.9)$, and the full derivation of $(A.9)$ is detailed in Appendix A.2 of Part (II).

$$P(\mathbf{x} \to \hat{\mathbf{x}}) = \left(\frac{1}{2n}\right)\left[\left(\frac{1}{2}\right)\left(1 + \frac{\rho\left[\sum_{l=1}^{2}(D_l)^2\right]}{8}\right)^{-N_R} + \sum_{v=1}^{n-1}\left(1 + \frac{\rho\left[\sum_{l=1}^{2}(D_l)^2\right]}{4\mu_v}\right)^{-N_R}\right], \tag{A.9}$$

where $\mu_v = 2\sin^2\left(\frac{v\pi}{2n}\right)$, $D_i = |d_i|$, with $d_1 = \left(S_q^1 - S_{\hat{q}}^1\right)$, $d_2 = \left(S_q^2 - S_{\hat{q}}^2\right)$ and finally, $n \geq 6$ is the number of summations for convergence.

5.3 Diversity analysis of the GCW-GSM scheme

It follows on the simplification of A.9 that,

$$P(\mathbf{x} \to \hat{\mathbf{x}}) = \left(\frac{1}{2n}\right)\left[\left(\frac{1}{2}\right)\left(1 + \frac{\rho D_u}{8}\right)^{-N_R} + \sum_{v=1}^{n-1}\left(1 + \frac{\rho D_u}{4\mu_v}\right)^{-N_R}\right], \tag{A.10}$$

where $D_u = \sum_{l=1}^{2}(D_l)^2$. At high SNR, $\left(\frac{\rho D_u}{8} >> 1\right)$ and $\left(\frac{\rho D_u}{4\mu_v} >> 1\right)$. Hence, $P(\mathbf{x} \to \hat{\mathbf{x}})$ can be approximated at high SNRs as

$$P(\mathbf{x} \to \hat{\mathbf{x}}) \cong \left(\frac{1}{2n}\right)\left[\left(\frac{1}{2}\right)\left(\frac{\rho D_u}{8}\right)^{-N_R} + \sum_{v=1}^{n-1}\left(\frac{\rho D_u}{4\mu_v}\right)^{-N_R}\right]. \tag{A.11}$$

Further simplification leads (A.11) into (A.12),

$$P(\mathbf{x} \to \hat{\mathbf{x}}) \cong \left(\frac{1}{2n}\right)\left[\left(\frac{1}{2}\right) + \sum_{v=1}^{n-1}\left(\frac{2}{\mu_v}\right)^{-N_R}\right]\left(\frac{D_u}{8}\right)^{-N_R}\rho^{-N_R}. \tag{A.12}$$

The overall diversity gain (G_c) attained by a MIMO-SM scheme has been defined in [20], as

$$-G_c = \lim_{SNR\to\infty}\left\{\frac{\log\left(P_b(SNR)\right)}{\log(SNR)}\right\}, \tag{A.13}$$

where P_b denotes the overall probability of error as a function of SNR. Hence given $P_b(SNR) = P(\mathbf{x} \to \hat{\mathbf{x}})$ as given in (A.12), then (A.13) becomes

$$-G_c = \lim_{\rho\to\infty}\left\{\frac{\log\left(P(\mathbf{x}\to\hat{\mathbf{x}})\right)}{\log(\rho)}\right\}. \tag{A.14}$$

Hence substituting (A.12) into (A.14), leads to (A.15).

$$-G_c = \lim_{\rho\to\infty}\left\{\frac{\log\left(\beta\rho^{-N_R}\right)}{\log(\rho)}\right\}, \tag{A.15}$$

where $\beta = \left(\frac{1}{2n}\right)\left[\left(\frac{1}{2}\right) + \sum_{v=1}^{n-1}\left(\frac{2}{\mu_v}\right)^{-N_R}\right]\left(\frac{D_u}{8}\right)^{-N_R}$.

Since $\lim_{\rho\to\infty}\left(\frac{\log(\beta)}{\log(\rho)}\right) = 0$, therefore $G_c = N_R$. Hence the diversity gain of the proposed system is N_R.

6 Simulation results

This section presents simulation results for the GCW-GSM system with different numbers of transmit antennas and comparisons with C-SM, C-GSM, C-QSM, GQSM-AG, GSM-CR and MIMO-GSM. The theoretical ABEP for the C-SM scheme was based on (9) in Naidoo *et al.* [17], that of GSM-CR was based on (A.6) in Naidoo *et al.* [15] and that of C-GSM scheme was based on (5) in Pillay *et al.* [16]. The theoretical ABEP of C-QSM was based on (3) and (4) in Oladoyinbo *et al.* [21], that of GQSM-AG was based on (10) in Castillo-Soria *et al.* [19], and that of MIMO-GSM was based on (16) in Wang *et al.* [9]. Another aim of this section is to validate the theoretical performance bound derived in (A.5). The ABER performance of the aforementioned systems was evaluated using Monte Carlo simulations over i.i.d Rayleigh frequency-flat fading channels with AWGN. The BER performance was assessed for various SEs as a function of the average SNR per receive antenna. The comparison was evaluated under the same conditions, which are; $N_R = 4$, same SE, similar MLD method and at a BER value of 1×10^{-5}.

Firstly, Fig. A.5 presents the BER performance curves of the GCW-GSM scheme over the Rayleigh frequency-flat fading channel, with $N_T = 4$ and $N_T = 6$, respectively. In Fig. A.5, the theoretical upper bounds are increasingly tight at high SNR values, thereby validating analytical frameworks. This might be because of that the transmitted symbol pair estimation error (P_d) dominates the BER performance in configurations of GCW-GSM. Different spectral efficiencies were used to prove that

even at bigger spectral efficiencies the scheme still corresponds with the analytical.

Secondly, Fig. A.6 presents the comparison of the BER performance of 4×4 16-QAM GCW-GSM with various 4×4 schemes with an SE of 10 $bits/s/Hz$. Table A.5 supports Figure A.6 to show that the proposed scheme outperformed most of the various schemes incorporated in this paper. An example is where the 4×4 16-QAM GCW-GSM scheme outperformed 4×4 256-QAM C-SM and the 4×4 256-QAM GSM-CR schemes by 6.0 dB and 2.0 dB, respectively. The other performance gains of the proposed scheme are shown in Fig. A.6 and Table A.5. The improved error performance over the C-SM scheme can be attributed to the fact that GCW-GSM achieves both coding gain and transmit diversity as compared to C-SM [16]. The enhanced error performance between GCW-GSM and GSM-CR could be due to the full rank and cubic shaping of GCW-GSM codewords that increase coding gain for the system as compared to the C-M-QAM symbols transmitted in GSM-CR [5, 15].

However, as seen in Fig. A.6, the 4×4 16-QAM GCW-GSM scheme has no performance gain over the 4×4 8-QAM GQSM-AG and 4×4 16-QAM MIMO-GSM schemes. The 4×4 8-QAM GQSM-AG exhibits a performance gain of approximately 4.0 dB over the 4×4 16-QAM GCW-GSM scheme at a BER of 1×10^{-5} and the 4×4 16-QAM MIMO-GSM scheme exhibits a performance gain of approximately 2.0 dB over the 4×4 16-QAM GCW-GSM scheme at a BER of 1×10^{-5}. The lack of performance gain of GCW-GSM scheme compared to the GQSM-AG scheme could be due to more transmit diversity in GQSM-AG. More transmit diversity in GQSM-AG because symbols are transmitted in real and imaginary parts thereby reducing ICI and fading by the channel on different components of the signal as compared to the GCW-GSM scheme, which sends symbols as they are [19]. The lack of performance gain of the GCW-GSM scheme compared to the MIMO-GSM scheme could be due to that, MIMO-GSM antennas send less information (a single M-QAM symbol per transmit antenna per time slot) as compared to GCW-GSM scheme which sends a GC super symbol which has two M-QAM symbols combined. Hence the larger the sent signals are, the more errors are as compared to the smaller symbols in the MIMO-GSM scheme.

Finally, Fig. A.7 shows a comparison of various 4×4 and 6×4 GCW-GSM systems over the Rayleigh frequency-flat fading channel environment compared to similar schemes under the Rician channel (K = 3). It is clear from Fig. A.7 that the proposed scheme has a better error performance under the Rayleigh fading channel as compared to the performance under the Rician channel. An example is seen where 4×4 16-QAM GCW-GSM under Rayleigh fading has a performance gain of

5 dB over 4×4 16-QAM GCW-GSM under Rician fading.

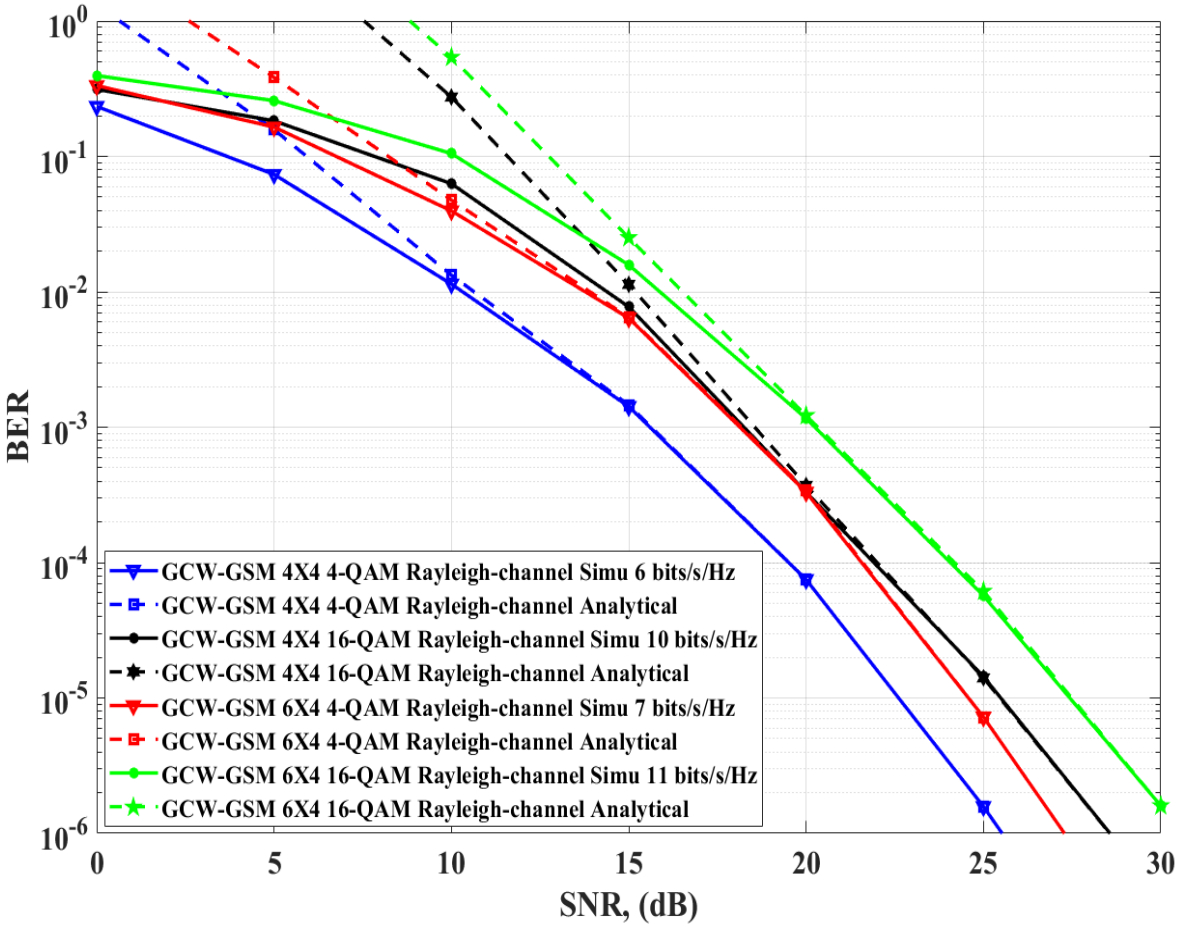

Fig. A.5: ABER results of the proposed analytical and simulated (4×4 and 6×4) (4-QAM and 16-QAM) GCW-GSM systems over Rayleigh frequency-flat fading channels.

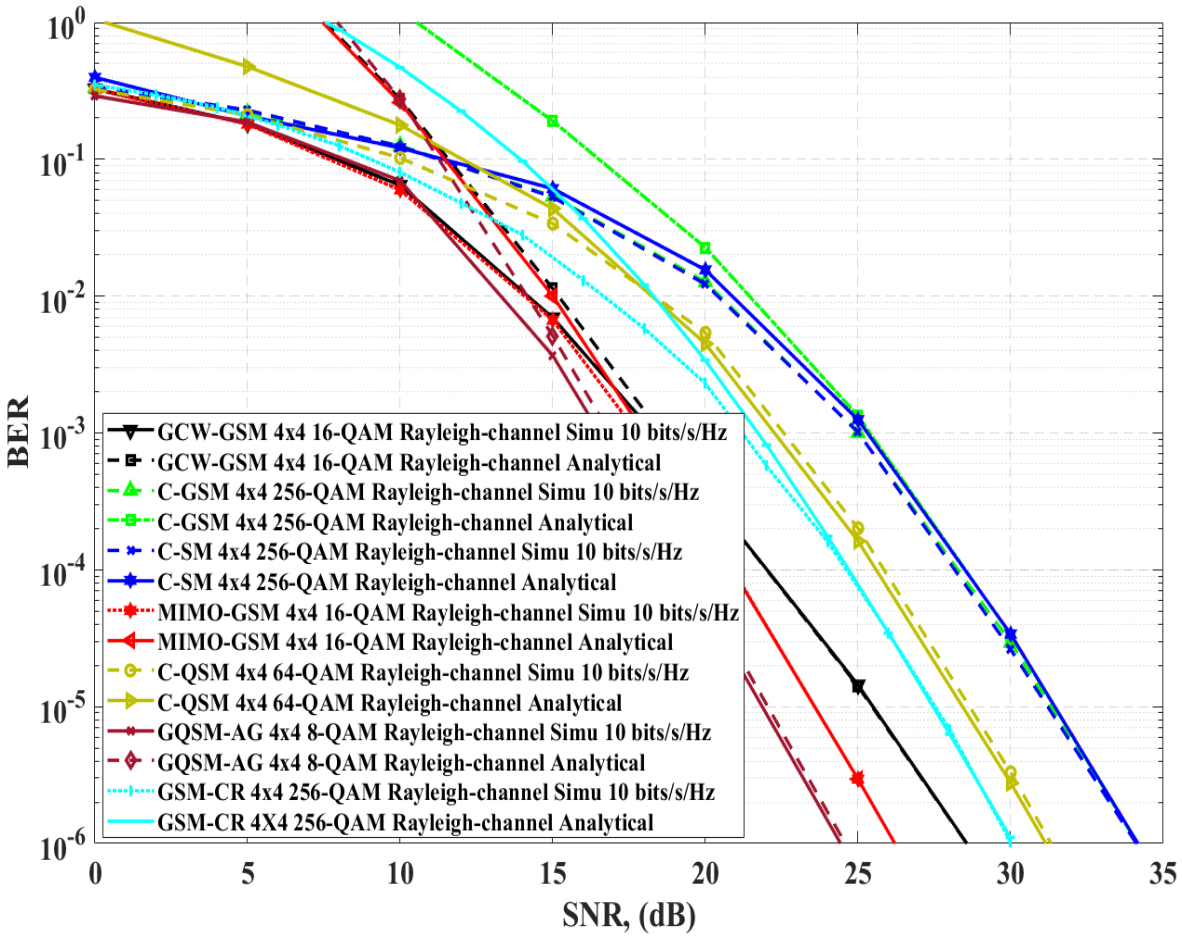

Fig. A.6: Comparison of ABER performance of various 4×4 SM systems against the proposed GCW-GSM scheme with an SE of 10 $bits/s/Hz$

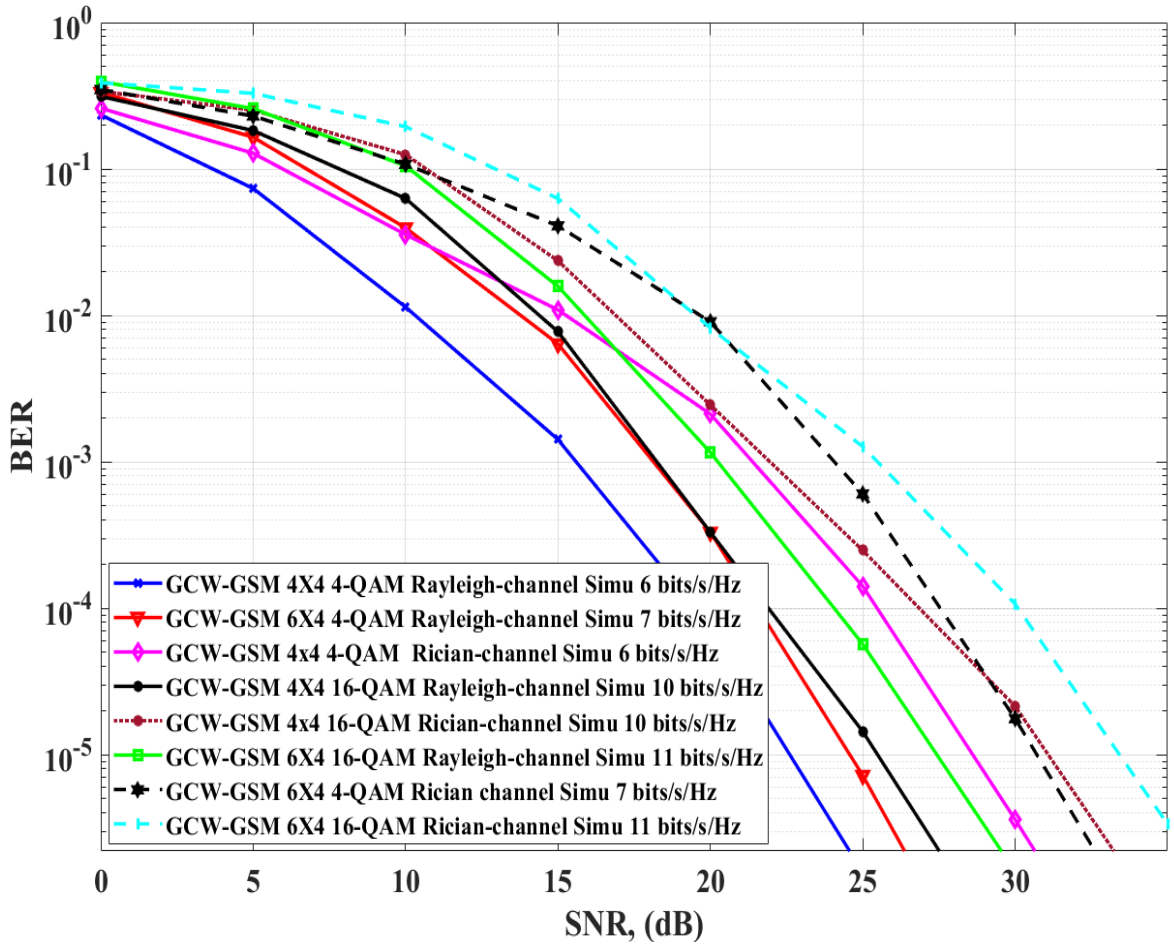

Fig. A.7: ABER comparison of the simulated (4×4 and 6×4) (4-QAM and 16-QAM) GCW-GSM systems over Rayleigh frequency-flat fading channel against the Rician channel.

Table A.5: 4×4 16-QAM GCW-GSM error performance gains over various 4×4 schemes at the same SE of $\mathfrak{m} = 10\ bits/s/Hz.$ and at BER of 10^{-5}

Scheme	Proposed scheme GCW-GSM (dB) gain
4×4 256-QAM C-SM	6.0
4×4 64-QAM C-QSM	2.9
4×4 256-QAM C-GSM	6.0
4×4 256-QAM GSM-CR	2.0
4×4 16-QAM MIMO-GSM	-2.0
4×4 8-QAM GQSM-AG	-4.0

7 Conclusion

A performance-enhanced GCW-GSM scheme was proposed and analysed. The GCW-GSM system modified the C-SM and C-GSM approach by utilising GCWs in conjunction with C-GSM. As a result, GCW-GSM achieves more diversity gain compared to C-SM and C-GSM. A closed-form analytical performance bound for GCW-GSM in i.i.d Rayleigh frequency-flat fading channels was derived, and Monte Carlo simulations were used to demonstrate the accuracy of the theoretical bound. Furthermore, the GCW-GSM SNR gains shown were significant compared to those of C-SM and C-GSM. Also, it was shown that the proposed scheme has a better error performance over the Rayleigh channel as compared to the Rician channel. However, the proposed GCW-GSM scheme has a high CC and uses many transmit antennas to further improve its error performance. Hence with this aforementioned drawback of the GCW-GSM scheme, as future work, the authors intend to propose low complexity detection methods for the GCW-GSM scheme, we also intend to fuse the GSM schemes with hexagonal quadrature modulation and optimised labelling maps to further enhance the spatial diversity of the system so as to further enhance the error performance of C-GSM schemes.

References

[1] D. J. Love and R. W. Heath, "Equal gain transmission in multiple-input multiple-output wireless systems," *IEEE Transactions on Communications*, vol. 51, no. 7, pp. 1102–1110, Jul. 2003.

[2] C. K. Agubor, F. K. Opara, and G. N. Eze, "A Review of Diversity Techniques for Wireless Communications," *Academic Research International (ARInt.)*, vol. 4, no. 2, pp. 157–167, Mar. 2013.

[3] J. C. Belfiore, G. Rekaya, and E. Viterbo, "Space Time Block Codes," *IEEE Transactions on information theory*, vol. 51, no. 4, pp. 1432–1436, Jul. 2005.

[4] K. Govindasamy, H. Xu, and N. Pillay, "Uncoded space-time labeling diversity," *IEEE Communications Letters*, vol. 20, no. 8, pp. 1511–1514, Jun. 2016.

[5] H. XU and N. Pillay, "Golden codeword-based modulation schemes for single-input multiple-output systems," *International Journal of communication Systems*, vol. 32, no. 10, p. e3963, Jul. 2019.

[6] M. Liu, M. Helard, J. F. Helard, and M. Crussiere, "A fast decodable full-rate STBC with high coding gain for 4$\times$ 2 MIMO systems," in *2013 IEEE 24th Annual International Symposium on Personal, Indoor, and Mobile Radio Communications (PIMRC)*. IEEE, Sep. 2013, pp. 677–681.

[7] R. Y. Mesleh, H. Haas, S. Sinanovic, C. W. Ahn, and S. Yun, "Spatial modulation," *IEEE Transactions on vehicular technology*, vol. 57, no. 4, pp. 2228–2241, Jul. 2008.

[8] J. Jeganathan, A. Ghrayeb, and L. Szczecinski, "Spatial modulation: Optimal detection and performance analysis," *IEEE Communications Letters*, vol. 12, no. 8, pp. 545–547, Aug. 2008.

[9] J. Wang, S. Jia, and J. Song, "Generalised spatial modulation system with multiple active transmit antennas and low complexity detection scheme," *IEEE Transactions on Wireless Communications*, vol. 11, no. 4, pp. 1605–1615, Mar. 2012.

[10] A. Younis, N. Serafimovski, R. Mesleh, and H. Haas, "Generalised spatial modulation," in *2010 Conference Record of the Forty Fourth Asilomar Conference on Signals, Systems and Computers*. IEEE, Nov. 2010, pp. 1498–1502.

[11] H. S. Hussein, H. Esmaiel, and D. Jiang, "Fully generalised spatial modulation technique for underwater communication," *Electronics Letters*, vol. 54, no. 14, pp. 907–909, Jul. 2018.

[12] S. Afridi and S. A. Hassan, "Spectrally efficient adaptive generalized spatial modulation MIMO systems," in *2017 14th IEEE Annual Consumer Communications & Networking Conference (CCNC)*. IEEE, Jan. 2017, pp. 260–263.

[13] F. Oggier, "On the Optimality of the golden code," in *2006 IEEE Information Theory Workshop - ITW '06 Chengdu*. IEEE, Oct. 2006, pp. 468–472.

[14] N. Pillay and H. Xu, "RF mirror media-based modulation for Golden codes," *Journal of Telecommunication, Electronic and Computer Engineering (JTEC)*, vol. 10, no. 3, pp. 21–24, Aug. 2018.

[15] N. R. Naidoo, "Enhanced performance and efficiency schemes for generalised spatial modulation," Ph.D. dissertation, University of KwaZulu-Natal, 2017.

[16] R. Pillay, N. Pillay, and H. Xu, "Improved error performance for generalised spatial modulation with enhanced spectral efficiency," *International Journal of Communication Systems*, vol. 33, no. 2, p. e4176, Jan. 2020.

[17] N. R. Naidoo, H. Xu, and T. A. Quazi, "Spatial modulation: optimal detector asymptotic performance and multiple-stage detection," *IET communications*, vol. 5, no. 10, pp. 1368–1376, Jul. 2011.

[18] R. Y. Mesleh, S. S. Ikki, and H. M. Aggoune, "Quadrature spatial modulation," *IEEE Transactions on Vehicular Technology*, vol. 64, no. 6, pp. 2738–2742, Jul. 2014.

[19] F. Castillo-Soria, J. Cortez-González, R. Ramirez-Gutierrez, M. M.-B. Fermín, and L. Soriano-Equigua, "Generalized quadrature spatial modulation scheme using antenna grouping," *ETRI Journal*, vol. 39, no. 5, pp. 707–717, Oct. 2017.

[20] L. Zheng and D. Tse, "Diversity and multiplexing: A fundamental tradeoff in multiple-antenna channels," *IEEE Transactions on information theory,*, vol. 49, no. 5, pp. 1073–1096, May. 2003.

[21] S. Oladoyinbo, N. Pillay, and H. Xu, "Adaptive quadrature spatial modulation," *IETE Technical Review*, vol. 37, no. 6, pp. 579–590, Nov. 2020.

[22] A. Koc, I. Altunbas, and E. Basar, "Full-duplex spatial modulation systems under imperfect channel state information," in *2017 24th International Conference on Telecommunications (ICT)*. IEEE, May. 2017, pp. 1–5.

[23] M. K. Simon and M. S. Alouini, *Digital communication over generalized fading channels: a unified approach to performance analysis*. New York: Wiley-Interscience Publication, 2000.

[24] H. Xu, "Symbol Error probability for Generalised Selection Combining reception of M-QAM," *SAIEE Africa Research Journal*, vol. 100, no. 3, pp. 68–71, Sep. 2009.

A Appendix A

A.1 Definition 1

Given a pair of qth symbols $\mathbf{X}_q = (S_q^1, S_q^2)$ in GCW-GSM M-QAM and $D_u > 0$, a signal detection subset of $\mathbf{X}_q$ is defined as $\mathfrak{S}_3(\mathbf{X}_q, D_u) = \left\{ (S_j^1, S_j^2), \prod_{i=1}^{2} |S_j^i - S_q^i|^2 \leq D_u,\, j \in [1 : M^2] \right\}$, and correspondingly, the index subset of the signal detection subset is defined as $Q(\mathbf{X}_{\hat{q}}, D_u)$ [5].

Let M_S be the cardinality of $\mathfrak{S}_3(\mathbf{X}_q, D_u)$. Hence, as an example, if we set $D_u = 12.8$ then M_S is 24 and 42 for 16-QAM and 64-QAM, respectively. The *CC* of (A.4) can be greatly reduced when this new subset is used to replace the whole super-symbol set.

A.2 Derivation of the PEP event between the transmitted vector and the estimated received vector

Based on the equivalent system model in (A.3), the conditional PEP, $P(\mathbf{x} \to \hat{\mathbf{x}})$ can be formulated as

$$P(\mathbf{x} \to \hat{\mathbf{x}}|\mathbf{H}) = P\left(\left\| \mathbf{y} - \sqrt{\frac{\rho}{2}}\mathbf{H}\mathbf{x} \right\|_F^2 > \left\| \mathbf{y} - \sqrt{\frac{\rho}{2}}\mathbf{H}\hat{\mathbf{x}} \right\|_F^2 \right). \tag{A.16}$$

Substituting (A.3) into (A.16) leads to

$$P(\mathbf{x} \to \hat{\mathbf{x}}|\mathbf{H}) = P\left(B > C\right), \tag{A.17}$$

where $B = \left\| \sqrt{\frac{\rho}{2}} \left(\mathbf{h}_{k_1} \left(S_q^1 - S_q^1 \right) + \mathbf{h}_{k_2} \left(S_q^2 - S_q^2 \right) \right) + \mathbf{n} \right\|_F^2$,
$C = \left\| \sqrt{\frac{\rho}{2}} \left(\mathbf{h}_{k_1} \left(S_q^1 - S_{\hat{q}}^1 \right) + \mathbf{h}_{k_2} \left(S_q^2 - S_{\hat{q}}^2 \right) \right) + \mathbf{n} \right\|_F^2$, $\mathbf{h}_{k_1}$ and $\mathbf{h}_{k_2}$ represent column vectors of channel gain matrix $\mathbf{H}$. k_1 and k_2 correspond to the possible active transmit antenna pair positions. Hence, (A.17) simplifies to (A.18).

$$P(\mathbf{x} \to \hat{\mathbf{x}}|\mathbf{H}) = P\left(\|\mathbf{n}\|_F^2 > \left\| \sqrt{\frac{\rho}{2}} \left(\sum_{l=1}^{2} \mathbf{h}_{k_l} d_l \right) + \mathbf{n} \right\|_F^2 \right), \tag{A.18}$$

where $d_1 = \left(S_q^1 - S_q^1 \right)$ and $d_2 = \left(S_q^2 - S_q^2 \right)$. However, we have

$$D = E + G + P, \tag{A.19}$$

where $D = \left\| \sqrt{\frac{\rho}{2}} \left(\sum_{l=1}^{2} \mathbf{h}_{k_l} d_l \right) + \mathbf{n} \right\|_F^2$, $E = \left\| \sqrt{\frac{\rho}{2}} \left(\sum_{l=1}^{2} \mathbf{h}_{k_l} d_l \right) \right\|_F^2$, $G = \|\mathbf{n}\|_F^2$, and $P = 2\Re\left\{ \sqrt{\frac{\rho}{2}} \mathbf{n}^H \left(\sum_{l=1}^{2} \mathbf{h}_{k_l} d_l \right) \right\}$.

Further simplification by substituting (A.19) in (A.18) leads to

$$\begin{aligned} P(\mathbf{x} \to \hat{\mathbf{x}}|\mathbf{H}) &= P\left(G > E + G + P\right) \\ &= P\left(0 > E + P\right) \\ &= P\left(\Re\left\{ \sqrt{\frac{\rho}{2}} \mathbf{n}^H \left(\sum_{l=1}^{2} \mathbf{h}_{k_l} d_l \right) \right\} > \frac{\rho}{4} \left\| \left(\sum_{l=1}^{2} \mathbf{h}_{k_l} d_l \right) \right\|_F^2 \right). \end{aligned} \tag{A.20}$$

Since $\mathbf{n}^H \in \mathbb{C}^{1 \times N_R}$ and each entry of $\mathbf{n}^H = \begin{bmatrix} n_1^* & n_2^* & n_3^* & \dots & n_{N_R}^* \end{bmatrix}$ is Gaussian distributed, it implies that each entry of $\Re\left\{ \sqrt{\frac{\rho}{2}} \mathbf{n}^H \mathbf{h}_{k_z} d_z \right\}$, $z \in [1 : 2]$ is also a GRV with distribution $N\left(0, \frac{\rho}{2} |d_z|^2 \sum_{l=1}^{N_R} \left|h_{k_z}^l\right|^2\right)$. This also implies that our decision variable is also Gaussian distributed as $\Re\left\{ \sqrt{\frac{\rho}{2}} \mathbf{n}^H \left(\sum_{l=1}^{2} \mathbf{h}_{k_l} d_l \right) \right\} \sim N\left(0, \frac{\rho}{4} \left\| \left(\sum_{l=1}^{2} \mathbf{h}_{k_l} d_l \right) \right\|_F^2 \right)$ and it leads to

$$P(\mathbf{x} \to \hat{\mathbf{x}}|\mathbf{H}) = Q\left(\frac{\omega_g}{\sqrt{\omega_g}} \right) = Q\left(\sqrt{\omega_g} \right), \tag{A.21}$$

where $\omega_g = \frac{\rho}{4} \left\| \left(\sum_{l=1}^{2} \mathbf{h}_{k_l} d_l \right) \right\|_F^2 = \frac{\rho}{4} \|\mathbf{H}_k \mathbf{G}_k\|_F^2 = \frac{\rho}{4} \|\mathbf{H}_k\|_F^2 \|\mathbf{G}_k\|_F^2$, with $\mathbf{H}_k = \begin{bmatrix} \mathbf{h}_{k_1} & \mathbf{h}_{k_2} \end{bmatrix}$ and $\mathbf{G}_k = \begin{bmatrix} d_1 & d_2 \end{bmatrix}^T$. Similarly, based on (11) in Koc *et al.* [22], ω_g are chi-squared random variables with $2N_R$ degrees of freedom defined as $\omega_g = \sum_{t=1}^{2N_R} \alpha_{\omega_g,t}^2$ with $\alpha_{\omega_g,t}^2 \sim N(0, \sigma_{\omega_g}^2)$ and $\sigma_{\omega_g}^2 = \frac{\rho}{4}\left(\sum_{l=1}^{2} (D_l)^2 \right)$. $D_i = |d_i|, i \in [1 : 2]$.

The conditional PEP can then be expressed as

$$P(\mathbf{x} \to \hat{\mathbf{x}}) = \int_0^\infty Q\left(\sqrt{\omega_g} \right) f_{\omega_g}\left(\omega_g \right) d\omega_g, \tag{A.22}$$

where the probability density function of ω_g is given in [23] as

$$f_{\omega_g}(\omega_g) = \frac{1}{\left(2\sigma^2_{\omega_g}\right)^{N_R}(N_R-1)!}\omega_g^{N_R-1}\exp(-\frac{\omega_g}{2\sigma^2_{\omega_g}}). \tag{A.23}$$

The trapezoidal transformation of the Q-function in [24], is given as

$$Q(z) \cong \frac{1}{2n}\left(\frac{1}{2}\exp(-\frac{z^2}{2}) + \sum_{i=1}^{n-1} S_v\right), \tag{A.24}$$

where $n \geq 6$ is the number of summations for convergence and $S_v = \exp(-\frac{z^2}{2\sin^2\left(\frac{v\pi}{2n}\right)})$.

Using the trapezoidal transformation (A.24) on (A.21) and then substituting into (A.22) yields

$$P(\mathbf{x} \to \hat{\mathbf{x}}) = \left(\frac{1}{2n}\right)\left[\left(\frac{1}{2}\right)\left(1 + \frac{\rho\left(\sum_{l=1}^{2}(D_l)^2\right)}{8}\right)^{-N_R} + \sum_{v=1}^{n-1}\left(1 + \frac{\rho\left(\sum_{l=1}^{2}(D_l)^2\right)}{4\mu_v}\right)^{-N_R}\right], \tag{A.25}$$

where $\mu_v = 2\sin^2\left(\frac{v\pi}{2n}\right)$.

Part III

Paper B

Paper B

Error Performance Analysis of Generalised Quadrature Spatial Modulation using H-8QAM

1 Abstract

Motivated to enhance the error performance of generalised complex quadrature spatial modulation (GCQSM) systems, this study proposes a scheme that builds on GCQSM and uses hexagonal quadrature amplitude modulation (H-QAM) constellations which have the advantages of a maximised Euclidean distance with relatively low peak-to-average power ratio, compared to conventional-QAM (C-QAM) systems. This, in turn, leads to an enhancement of the error performance of GCQSM schemes. The proposed scheme utilises a rotated hexagonal 8QAM (H-8QAM) set. Thus, the proposed scheme is herein named; Generalised QSM using H-8QAM (GQSM-H-8QAM). In this study, the error performance of the proposed GQSM-H-8QAM scheme is investigated over Rayleigh frequency flat-fading channels with additive white Gaussian noise. Additionally, a theoretical average bit error probability (ABEP) expression of the GQSM-H-8QAM scheme is formulated and validated using Monte Carlo simulations. Compared to simulation results, the ABEP is increasingly tight at high signal-to-noise ratio values. Obtained simulation results also show an improvement in the error performance of the GQSM-H-8QAM scheme over various SM schemes like GCQSM, conventional-quadrature spatial modulation (C-QSM) and conventional-generalised spatial modulation (C-GSM), at the same spectral efficiency (SE). An improvement in the error performance of $0.61\ dB$ with an SE of $8\ bits/s/Hz$ is seen in 4×4 GQSM-H-8QAM over 4×4 GCQSM using C-8QAM, $2.58\ dB$ over 4×4 C-QSM-C-64QAM and a gain of $4.85\ dB$ over 4×4 C-GSM-C-64QAM.

***Index Terms*—-Error performance; generalised quadrature spatial modulation; hexagonal-quadrature amplitude modulation; multiple-input multiple-output.**

2 Introduction

Nowadays, the world has been forced to adapt to COVID-19 living conditions. Thus, there has been a high demand and compulsory need for the human race to work at home/indoors with no/minimum physical interaction. This has resulted in a high dependence on the Internet and wireless communications networks. Hence, a need for wireless communications with reliable link margins and high data rates. Multiple-input multiple-output (MIMO) systems have been shown to improve/enhance spectral efficiency (SE) and /or improve the link reliability of wireless networks against multi-path fading [1]. The idea behind MIMO systems is to improve the error performance of wireless communication networks using spatial diversity and/or enhancing SE using spatial multiplexing [1].

Conventional spatial modulation (C-SM) is one of many MIMO techniques that can improve the SE by the utilisation of both the spatial constellation (transmit antenna indices) and the signal constellation [2]. In C-SM, information bits are categorised into two; the bits for transmitting antenna indices and the symbols bits [2]. Only a single transmit antenna per channel use is needed in C-SM. Hence, compared to other transmission schemes like Alamouti space-time block codes and vertical Bell layered space-time scheme (V-BLAST), C-SM was found to have a better error performance because it precludes inter-channel interference (ICI) and inter-antenna synchronisation (IAS) [3]. Also, C-SM was found to be more bandwidth efficient when compared to conventional modulation with a single transmit antenna [4]. This is because its specified transmit antenna per time slot also conveys additional information [4]. However, the number of physical antennas that can be employed at the transmission side limits the SE of C-SM schemes, and thus, conventional generalised spatial modulation (C-GSM) was proposed to alleviate this disadvantage [5].

C-GSM overcomes the C-SM disadvantage by curbing the restriction of transmit antennas being a power of two in C-SM schemes [5]. Thus, in C-GSM, the input data stream bits are mapped into two categories, the symbol signal bits and the spatial constellation bits (antenna pairs combination bits). In C-GSM, a unique combination/grouping of active transmit antennas per time slot is represented by an index. This unique combination/grouping relies on the input random data stream [5]. Thus, C-GSM differs from C-SM as two or more transmit antennas are activated per channel use compared to one active transmit antenna per channel use in C-SM [5]. Hence, C-GSM enhances the overall SE by $\log_2(N_c)$; where $N_c = \left\lfloor \log_2 \binom{N_T}{N_A} \right\rfloor_{2^p}$ pairs of permissible transmit antennas for transmission,

with $\lfloor \cdot \rfloor_{2^p}$ representing the largest integer less than or equal to the argument that is a positive integer p power of 2. Whereas, $\binom{\cdot}{\cdot}$ represents the binomial coefficient of the argument. N_T is the total number of transmit antennas for the C-GSM scheme, and N_A has been discussed before in [5]. The chosen value of use for N_A in this paper, is 2.

In the past decade, an effort to improve the error performance and/or SE of SM systems, led to the derivation of conventional-quadrature spatial modulation (C-QSM) in Mesleh *et al.* [6]. C-QSM extends the spatial constellation into two dimensions (the in-phase (*I*) and quadrature (*Q*) dimensions). The *I* dimension is for transmitting the real part of a single amplitude/phase modulated symbol, and the *Q* dimension is for transmitting the imaginary part of the single amplitude/phase modulated symbol [6, 7]. The *I* components are modulated into cosine carriers and *Q* components are modulated into sine carriers, respectively. Hence with that, C-QSM eliminates ICI, thereby enhancing the error performance of SM systems [8]. Additionally, C-QSM enhances the SE ($\mathfrak{m}$) by $\log_2(N_T)$ $bits/s/Hz$ compared to the C-SM, which achieves $\mathfrak{m} = \log_2(M) + \log_2(N_T)$ $bits/s/Hz$; where M is the amplitude/phase modulation order [6]. In Li *et al.* [9], C-QSM is used where indexes of the designated receive antennas (N_R) are used to convey information. Thus, in Li *et al.* [9], an amplitude/phase modulated symbol is precoded so that only a single receive antenna is activated, thereby conveying more information to the receiver. Also, in Kim [10], C-QSM has been used in antenna selection schemes to improve the error performance and simultaneously reduce the detection complexity. However, despite the capability of improving the error performance and SE of SM wireless communication networks, C-QSM has the disadvantage of utilising many transmit antennas as compared to conventional spatial multiplexing (C-SMux) techniques, thereby governing the improvement of the error performance of SM systems [11].

2.1 Motivation

Motivated to improve the error performance and/or SE of SM systems with a minimal number of transmit antennas, a generalised complex quadrature spatial modulation (GCQSM) scheme was proposed in Mohaisen *et al.* [12]. The GCQSM scheme builds on C-QSM by adding the attributes of C-GSM to the C-QSM scheme. It improves the SE by transmitting two amplitude/phase modulated symbols drawn from two different constellation sets at each channel use, using unique combinations of generalised *I* domain antennas and *Q* domain antennas. The two symbols could be transmitted from the same antenna at one point, and thus the total modulation set at the transmitter becomes the

Minkowski sum of the original two constellation sets [12]. Therefore, compared to C-SM and C-QSM, this leads to an increase in the size of the modulation set and a decrease in the minimum distance between transmitted symbols at the transmitter of GCQSM systems, which in turn results in the degradation of the error performance of the GCQSM scheme [13]. This results in a poor error performance because the detector depends on the minimum Euclidean distance (MED) between the transmitted vector symbols [14].

To further enhance/improve the error performance of SM systems, this paper proposes to build on GCQSM by equipping it with hexagonal QAM (H-QAM) constellations which have the benefits of a maximised MED (M-MED) with relatively low peak-to-average (PA) power ratio [15]. H-QAM systems are QAM systems with a hexagonal structure and they are densely packed with a M-MED. In [15], it was found that the structure of H-QAM systems gave them an advantage of outperforming conventional-QAM (C-QAM) systems by approximately $0.6\ dB$. SM and QSM systems with H-QAM were introduced by Cogen *et al.* in [16] and in [17]. H-QAM was found to be more energy efficient than square QAM, rectangular QAM and cross-QAM. Hence, its use was found for many applications including multi-carrier systems, MIMO systems, SM, QSM and advanced channel coding [15] and [17]. Cogen *et al.* [17], also solved the error floor degradation of the error performance of QSM systems by rotating the H-QAM symbols. Also, in [12], Mohaisen *et al.*, investigated the rotation of symbols in GCQSM systems which also led to an improvement in the error performance of GCQSM systems. In Naidoo *et al.* [14], and Singya *et al.* [15], the error performance of SM systems was also found to depend on the M-MED between two neighbouring constellation points and the average symbol energy. Hence, this paper proposes to use H-QAM systems as they have been proven to have an M-MED and relatively low PA which improves the error performance of SM schemes, as compared to C-QAM systems.

Thus, to improve the error performance of SM systems, this study proposes a GQSM scheme that builds on GCQSM [13], by combining it with rotated H-QAM systems like Cogen *et al.* [17]. The proposed scheme adopts rotated H-8QAM and utilises generalised combinations of the I and Q domain antennas. This is because H-8QAM has an M-MED between neighbouring symbols and a relatively low PA as compared to C-8QAM [18]. Also, the proposed scheme uses generalised antenna combinations because they help enhance and/or improve error performance and SE [5]. Thus, the benefits of GCQSM and rotated H-QAM systems lead to improved error performance. The H-8QAM concept could be extended to other various H-QAM constellations like H-32QAM and

others, however as discussed in [18], this results in a poor error performance as the size of the hexagonal lattice structure increases. Hence the proposed scheme utilises only H-8QAM as it is the optimum H-8QAM compared to others of the same family [18]. A constellation comparison diagram between rotated H-8QAM and C-8QAM is included in Appendix A.1 of Part (III). The creation of H-8QAM symbols was discussed in [18]. It was also well covered including the solution of the error floor in the error performance of QSM systems by Cogen *et al.* [17]. This paper adopts the same way of creation and rotation of H-8QAM symbols as in [17].

In summary, in this paper, a GQSM scheme that improves the error performance of SM systems by equipping GCQSM systems with rotated H-8QAM is proposed [17]. The proposed scheme uses the C-QSM approach of splitting two rotated H-8QAM symbols into their respective *I* and *Q* components. The split symbols are then transmitted by generalised combinations of the *I* and *Q* domain antennas like in C-QSM. This helps with eliminating ICI and thereby further enhancing the error performance of the proposed scheme, since the *I* and *Q* components of the C-QSM scheme are modulated into cosine and sine carriers [8]. Thus, the main contributions of this paper are:

1. Proposal of a new GQSM scheme called GSM with H-QAM (GQSM-H-8QAM), that improves the error performance of GCQSM systems by equipping them with rotated H-8QAM. The H-8QAM systems have a lattice structure that has an M-MED and relatively low PA compared to C-QAM. This helps improve the error performance of SM schemes.
2. Derivation of an upper bound ABER expression for the GQSM-H-8QAM scheme over independent and identically distributed (i.i.d) Rayleigh frequency-flat fading channels.
3. Validation of the derived analytical bound using Monte Carlo simulation results.

Finally, the paper is organised as follows. Introduction of the proposed GQSM-H-8QAM system is detailed in Section 3. It is presented in the form of a MIMO $N_T \times N_R$ H-8QAM system shown in Figs. B.1 and B.2. For this system, there exists $n = \binom{N_T}{N_A}$ possible transmission antenna pairs of which only N_c pairs are allowed for transmission, with $N_c \leq n$. The receiver computational complexity analysis (CCA) based on real-valued multiplications and additions of the GQSM-H-8QAM scheme is then presented in Section 4, followed by the performance analysis of the proposed scheme in Section 5. Section 6 then dwells on the results and performance comparisons. Finally, the paper is concluded in Section 7.

2.2 Notation

$(\cdot)^*$ represents the conjugate and $|\cdot|$ denotes the Euclidean norm operator. Bold lowercase letters denote column vectors and uppercase letters denote matrices, respectively. Scalar quantities are then represented by regular letters. For a set of $S \times L$ complex matrices, this paper uses $\mathbb{C}^{S\times L}$. For complex arguments, this paper uses $\Re(\cdot)$ and $j(\cdot)$ to represent the real and imaginary parts, respectively. $Q(\cdot)$ is for representing the Gaussian Q-function, $E\{\cdot\}$ is for denoting the expectation operator, $\underset{w}{\text{argmin}}\{\cdot\}$ and $\underset{w}{\text{argmax}}\{\cdot\}$ represent the minimum or maximum value of an argument with respect to w, respectively. $[\cdot]^T$ and $(\cdot)^H$ are the transpose and Hermitian operators, respectively. $\|\cdot\|_F$ denotes the Frobenius norm operator. $\lfloor\cdot\rfloor_{2^p}$ denotes the largest integer less than or equal to the argument that is a positive integer p power of 2 and finally, $\binom{\cdot}{\cdot}$ represents the binomial coefficient of the argument.

3 System model

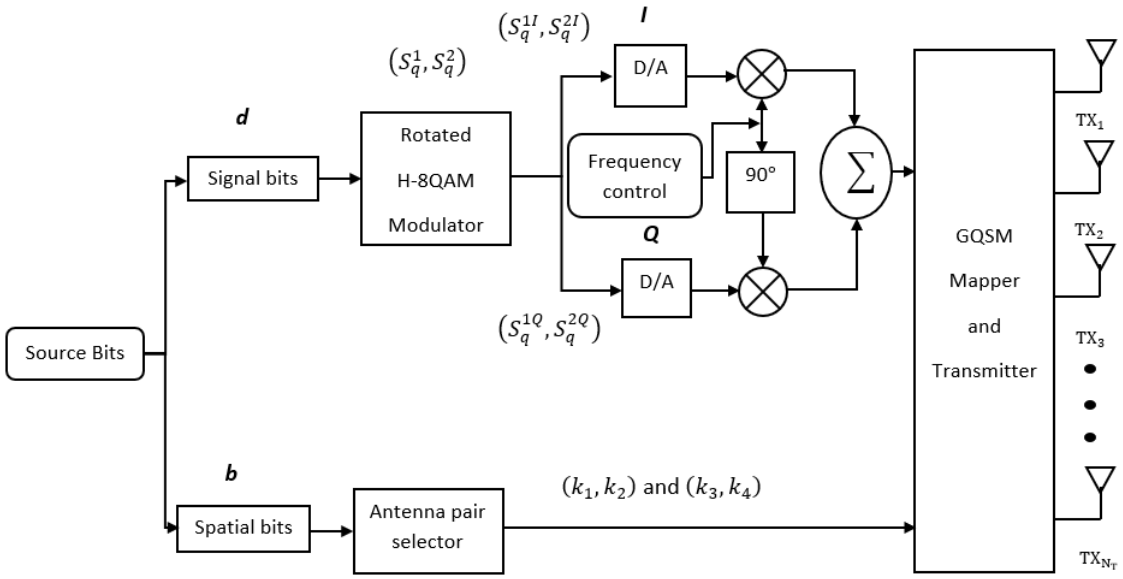

Fig. B.1: Transmission side of the proposed GQSM-H-8QAM system model.

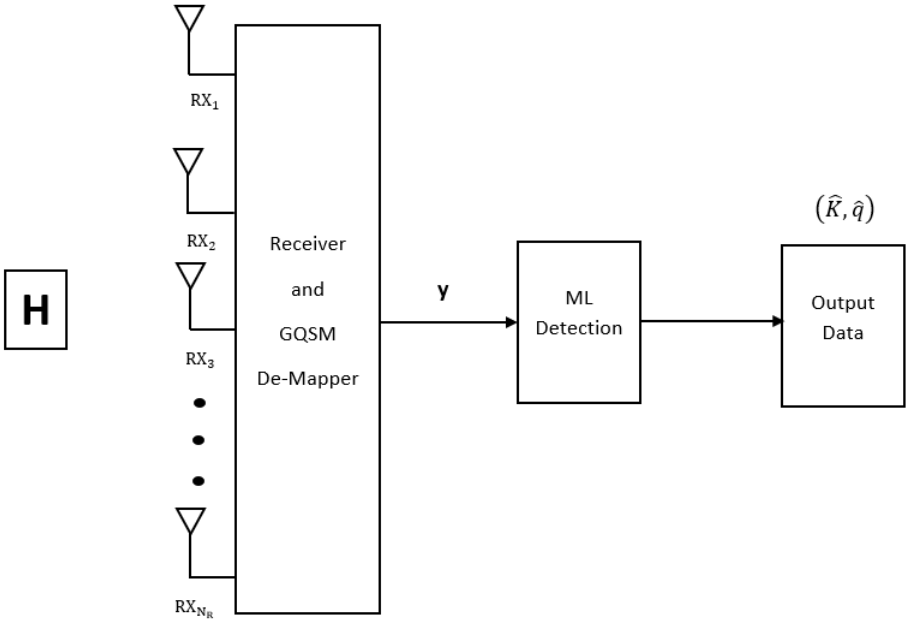

Fig. B.2: Receiver side of the proposed GQSM-H-8QAM system model.

Figs. B.1 and B.2 show the proposed GQSM-H-8QAM system model, with an input data stream that is divided into two categories, the spatial input bits (antenna pair indices) and two rotated H-8QAM symbol bits. The first input category is spatial information. Spatial input bits ($\mathfrak{D} = \log_2 N_c$) are assigned to a unique generalised K^{th} antenna pair of transmit antennas (k_1 and k_2), which are for the *I* dimension of the system. The same $\mathfrak{D}$ bits are assigned to a second but different generalised K^{th} antenna pair of transmit antennas (k_3 and k_4), which are for the *Q* dimension of the system. An example is where $N_T = 4$, two possible sets of antenna pairs $\Big[(1,3);(1,4);(2,3);(2,4)\Big]$ for the *I* dimension and $\Big[(2,4);(2,3);(1,4);(1,3)\Big]$ for the *Q* dimension are assigned the same bit indices $\Big[00;01;10;11\Big]$. A mapping table of the grouped bits (*I* dimension transmit antenna pairs and *Q* dimension transmit antenna pair combinations), is given in Tables B.1 and B.2. The antenna mapping for the *I* and *Q* dimensions are different in order to avoid ICI or the use of the same pair of antennas to simultaneously transmit a mixed signal of the real and imaginary parts. This enhances the error performance of the proposed system.

Table B.1: I and Q dimension antenna combinations and mapping ($N_T = 4$ and $N_c = 4$).

Spatial input bits	Antenna pair bit indices	I-dimension antenna pairs	Q-dimension antenna pairs	Rotation angle
$\boldsymbol{d}$	00	T_{X1}, T_{X3}	T_{X2}, T_{X4}	0
$\boldsymbol{d}$	01	T_{X1}, T_{X4}	T_{X2}, T_{X3}	$\frac{\pi}{4}$
$\boldsymbol{d}$	10	T_{X2}, T_{X3}	T_{X1}, T_{X4}	$\frac{\pi}{4}$
$\boldsymbol{d}$	00	T_{X2}, T_{X4}	T_{X1}, T_{X3}	0

Table B.2: I and Q dimension antenna combinations and mapping ($N_T = 6$ and $N_c = 8$)

Spatial input bits	Antenna pair bit indices	I-dimension antenna pairs	Q-dimension antenna pairs	Rotation angle
$\boldsymbol{d}$	000	T_{X1}, T_{X2}	T_{X5}, T_{X6}	0
$\boldsymbol{d}$	001	T_{X1}, T_{X3}	T_{X4}, T_{X6}	0
$\boldsymbol{d}$	010	T_{X1}, T_{X4}	T_{X3}, T_{X6}	0
$\boldsymbol{d}$	011	T_{X1}, T_{X5}	T_{X2}, T_{X6}	$\frac{\pi}{3}$
$\boldsymbol{d}$	100	T_{X1}, T_{X6}	T_{X4}, T_{X5}	$\frac{\pi}{3}$
$\boldsymbol{d}$	101	T_{X2}, T_{X3}	T_{X1}, T_{X4}	$\frac{\pi}{3}$
$\boldsymbol{d}$	110	T_{X2}, T_{X4}	T_{X1}, T_{X3}	$\frac{2\pi}{3}$
$\boldsymbol{d}$	111	T_{X2}, T_{X5}	T_{X3}, T_{X4}	$\frac{2\pi}{3}$

The second category of the input data stream is the symbols bit stream. A bit stream $\boldsymbol{b} = \left[b_1 b_2 ... b_{2r}\right]$, with r =$\log_2 M$ is fed into a mapper ($\mathfrak{G}_1$). In mapper ($\mathfrak{G}_1$), the $2r$ input bits are mapped onto a rotated H-8QAM signal constellation set to yield two symbols S_q^1 and S_q^2, where $q = 1 + \sum_{v=1}^{2r} 2^{2r-v} b_v$, $q \in [1 : M^2]$ and $E\{|S_q^i|^2\} = 1$, $i \in [1 : 2]$. The creation of the H-8QAM symbol constellation and its rotation is well discussed by Cogen *et al.* [17]. This paper adopts the same way of creating H-8QAM systems. Also, Cogen *et al.* [17], discusses the degrading effect of error floor on the error performance of QSM systems when using H-QAM without rotation. Thus, Cogen *et al.* [17], then devised a solution of using optimum rotation angles on H-QAM-QSM systems to curb the error floor on the error performance of H-QAM-QSM schemes. The optimum rotation angle for the chosen H-8QAM schemes in this paper is $\frac{\pi}{4}$ [17]. The mapping of the rotated H-8QAM symbols to bits is provided in Table B.3 and Fig.B.10. The SE of the proposed GQSM-H-8QAM scheme is given as

$$\mathfrak{m} = 2\log_2(M) + \lfloor \log_2 \binom{N_T}{2} \rfloor_{2^p}. \tag{B.1}$$

The modulated symbols (S_q^1 and S_q^2) are split into their respective real parts and imaginary parts ($S_q^{1I} + jS_q^{1Q}$ and $S_q^{2I} + jS_q^{2Q}$). The real parts of the symbols are transmitted via the *I* dimension using the in-phase transmit antenna pairs (k_1 and k_2). The imaginary parts of the symbols are in turn transmitted through the *Q* dimension using the quadrature antenna pairs (k_3 and k_4). Thus, the split symbols are transmitted by four transmit antennas concurrently per time slot, in the form of an $N_T \times 1$ transmit vector $\mathbf{x}$ shown in Fig. B.3. Vector $\mathbf{x}$ has four non-zero elements, which are the two real parts (S_q^{1I} and S_q^{2I}) and the two imaginary parts (S_q^{1Q} and S_q^{2Q}) of the symbols. Moreover, the positions of these four nonzero elements correspond to the indices of the four chosen active transmit antennas. θ_k is the rotation angle applied to different transmit antenna pairs as shown in Tables B.1 and B.2. This is done in order to further minimise ICI that could be generated by overlapping antenna pairs [14]. The discussion of the selection of the antenna pairs and the optimum θ_k was discussed in [14] and [19]. Hence, Tables B.1 and B.2 show the chosen transmit antenna pairs and the corresponding optimum θ_k values used in this paper according to [14, 17].

Table B.3: rotated H-8QAM symbol mapping table

Data symbol input bits	q	Rotated H-8QAM Symbol (S)
000	0	$-1+1j$
001	1	$+1+3j$
010	2	$+1-1j$
011	3	$+3+1j$
100	4	$-3+3j$
101	5	$-3-1j$
110	6	$-1-3j$
111	7	$+3-3j$

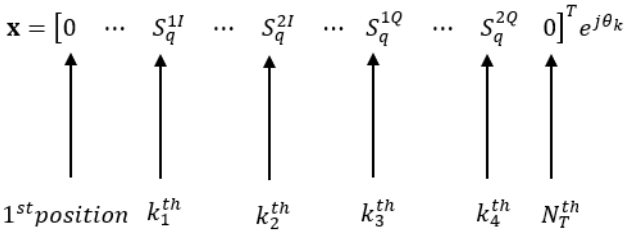

Fig. B.3: Transmitted signal vector $\mathbf{x}$, for the GQSM-H-8QAM scheme.

At the receiver, the signal is given by $\mathbf{y} \in \mathbb{C}^{N_R \times 1}$ (B.2), as

$$\begin{aligned}\mathbf{y} &= \sqrt{\frac{\rho}{4}}\mathbf{H}\mathbf{x} + \mathbf{n}, \\ &= \sqrt{\frac{\rho}{4}}\left[\left(\mathbf{h}_{k_1} S_q^{1I} + \mathbf{h}_{k_2} S_q^{2I}\right) e^{j\theta_k} + j\left(\mathbf{h}_{k_3} S_q^{1Q} + \mathbf{h}_{k_4} S_q^{2Q}\right) e^{j\theta_k}\right] + \mathbf{n},\end{aligned} \tag{B.2}$$

where the fading channel matrix is represented by $\mathbf{H} \in \mathbb{C}^{N_R \times N_T}$ and $\mathbf{n} \in \mathbb{C}^{N_R \times 1}$ is the AWGN vector. $\mathbf{h}_{k_l} (1 \leq l \leq N_T)$ is the lth column vector of the channel gain matrix $\mathbf{H} = \begin{bmatrix}\mathbf{h}_{k_1} & \mathbf{h}_{k_2} & \mathbf{h}_{k_3} & \dots & \mathbf{h}_{k_{N_T}}\end{bmatrix}$ and $\mathbf{h}_{k_l} = \begin{bmatrix}h_{1k_l} & h_{2k_l} & h_{3k_l} & \dots & h_{N_R k_l}\end{bmatrix}^T$. The elements of both $\mathbf{n}$ and $\mathbf{H}$ are assumed to be i.i.d Gaussian random variables (GRVs) with distribution $CN(0, 1)$, respectively. Finally, ρ is the average signal-to-noise ratio (SNR).

The optimum maximum likelihood detection (MLD) for the proposed scheme, can be written as in (B.3) and it entails a joint estimation of the transmission antenna pairs indices ($\hat{K}$) and the sent symbols ($S_{\hat{q}}^1$ and $S_{\hat{q}}^2$) [11] and [12], as follows,

$$\begin{aligned}\left[\hat{K}, S_{\hat{q}}^1, S_{\hat{q}}^2\right] &= \underset{\substack{q \in 1:M^2 \\ K \in 1:N_c}}{\operatorname{argmin}} \left\{ \left\| \mathbf{y} - \sqrt{\frac{\rho}{4}}\mathbf{H}\hat{\mathbf{x}} \right\|_F^2 \right\}, \\ &= \underset{\substack{q \in 1:M^2 \\ K \in 1:N_c}}{\operatorname{argmin}} \left\{ \|\mathfrak{g}\|_F^2 - 2\Re\left\{\mathbf{y}^H \mathfrak{g}\right\} \right\},\end{aligned} \tag{B.3}$$

where $\mathfrak{g} = \sqrt{\frac{\rho}{4}}\left(\left(\mathbf{h}_{k_1} S_q^{1I} + \mathbf{h}_{k_2} S_q^{2I}\right) e^{j\theta_k} + j\left(\mathbf{h}_{k_3} S_q^{1Q} + \mathbf{h}_{k_4} S_q^{2Q}\right) e^{j\theta_k} \right)$ and $\hat{\mathbf{x}}$ is the estimated received vector shown in Fig. B.4, respectively.

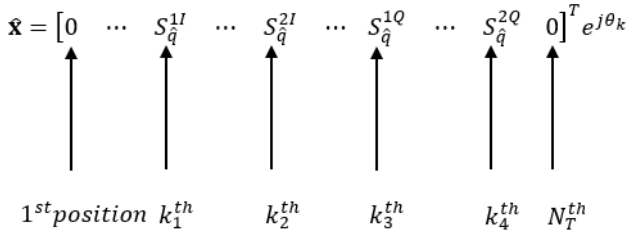

Fig. B.4: Estimated received signal vector for the GQSM-H-8QAM scheme.

4 MLD CCA of the GQSM-H-8QAM scheme - based on real valued multiplications and additions

The CCA of the GQSM-H-8QAM scheme is similar to that discussed in Holoubi *et al.* [20]. It is based on real value multiplications and additions. In [20], it is given as $(20N_R - 1)2^{\mathfrak{m}}$. In this section, all the incorporated CCAs of various schemes in this paper (including enhanced SE-GSM (ESE-GSM), GSM multiplexing two symbols (MIMO-GSM), Golden codeword based GSM (GCW-GSM) and constellation reassigned GSM (GSM-CR)), have been discussed before in Part(II), [6] and [21]. As seen in Tables B.4 and B.5, the GQSM-H-8QAM scheme has the highest CC as compared to all the schemes included in this paper. GQSM-H-8QAM has an optimal MLD at the expense of a high CC. However, it is essential to also consider that the proposed scheme uses fewer transmit antennas as compared to various MIMO-SM schemes under the same conditions. An example is shown in Tables B.9 and B.10 found in Appendix A.1 of Part (III). Table B.10 shows that the proposed scheme requires 4 transmit antennas to achieve an SE of $\mathfrak{m} = 8\ bits/s/Hz$ as compared to C-SM and C-GSM with $N_T = 32$ and 10, to achieve the same SE under the same conditions, respectively. Hence, the disadvantage of a high CC in the proposed scheme is compensated by the advantage of using a less number of transmit antennas as compared to other various MIMO-SM schemes incorporated in this paper. Due to a high CC shown by the proposed scheme, as upcoming work, the author intends to formulate low complexity detection algorithms to overcome this disadvantage.

Table B.4: MLD CCA under similar parameter settings ($N_T = 4$, $N_R = 4$ and $\mathfrak{m} = 8\ bits/s/Hz$).

Scheme	*CCA* Formulae	Simulation parameters	CC
GQSM-H-8QAM	$(20N_R - 1)2^{\mathfrak{m}}$	$M = 8$	$20,224$
GCQSM	$2^{\mathfrak{m}}(8N_R)$	$M = 8$	$8,192$
C-SM	$N_T M(3N_R + 1)$	$M = 64$	$3,328$
C-QSM	$2^{\mathfrak{m}}(8N_R)$	$M = 16$	$8,192$
C-GSM	$N_R M(N_A + 2)N_c$	$M = 64, N_c = 4, N_A = 2$	$4,096$
GSM-CR	$N_R M(N_A + 2)N_c$	$M = 64, N_c = 4, N_A = 2$	$4,096$
MIMO-GSM	$N_R M^{N_A}(N_A + 2)N_c$	$M = 8, N_c = 4, N_A = 2$	$4,096$
GCW-GSM	$N_R M^2(N_A + 2)N_c$	$M = 8, N_c = 4, N_A = 2$	$4,096$

Table B.5: MLD CCA ratios under the same parameter settings ($N_T = 4$, $N_R = 4$ and $\mathfrak{m} = 8$ $bits/s/Hz$).

Ratios ($\mathfrak{r}$)	Ratios scheme	Ratio Formulae	CC ratio
$\mathfrak{r}_1$	$\frac{GQSM-H-8QAM}{C-SM}$	$\frac{(20N_R-1)2^{\mathfrak{m}}}{N_T M(3N_R+1)}$	6.08
$\mathfrak{r}_2$	$\frac{GQSM-H-8QAM}{GCQSM}$	$\frac{(20N_R-1)2^{\mathfrak{m}}}{8N_R}$	4.94
$\mathfrak{r}_3$	$\frac{GQSM-H-8QAM}{C-GSM}$	$\frac{(20N_R-1)2^{\mathfrak{m}}}{N_c M(N_A+2)}$	4.94
$\mathfrak{r}_4$	$\frac{GQSM-H-8QAM}{GSM-CR}$	$\frac{(20N_R-1)2^{\mathfrak{m}}}{N_c M(N_A+2)}$	2.47
$\mathfrak{r}_5$	$\frac{GQSM-H-8QAM}{MIMO-GSM}$	$\frac{(20N_R-1)2^{\mathfrak{m}}}{N_c M^{N_a}(N_A+2)}$	4.94
$\mathfrak{r}_6$	$\frac{GQSM-H-8QAM}{C-QSM}$	$\frac{20N_R-1}{8N_R}$	2.47

5 Error performance analysis of GQSM-H-8QAM

In this section, the ABEP of GQSM-H-8QAM is formulated. The detection discussed in Section 3 follows the same approach as [6], [11] and [12]. Hence the ABEP of GQSM-H-8QAM is upper-bounded by

$$P_e \leq \frac{1}{2^{\mathfrak{m}}} \sum_{q=1}^{2^{\mathfrak{m}}} \sum_{\hat{q}=1}^{2^{\mathfrak{m}}} \frac{1}{\mathfrak{m}^2} N\left(q, \hat{q}\right) P(\mathbf{x} \rightarrow \hat{\mathbf{x}}), \tag{B.4}$$

where $N\left(q, \hat{q}\right)$ is the total number of bit errors for the associated pairwise error probability (PEP) event $P(\mathbf{x} \rightarrow \hat{\mathbf{x}})$ between the transmitted vector $\mathbf{x}$ and the received vector $\hat{\mathbf{x}}$. The conditional PEP $P(\mathbf{x} \rightarrow \hat{\mathbf{x}})$ is formulated as

$$P(\mathbf{x} \rightarrow \hat{\mathbf{x}}) = \left(\frac{1}{2n}\right) \left[\left(\frac{1}{2}\right) \left(1 + \frac{\rho\left(\sum_{l=1}^{4} (D_l)^2\right)}{16}\right)^{-N_R} + \sum_{v=1}^{n-1} \left(1 + \frac{\rho\left(\sum_{l=1}^{4} (D_l)^2\right)}{8\mu_v}\right)^{-N_R} \right], \tag{B.5}$$

where $\mu_v = 2\sin^2\left(\frac{v\pi}{2n}\right)$, $n \geq 6$ is the number of summations for convergence, $d_i = \left[\left(S_q^{iI} - S_{\hat{q}}^{iI}\right) e^{j\theta_k}\right]$, $d_{(i+2)} = \left[\left(S_q^{lQ} - S_{\hat{q}}^{lQ}\right) e^{j\theta_k}\right]$, $i \in [1:2]$ and $D_l = |d_l|, l \in [1:4]$. The derivation of the conditional PEP is found in Appendix A.2 of Part (III).

5.1 Diversity analysis of the GQSM-H-8QAM scheme

It follows on the simplification of (B.5) that,

$$P(\mathbf{x} \to \hat{\mathbf{x}}) = \left(\frac{1}{2n}\right)\left[\left(\frac{1}{2}\right)\left(1+\frac{\rho D_u}{16}\right)^{-N_R} + \sum_{v=1}^{n-1}\left(1+\frac{\rho D_u}{8\mu_v}\right)^{-N_R}\right], \tag{B.6}$$

where $D_u = \sum_{l=1}^{4}(D_l)^2$. At high SNRs, $\left(\frac{\rho D_u}{8} >> 1\right)$ and $\left(\frac{\rho D_u}{4\mu_v} >> 1\right)$. Hence, $P(\mathbf{x} \to \hat{\mathbf{x}})$ can be approximated at high SNRs as

$$P(\mathbf{x} \to \hat{\mathbf{x}}) \cong \left(\frac{1}{2n}\right)\left[\left(\frac{1}{2}\right)\left(\frac{\rho D_u}{16}\right)^{-N_R} + \sum_{v=1}^{n-1}\left(\frac{\rho D_u}{8\mu_v}\right)^{-N_R}\right]. \tag{B.7}$$

Further simplification leads (B.7) into (B.8),

$$P(\mathbf{x} \to \hat{\mathbf{x}}) \cong \left(\frac{1}{2n}\right)\left[\left(\frac{1}{2}\right) + \sum_{v=1}^{n-1}\left(\frac{2}{\mu_v}\right)^{-N_R}\right]\left(\frac{D_u}{16}\right)^{-N_R}\rho^{-N_R}. \tag{B.8}$$

The overall diversity gain (G_c) attained by a MIMO-SM scheme has been defined in [22], as

$$-G_c = \lim_{SNR\to\infty}\left\{\frac{\log\left(P_b(SNR)\right)}{\log(SNR)}\right\}, \tag{B.9}$$

where P_b denotes the overall probability of error as a function of SNR. Hence given $P_b(SNR) = P(\mathbf{x} \to \hat{\mathbf{x}})$ as given in (B.8), then (B.9) becomes

$$-G_c = \lim_{\rho\to\infty}\left\{\frac{\log\left(P(\mathbf{x} \to \hat{\mathbf{x}})\right)}{\log(\rho)}\right\}. \tag{B.10}$$

Hence substituting (B.8) into (B.10), leads to (B.11).

$$-G_c = \lim_{\rho\to\infty}\left\{\frac{\log\left(\beta\rho^{-N_R}\right)}{\log(\rho)}\right\}, \tag{B.11}$$

where $\beta = \left(\frac{1}{2n}\right)\left[\left(\frac{1}{2}\right) + \sum_{v=1}^{n-1}\left(\frac{2}{\mu_v}\right)^{-N_R}\right]\left(\frac{D_u}{16}\right)^{-N_R}$.

Since $\lim_{\rho\to\infty}\left(\frac{\log(\beta)}{\log(\rho)}\right) = 0$, therefore $G_c = N_R$. Hence the diversity gain of the proposed system is N_R.

6 Simulation and numerical results analysis

This section presents simulation results for the proposed GQSM-H-8QAM system with a different number of transmit antennas and comparisons with C-SM, C-GSM, C-QSM, MIMO-GSM and ESE-GSM. The theoretical ABEP for C-SM schemes was based on (9) in Naidoo *et al.* [4], that of C-GSM schemes was based on (5) in Pillay *et al.* [19], and that of ESE-GSM was based on (5) and (12) in Pillay *et al.* [19]. The theoretical ABEP of C-QSM was based on (3) and (4) in Oladoyinbo *et al.* [8], and that of MIMO-GSM was based on (16) in Wang *et al.* [21]. Another aim of this section is to validate the theoretical performance bound derived in (B.4). The ABER of the proposed scheme was evaluated using Monte Carlo simulations over i.i.d Rayleigh frequency-flat fading channels with AWGN. The BER performance was assessed for various SEs ($\mathfrak{m} = 8\ bits/s/Hz$, $\mathfrak{m} = 9\ bits/s/Hz$ and $\mathfrak{m} = 10\ bits/s/Hz$) as a function of the average SNR. These three SEs considered, are shown in Figs. B.5-B.9. The comparisons were made under the same conditions, which are; $N_R = 4$ assumed in all scenarios, identical SE, optimal MLD method, and at a BER value of 1×10^{-5} for comparison. The formulae for evaluating the SEs of all the various schemes in Figs. B.5-B.9 are found in Table B.8 of Appendix A.1 of Part (III).

Firstly, Fig. B.5 presents the BER performance curves of the GQSM-H-8QAM scheme with $N_T = 4$, 6 and 8, respectively. In Fig. B.5, the analytical results are validated by simulation results and it is seen that they are tighter as the SNR values increase. They are tight at high SNR values because of the upper-bounded ABER performance in all the configurations of the GQSM-H-8QAM scheme.

Secondly, Figs. B.6 and B.7 with Table B.6 show the simulation results and the calculated error performance gains of the proposed 4×4 GQSM-H-8QAM scheme over 4×4 various schemes of the same SE ($\mathfrak{m} = 8\ bits/s/Hz$). As seen from Figs. B.6 and B.7 together with Table B.6, the proposed scheme has an error performance gain of $0.61\ dB$ over 4×4 GCQSM-C-8QAM, $0.93\ dB$ over 4×4 GSM-CR-64QAM scheme and $0.75\ dB$ over 4×4 MIMO-GSM-C-8QAM scheme. Furthermore, Wang *et al.* [21], discussed MIMO-GSM and it was shown to outperform C-SM and C-GSM schemes of the same SE. In [14], it is also seen that GSM-CR outperforms C-SM and C-GSM schemes. Thus, the proposed scheme has performance gain over all the schemes included in this paper, as it outperformed the best of those discussed in literature [14, 21]. This might be because of the use of generalised antennas and H-8QAM with an M-MED that improved the error performance of the proposed scheme.

Thirdly, Fig. B.8 shows the proposed GQSM-H-8QAM scheme performance compared with the same schemes in Figs. B.6 and B.7 at an SE of $\mathfrak{m} = 9\ bits/s/Hz$, $N_R = 4$, but under different number of transmit antennas. Fourthly, Fig. B.9 shows the proposed GQSM-H-8QAM scheme performance compared with the same schemes in Fig. B.6 but under different SEs and different numbers of transmit antennas. In Fig. B.9, the 8×4 GQSM-H-8QAM scheme is compared with other various 8×4 schemes with an SE of $\mathfrak{m} = 10\ bits/s/Hz$. Fig. B.9 together with Table B.7 also exhibits the same behaviour as Figs. B.6 and B.7. The proposed scheme outperformed all the various schemes that were compared to it.

It is also important, to note that the proposed scheme (GQSM-H-8QAM), has another advantage of using a less number of transmit antennas under conditions of fixed N_R and fixed M at a certain SE ($\mathfrak{m}$) as compared to the other systems included in this paper. An example is shown in Tables B.9 and B.10 found in Appendix A.1 of Part (III), which show the number of N_T(s) required to achieve a certain SE at $N_R = 4$. Table B.9 shows that the GQSM-H-8QAM scheme requires 4 transmit antennas to achieve an SE of $\mathfrak{m} = 8\ bits/s/Hz$ using H-8QAM as compared to C-SM which requires $N_T = 32$, C-GSM which requires $N_T = 10$ and ESE-GSM which requires $N_T = 8$ to achieve the same SE under the same settings. This shows that the GQSM-H-8QAM scheme has the advantage of less hardware costs as it requires a less number of transmit antennas as compared to the other systems. The only exception seen in Tables B.9 and B.10, is the MIMO-GSM scheme which requires the same number of transmit antennas as the proposed scheme to achieve the same SE under identical settings as the proposed scheme. However, it is outperformed by the proposed scheme as seen from the results in Figs. B.6-B.9.

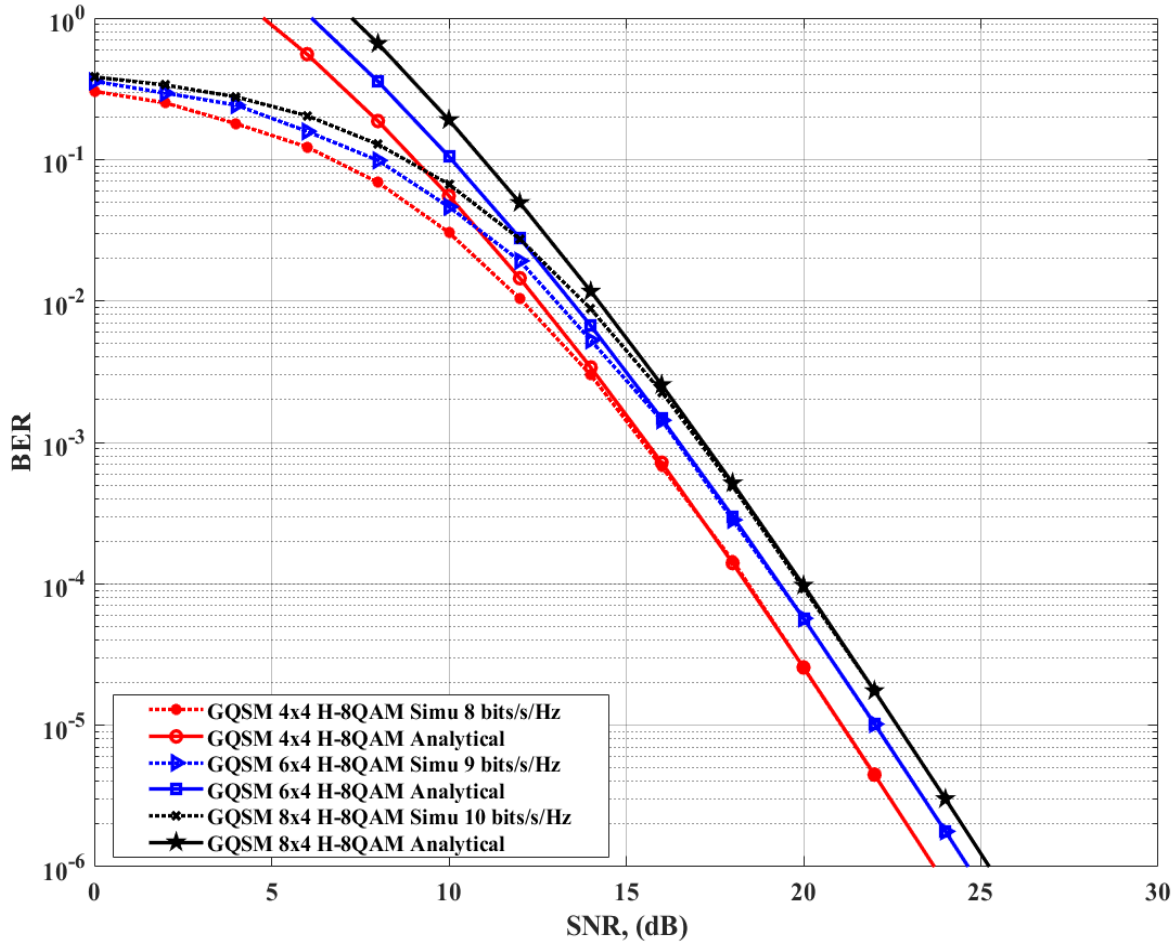

Fig. B.5: 4×4, 6×4 and 8×4 GQSM-H-8QAM analytical and simulation ABER results.

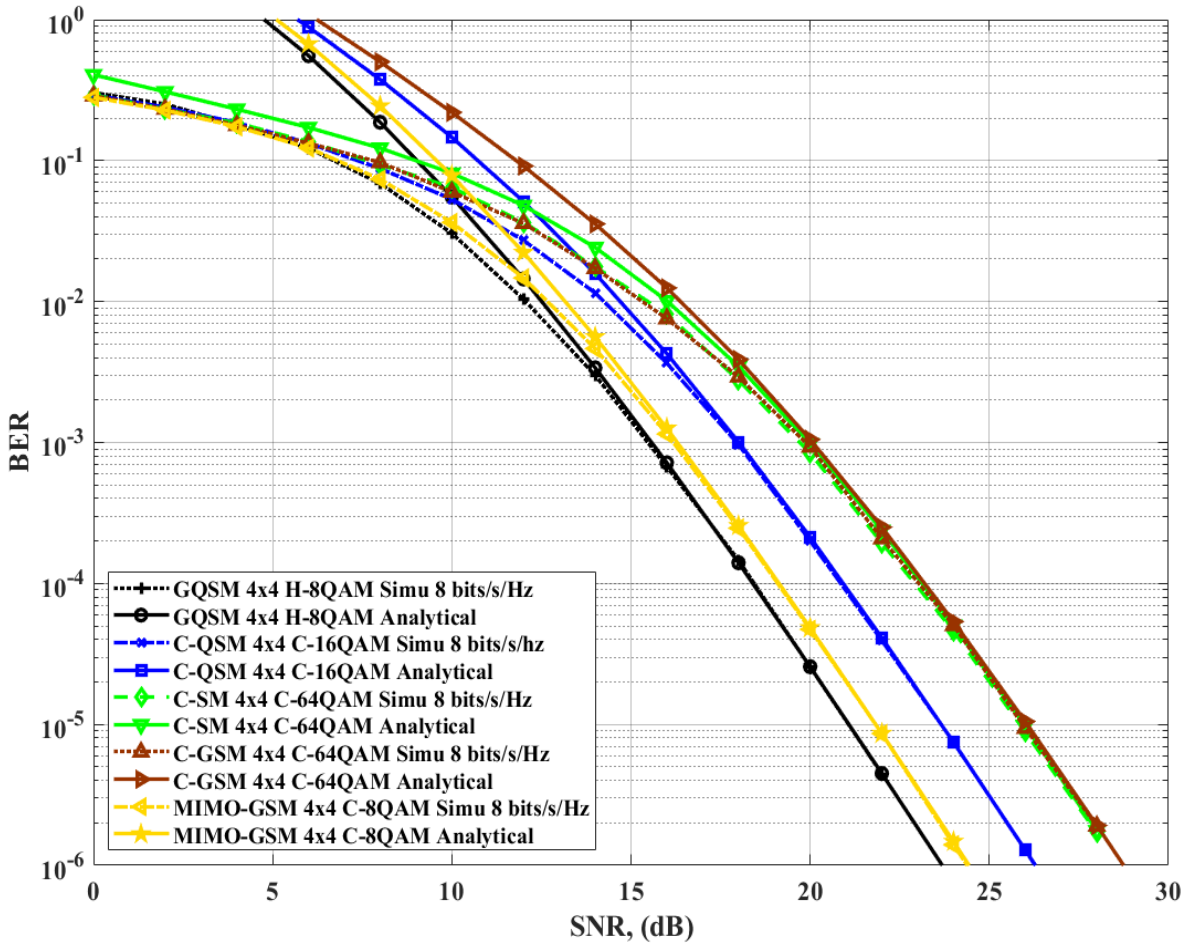

Fig. B.6: Comparison of 4×4 GQSM-H-8QAM with various schemes of the same SE, same N_T and N_R.

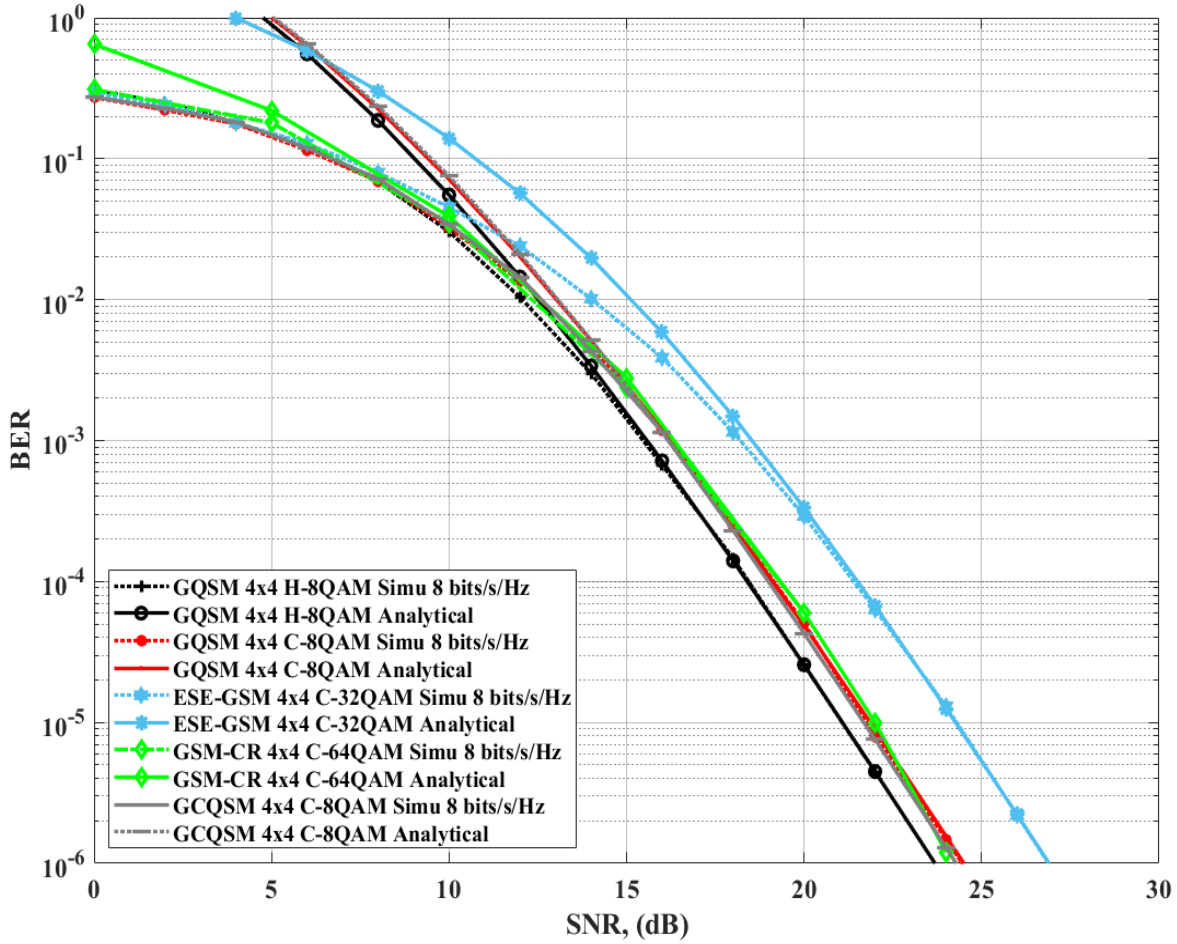

Fig. B.7: Comparison of 4×4 GQSM-H-8QAM with various schemes of the same SE, same N_T and N_R.

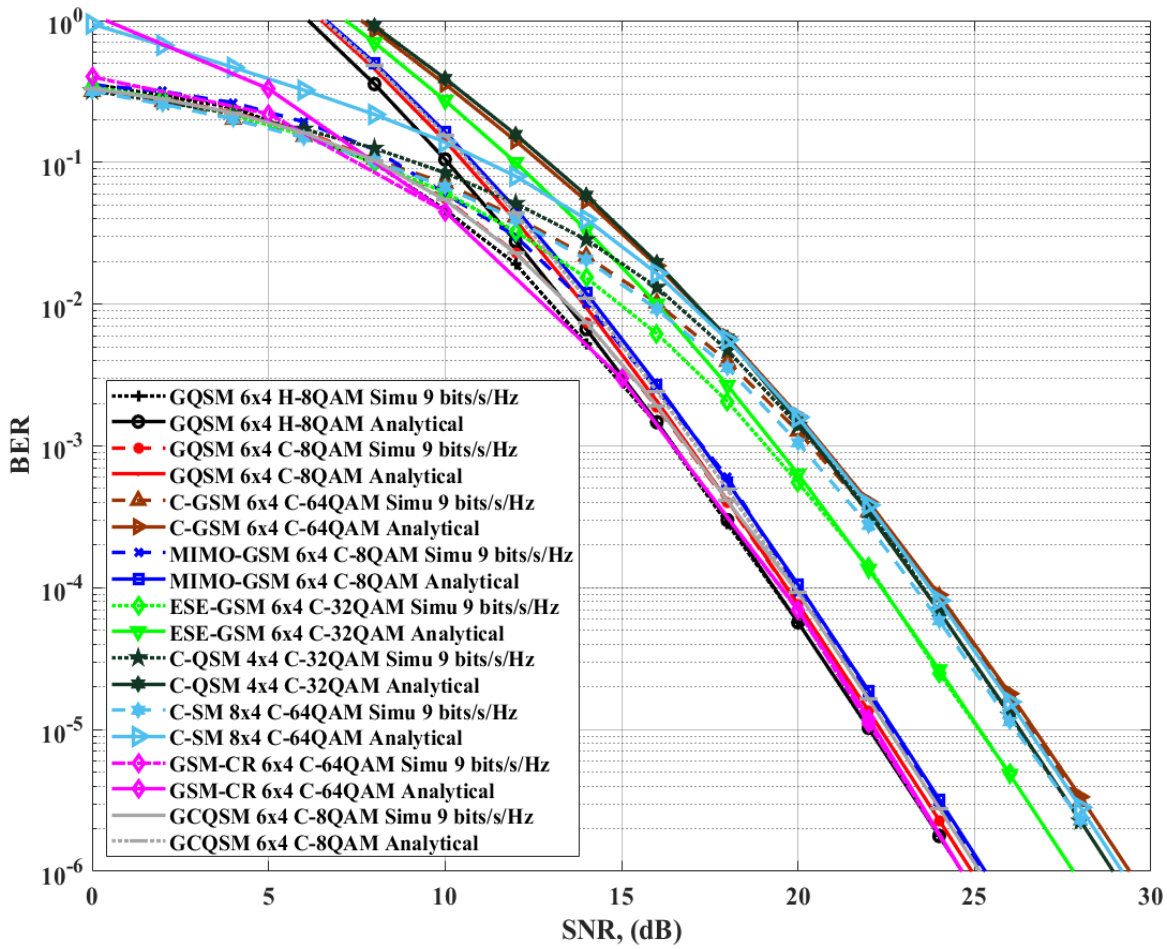

Fig. B.8: Comparison of 6×4 GQSM-H-8QAM with various schemes of the same SE, same N_T and N_R.

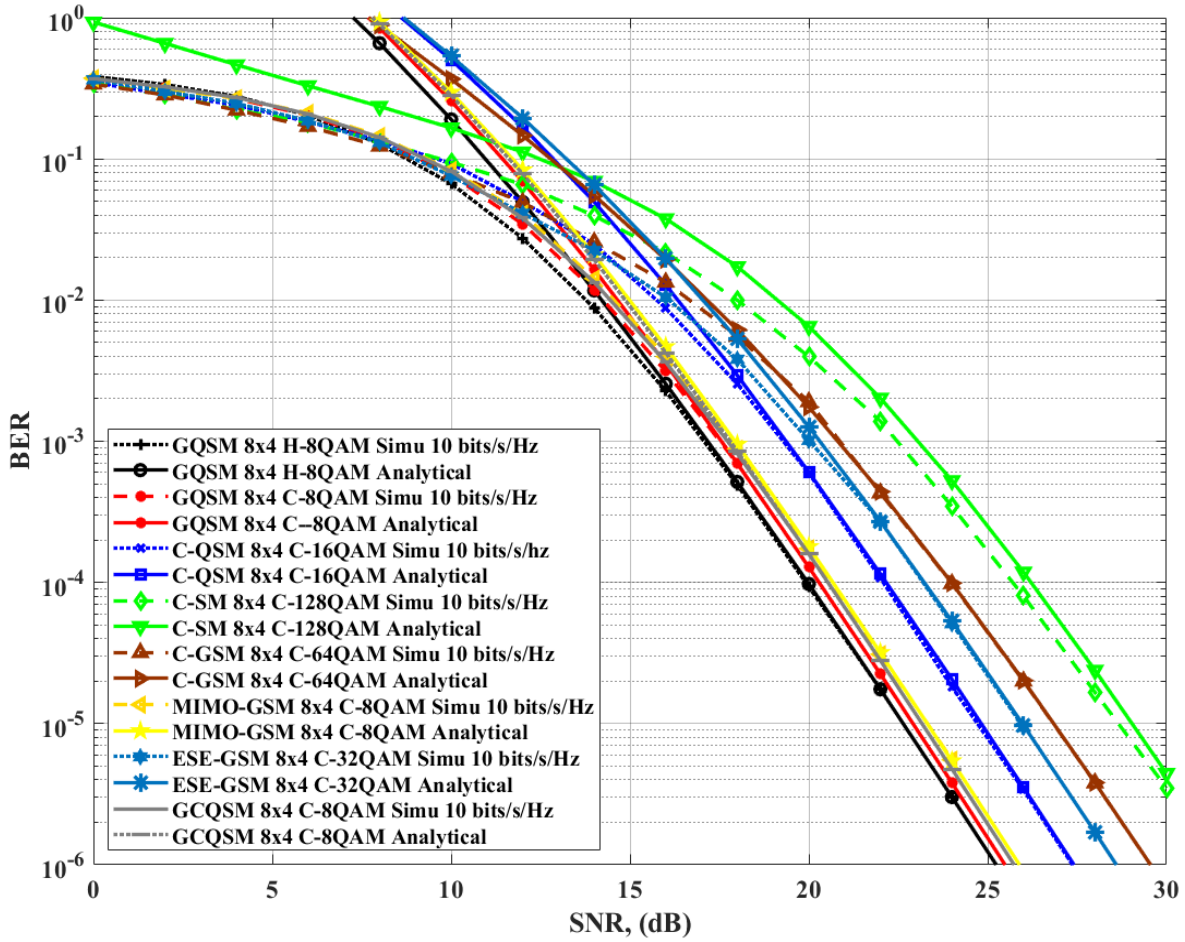

Fig. B.9: Comparison of 8×4 GQSM-H-8QAM with various schemes of the same SE, same N_T and N_R.

Table B.6: 4×4 GQSM-H-8QAM error performance gains over 4×4 various schemes of the same $\mathfrak{m} = 8\ bits/s/Hz$ and at a BER of 10^{-5}.

Scheme	GQSM-H-8QAM proposed scheme (dB) gain
4×4 GQSM-C-8QAM	0.68
4×4 GCQSM-C-8QAM	0.61
4×4 C-QSM-C-16QAM	2.58
4×4 C-SM-C-64QAM	4.78
4×4 C-GSM-C-64QAM	4.85
4×4 GSM-CR-C-64QAM	0.93
4×4 MIMO-GSM-C-8QAM	0.75
4×4 ESE-GSM-C-32QAM	3.22

Table B.7: 8×4 GQSM-H-8QAM error performance gains over various 8×4 schemes of the same $\mathfrak{m} = 10\ bits/s/Hz$ and at a BER of 10^{-5}.

Scheme	GQSM-H-8QAM proposed scheme (dB) gain
8×4 GQSM-C-8QAM	0.27
8×4 GCQSM-C-8QAM	0.43
8×4 C-QSM-C-16QAM	2.08
8×4 C-SM-C-64QAM	6.02
8×4 C-GSM-C-64QAM	4.19
8×4 MIMO-GSM-C-8QAM	0.68
8×4 ESE-GSM-C-32QAM	3.29

7 Conclusion

In this paper, the GQSM-H-8QAM scheme was proposed to improve the error performance of MIMO-SM schemes. The scheme builds on GCQSM and uses energy-efficient H-8QAM instead of the C-QAM, to improve the error performance of MIMO-SM schemes. Also, in this paper, an upper bound analytical error performance formula for the proposed scheme in i.i.d Rayleigh frequency-flat fading channels was derived. This analytical bound was validated using Monte Carlo simulations. The results showed that the derived analytical bound is increasingly tight with increasing SNR values. Furthermore, the proposed scheme outperformed GCW-GSM, GCQSM, C-SM, C-QSM, MIMO-GSM, C-GSM and other various MIMO-SM schemes incorporated in this paper. Hence,

from the results obtained, it can be concluded that the proposed scheme is a viable option for improving the error performance of MIMO-SM schemes. However, despite its capability of improving the error performance of MIMO-SM schemes, the proposed scheme was found to have a high complexity MLD. Hence, for future work, the authors intend to work on low-complexity detection methods for the proposed scheme. In addition, the authors also plan to build on the proposed scheme by fusing it with uncoded space-time labelling diversity and golden codewords to improve/enhance the SE of MIMO-SM systems.

References

[1] D. J. Love and R. W. Heath, "Equal gain transmission in multiple-input multiple-output wireless systems," *IEEE Transactions on Communications*, vol. 51, no. 7, pp. 1102–1110, Jul. 2003.

[2] R. Y. Mesleh, H. Haas, S. Sinanovic, C. W. Ahn, and S. Yun, "Spatial modulation," *IEEE Transactions on Vehicular Technology*, vol. 57, no. 4, pp. 2228–2241, Jul. 2008.

[3] J. Jeganathan, A. Ghrayeb, and L. Szczecinski, "Spatial modulation: Optimal detection and performance analysis," *IEEE Communications Letters*, vol. 12, no. 8, pp. 545–547, Aug. 2008.

[4] N. R. Naidoo, H. Xu, and T. A. Quazi, "Spatial modulation: optimal detector asymptotic performance and multiple-stage detection," *IET communications*, vol. 5, no. 10, pp. 1368–1376, Jul. 2011.

[5] A. Younis, N. Serafimovski, R. Mesleh, and H. Haas, "Generalised spatial modulation," in *2010 conference record of the forty fourth Asilomar conference on signals, systems and computers*. IEEE, Nov. 2010, pp. 1498–1502.

[6] R. Y. Mesleh, S. S. Ikki, and H. M. Aggoune, "Quadrature spatial modulation," *IEEE Transactions on Vehicular Technology*, vol. 64, no. 6, pp. 2738–2742, Jul. 2014.

[7] V. V. Gudla and V. B. Kumaravelu, "Permutation index-quadrature spatial modulation: A spectral efficient spatial modulation for next generation networks," *AEU-International Journal of Electronics and Communications*, vol. 111, no. 1, p. 152917, Nov. 2019.

[8] S. Oladoyinbo, N. Pillay, and H. Xu, "Adaptive quadrature spatial modulation," *IETE Technical Review*, vol. 37, no. 6, pp. 579–590, Nov. 2020.

[9] J. Li, M. Wen, X. Cheng, Y. Yan, S. Song, and M. H. Lee, "Generalized precoding-aided quadrature spatial modulation," *IEEE Transactions on Vehicular Technology*, vol. 66, no. 2, pp. 1881–1886, May. 2016.

[10] S. Kim, "Antenna selection schemes in quadrature spatial modulation systems," *ETRI Journal*, vol. 38, no. 4, pp. 606–611, Aug. 2016.

[11] F. Castillo-Soria, J. Cortez-González, R. Ramirez-Gutierrez, M. M.-B. Fermín, and L. Soriano-Equigua, "Generalized quadrature spatial modulation scheme using antenna grouping," *ETRI Journal*, vol. 39, no. 5, pp. 707–717, Oct. 2017.

[12] M. Mohaisen, "Generalised complex quadrature spatial modulation," *Wireless Communications and Mobile Computing*, vol. 2019, no. 1, p. 3137927, Apr. 2019.

[13] ——, "Increasing the minimum Euclidean distance of the complex quadrature spatial modulation," *IET Communications*, vol. 12, no. 7, pp. 854–860, May. 2018.

[14] N. R. Naidoo, "Enhanced performance and efficiency schemes for generalised spatial modulation," Ph.D. dissertation, University of KwaZulu-Natal, 2017.

[15] K. P. Singya, N. Kumar, V. Bhatia, and M. Alouini, "On the performance of hexagonal, cross, and rectangular qam for multi-relay systems," *IEEE Access*, vol. 7, no. 1, pp. 60 602–60 616, May. 2019.

[16] F. Cogen and E. Aydin, "Hexagonal quadrature amplitude modulation aided spatial modulation," in *2019 11th International Conference on Electrical and Electronics Engineering (ELECO)*. IEEE, Nov. 2017, pp. 730–733.

[17] ——, "Performance analysis of hexagonal qam constellations on quadrature spatial modulation with perfect and imperfect channel estimation," *Physical Communication*, vol. 47, no. 1, p. 101379, May. 2021.

[18] P. K. Singya, P. Shaik, N. Kumar, V. Bhatia, and M. Alouini, "A survey on design and performance of higher-order qam constellations," *arXiv preprint arXiv:2004.14708*, Apr. 2020.

[19] R. Pillay, N. Pillay, and H. Xu, "Improved error performance for generalised spatial modulation with enhanced spectral efficiency," *International Journal of Communication Systems*, vol. 33, no. 2, p. e4176, Jan. 2020.

[20] T. Holoubi, S. Murtala, N. Muchena, and M. Mohaisen, "On the performance of improved quadrature spatial modulation," *ETRI Journal*, vol. 42, no. 4, pp. 562–574, Aug. 2020.

[21] J. Wang, S. Jia, and J. Song, "Generalised spatial modulation system with multiple active transmit antennas and low complexity detection scheme," *IEEE Transactions on Wireless Communications*, vol. 11, no. 4, pp. 1605–1615, Mar. 2012.

[22] L. Zheng and D. Tse, "Diversity and multiplexing: A fundamental tradeoff in multiple-antenna channels," *IEEE Transactions on information theory,*, vol. 49, no. 5, pp. 1073–1096, May. 2003.

[23] A. Koc, I. Altunbas, and E. Basar, "Full-duplex spatial modulation systems under imperfect channel state information," in *2017 24th International Conference on Telecommunications (ICT)*. IEEE, May. 2017, pp. 1–5.

[24] M. K. Simon and M. S. Alouini, *Digital communication over generalized fading channels: a unified approach to performance analysis*. New York: Wiley-Interscience Publication, 2000.

[25] H. Xu, "Symbol Error probability for Generalised Selection Combining reception of M-QAM," *SAIEE Africa Research Journal*, vol. 100, no. 3, pp. 68–71, Sep. 2009.

A Appendix B

A.1 H-8QAM constellation set

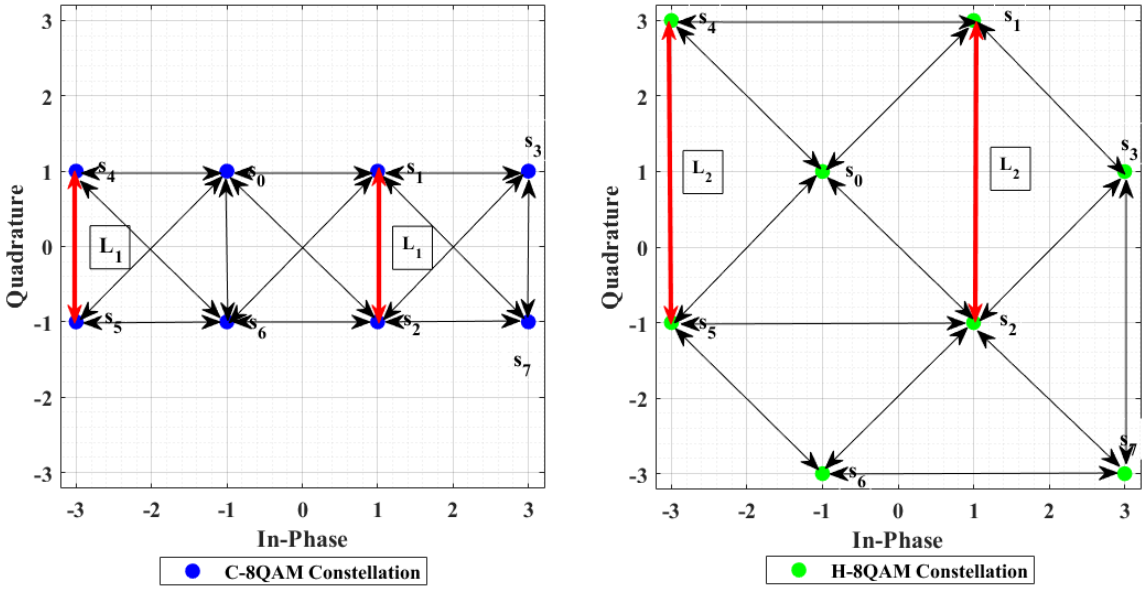

Fig. B.10: Comparison of the C-8QAM and rotated H-8QAM constellations with $L_2 = \frac{4}{\sqrt{10}} > L_1 = \frac{2}{\sqrt{6}}$.

Table B.8: List of formulae for calculating the SE of various schemes [14], [19] and [21]

Model scheme	Formula
GQSM-H-8QAM	$\mathfrak{m} = 2\log_2(M) + \lfloor \log_2 \binom{N_T}{N_A} \rfloor_{2^p}$
GCQSM	$\mathfrak{m} = 2\log_2(M) + \lfloor \log_2 \binom{N_T}{N_A} \rfloor_{2^p}$
C-SM	$\mathfrak{m} = \log_2(M) + \log_2(N_T)$
C-GSM	$\mathfrak{m} = \log_2(M) + \lfloor \log_2 \binom{N_T}{N_A} \rfloor_{2^p}$
GSM-CR	$\mathfrak{m} = \log_2(M) + \lfloor \log_2 \binom{N_T}{N_A} \rfloor_{2^p}$
MIMO-GSM	$\mathfrak{m} = 2\log_2(M) + \lfloor \log_2 \binom{N_T}{N_A} \rfloor_{2^p}$
C-QSM	$\mathfrak{m} = \log_2(M) + 2\log_2(N_T)$
ESE-GSM	$\mathfrak{m} = \log_2(M) + 1 + \lfloor \log_2 \binom{N_T}{N_A} \rfloor_{2^p}$

For the following Tables B.9 and B.10, where other schemes are excluded, means that they were not compatible for the conditions under comparison.

Table B.9: Number of N_T required for $\mathfrak{m} = 8\ bits/s/Hz$ for $M = 8$ and $N_R = 4$

Model scheme	GQSM-H-8QAM	C-SM	C-GSM	GSM-CR	MIMO-GSM	ESE-GSM
N_T	4	32	10	10	4	8

Table B.10: Number of N_T required for $\mathfrak{m} = 10\ bits/s/Hz$ for $M = 8$ and $N_R = 4$

Model scheme	GQSM-H-8QAM	C-SM	C-GSM	GSM-CR	MIMO-GSM	ESE-GSM
N_T	8	128	18	18	8	12

A.2 Derivation of the PEP

Based on the equivalent system model in $(B.2)$, the conditional PEP, $P(\mathbf{x} \rightarrow \hat{\mathbf{x}})$ can be formulated as

$$P(\mathbf{x} \rightarrow \hat{\mathbf{x}}|\mathbf{H}) = P\left(\left\|\mathbf{y} - \sqrt{\frac{\rho}{4}}\mathbf{H}\mathbf{x}\right\|_F^2 > \left\|\mathbf{y} - \sqrt{\frac{\rho}{4}}\mathbf{H}\hat{\mathbf{x}}\right\|_F^2\right). \tag{B.12}$$

Substituting $(B.2)$ into $(B.12)$ leads to

$$P(\mathbf{x} \rightarrow \hat{\mathbf{x}}|\mathbf{H}) = P\left(A > B\right), \tag{B.13}$$

where $A = \|\mathbf{n}\|_F^2$, $B = \frac{\rho}{4}\left\|\sum_{l=1}^{4}\mathbf{h}_{k_l}d_l + \mathbf{n}\right\|_F^2$, $d_i = \left[\left(S_q^{iI} - S_{\hat{q}}^{iI}\right)e^{j\theta_k}\right]$ and $d_{(i+2)} = \left[\left(S_q^{lQ} - S_{\hat{q}}^{lQ}\right)e^{j\theta_k}\right], i \in [1:2]$.

Equation (B.13) can also be rewritten as;

$$P(\mathbf{x} \rightarrow \hat{\mathbf{x}}|\mathbf{H}) = P\left(A > C + A + E\right), \tag{B.14}$$

where $C = \frac{\rho}{4}\left\|\sum_{l=1}^{4}\mathbf{h}_{k_l}d_l\right\|_F^2$ and $E = 2\Re\left\{\sqrt{\frac{\rho}{4}}\mathbf{n}^H\left(\sum_{l=1}^{4}\mathbf{h}_{k_l}d_l\right)\right\}$.

Simplifying Equation (B.14) leads to (B.15).

$$P(\mathbf{x} \rightarrow \hat{\mathbf{x}}|\mathbf{H}) = P\left(\frac{1}{2}E < \frac{1}{2}C\right). \tag{B.15}$$

Since $\mathbf{n}^H \in \mathbb{C}^{1\times N_R}$ and each entry of $\mathbf{n}^H = \begin{bmatrix} n_1^* & n_2^* & n_3^* & \dots & n_{N_R}^* \end{bmatrix}$ is Gaussian distributed, it, therefore, means that each entry of $\Re\left\{\sqrt{\frac{\rho}{4}}\mathbf{n}^H\mathbf{h}_{k_z}d_z\right\}$, $z \in [1:4]$ is also a GRV with distribution $N\left(0, \frac{\rho}{4}|d_z|^2\sum_{l=1}^{N_R}|h_{k_z}^l|^2\right)$. Hence, this implies that our decision variable is also Gaussian distributed as $\Re\left\{\sqrt{\frac{\rho}{4}}\mathbf{n}^H\left(\sum_{l=1}^{4}\mathbf{h}_{k_l}d_l\right)\right\} \sim N\left(0, \frac{\rho}{8}\left\|\sum_{l=1}^{4}\mathbf{h}_{k_l}d_l\right\|_F^2\right)$ and it leads to

$$P(\mathbf{x} \rightarrow \hat{\mathbf{x}}|\mathbf{H}) = Q\left(\frac{\omega_g}{\sqrt{\omega_g}}\right) = Q\left(\sqrt{\omega_g}\right), \tag{B.16}$$

where $\omega_g = \frac{1}{2}C = \frac{\rho}{8}\|\mathbf{H}_k\mathbf{G}_k\|_F^2 = \frac{\rho}{8}\|\mathbf{H}_k\|_F^2\|\mathbf{G}_k\|_F^2$, with $\mathbf{H}_k = \begin{bmatrix}\mathbf{h}_{k_1} & \mathbf{h}_{k_2} & \mathbf{h}_{k_3} & \mathbf{h}_{k_4}\end{bmatrix}$ and $\mathbf{G}_k = \begin{bmatrix}d_1 & d_2 & d_3 & d_4\end{bmatrix}^T$. Similarly, based on (11) in Koc *et al.* [23], ω_g are chi-squared RVs with

$2N_R$ degrees of freedom defined as $\omega_g = \sum_{t=1}^{2N_R} \alpha_{\omega_{g,t}}^2$ with $\alpha_{\omega_{g,t}}^2 \sim N(0, \sigma_{\omega_g}^2)$ and $\sigma_{\omega_g}^2 = \frac{\rho}{8}\big(\sum_{l=1}^{4}(D_l)^2\big)$. $D_l = |d_l|, l \in [1:4]$.

The conditional PEP can then be expressed as

$$P(\mathbf{x} \to \hat{\mathbf{x}}) = \int_0^\infty Q\left(\sqrt{\omega_g}\right) f_{\omega_g}(\omega_g)\, d\omega_g, \tag{B.17}$$

where the probability density function of ω_g is given in [24] as

$$f_{\omega_g}(\omega_g) = \frac{1}{\left(2\sigma_{\omega_g}^2\right)^{N_R}(N_R-1)!}\omega_g^{N_R-1}\exp(-\frac{\omega_g}{2\sigma_{\omega_g}^2}). \tag{B.18}$$

The trapezoidal transformation of the Q-function in [25], is given as

$$Q(z) \cong \frac{1}{2n}\left(\frac{1}{2}\exp(-\frac{z^2}{2}) + \sum_{i=1}^{n-1} S_v\right), \tag{B.19}$$

where $n \geq 6$ is the number of summations for convergence and $S_v = \exp(-\frac{z^2}{2\sin^2\left(\frac{v\pi}{2n}\right)})$.

Using the trapezoidal transformation (B.19) on (B.16) and then substituting into (B.17) yields

$$P(\mathbf{x} \to \hat{\mathbf{x}}) = \left(\frac{1}{2n}\right)\left[\left(\frac{1}{2}\right)\left(1 + \frac{\rho\left(\sum_{l=1}^{4}(D_l)^2\right)}{16}\right)^{-N_R} + \sum_{v=1}^{n-1}\left(1 + \frac{\rho\left(\sum_{l=1}^{4}(D_l)^2\right)}{8\mu_v}\right)^{-N_R}\right], \tag{B.20}$$

where $\mu_v = 2\sin^2\left(\frac{v\pi}{2n}\right)$.

Part IV

Paper C

Paper C

Error Performance Analysis of Multiple Active Antennas GSM and GQSM with Labelling Diversity

1 Abstract

Multiple-input multiple-output (MIMO) generalised spatial modulation (GSM) systems represent a pivotal advancement in wireless communication technology. These systems have unlocked the potential for enhanced data rates and enhanced error performance. Therefore, this research delves into a strategy aimed at elevating the error performance within MIMO-GSM systems. This strategy involves the integration of MIMO-GSM systems with both generalised quadrature spatial modulation (GQSM) and the concept of labelling diversity (LD). Two schemes namely multiple active antenna generalised spatial modulation with labelling diversity (MAA-GSM-LD) and generalised complex quadrature spatial modulation with labelling diversity (GCQSM-LD) are proposed. The first scheme is MAA-GSM-LD, which builds on conventional generalised spatial modulation (C-GSM) by incorporating it with multiple active antennas and optimised labelling maps that have a maximised minimum product distance (M-MPD) between constellations. This M-MPD helps improve detection, thereby improving the error performance of MIMO-SM schemes. Four symbols are sent simultaneously per time slot in MAA-GSM-LD. The second scheme (GCQSM-LD), builds on MAA-GSM-LD by splitting the four symbols created in MAA-GSM-LD into the quadrature and in-phase dimensions, thereby avoiding inter-antenna synchronisation and improving the error performance of MIMO-GSM systems. Furthermore, in this research, analytical mathematical expressions for both the union-bound and upper-bound average bit error rate (ABER) for the MAA-GSM-LD and GCQSM-LD schemes were developed. These evaluations are conducted over Rayleigh frequency-flat fading channels that are independent and identically distributed. To verify the accuracy of these expressions, Monte Carlo simulations were employed. The results indicate that as the signal-to-noise ratio (SNR) increases, the average bit error probability (ABEP) closely aligns with the simulation outcomes. Obtained simulation results also show an improvement in the error performance of both MAA-GSM-LD and GCQSM-LD schemes over various MIMO-SM schemes like generalised complex quadrature spatial modulation (GCQSM) and generalised SM multiplexing two symbols (MIMO-GSM), at the same spectral efficiency (SE). For MAA-GSM-LD, an improvement in the error performance of $1.0\ dB$ with an SE of $11\ bits/s/Hz$ is seen in 6×4 MAA-GSM-LD C-16-QAM over 6×4 GQSM C-16-QAM and $4.3\ dB$ over 6×4 Golden codeword-GSM-C-64QAM. For GCQSM-LD, an improvement in the error performance of $4.7\ dB$ with an SE of $14\ bits/s/Hz$ is seen in 8×4 GCQSM-LD C-16-QAM over 4×4 GCQSM-C-64-QAM and $3.7\ dB$ over 4×4 Generalised quadrature spatial modulation with antenna grouping (GQSM-AG)-C-32QAM.

***Index Terms*—-Error performance; generalised quadrature spatial modulation; labelling diversity; multiple active antennas.**

2 Introduction

Due to the ever-growing demand for data-intensive applications and seamless connectivity, wireless communication networks have widely embraced multiple-input multiple-output (MIMO) systems [1, 2]. These MIMO systems utilise multiple antennas at both the transmitter and receiver ends, taking advantage of spatial diversity to enhance link capacity and reliability [1, 3]. However, the reliability of MIMO systems can be impacted by factors such as channel impairments, inter-symbol interference (ISI), and noise [4]. This research delves into an investigation of the synergistic incorporation of three innovative techniques: Conventional generalised spatial modulation (C-GSM), conventional generalised quadrature spatial modulation (C-GQSM), and space-time labelling diversity. This integration aims to enhance the error performance and/or spectral efficiency (SE) of MIMO systems.

Conventional spatial modulation (C-SM) is a technique designed to enhance SE by jointly mapping information bits onto the spatial constellation (transmit antenna indices) and the signal constellation [5–7]. Previous studies, such as Naidoo *et al.* [7], have compared C-SM with other MIMO transmission schemes, highlighting its advantages in terms of avoiding inter-channel interference (ICI) and achieving inter-antenna synchronization (IAS). However, the SE of C-SM is influenced by the practical number of transmit antennas, which led to the development of C-GSM to address this limitation [8, 9].

C-GSM overcomes the constraint imposed by C-SM, which requires the number of transmit antennas to be a power of two, and instead permits a block of information bits to be associated with a constellation symbol and a transmit antenna index. In contrast to C-SM, where only one transmit antenna is active at any given time, C-GSM enhances the SE by a factor equivalent to the base-two logarithm of the number of antenna combinations. This reduction in the necessary number of transmit antennas achieves the same SE [8, 10].

Furthermore, a spatial modulation scheme involving multiple active transmit antennas (MIMO-GSM), as proposed in Wang *et al.* [11], leverages C-GSM to enhance the SE of MIMO systems. It allows the simultaneous transmission of multiple symbols using multiple transmitters, thereby improving both SE and error performance by increasing spatial diversity.

To enhance the error performance of SM systems, Mesleh *et al.*, [12], introduced a scheme known as conventional quadrature spatial modulation (C-QSM). C-QSM expands the spatial constellation into two dimensions, specifically the in-phase (I) and quadrature (Q) dimensions. It effectively eliminates inter-channel interference (ICI) by modulating the I and Q components using cosine and sine carriers, respectively [12–14]. In a study by Kim *et al.*, [15], C-QSM was employed in antenna selection schemes to improve error performance while simultaneously reducing detection complexity. However, it is important to note that C-QSM has a drawback. It necessitates a higher number of transmit antennas when compared to conventional spatial multiplexing (C-SMux). This limitation can restrict the potential for error performance improvement in SM systems [13].

Additionally, in the quest to enhance the error performance of SM systems while minimising the required number of transmit antennas, Mohaisen *et al.* [16], introduced a generalised complex quadrature spatial modulation (GCQSM) scheme. GCQSM builds upon the foundation of C-QSM by fusing elements from C-GSM with those of C-QSM. This integration results in improved error performance by simultaneously transmitting two amplitude/phase modulated symbols sourced from two distinct constellations during each channel utilisation. Their study demonstrates that this amalgamation of C-GSM and C-QSM enhances robustness against IAS, consequently elevating the reliability and SE of wireless communication links. Despite the heightened complexity encountered at both the transmitter and receiver ends, the equilibrium between performance gains and added complexity renders GCQSM a practical choice for implementation.

Furthermore, Castillo *et al.* [13], introduced a technique called generalised quadrature spatial modulation with antenna grouping (GQSM-AG) to also enhance the error performance of SM systems. GQSM-AG similarly leverages attributes from both C-GSM and C-QSM. Their study illustrates that this combination results in an improved error performance compared to C-QSM, C-GSM, and various other MIMO-SM techniques.

Another important technique for improving reliability in wireless communication systems, especially in MIMO systems, is space-time labelling diversity (STLD). As an extension of space-time block coding (STBC) and spatial modulation (SM), STLD uses both spatial and temporal diversity to mitigate fading and improve overall system performance [17, 18]. Recently, STLD was proposed as a novel diversity technique that achieves higher diversity gain without requiring additional transmit or receive antennas [19]. By using optimised labelling maps, STLD can maximise the minimum product

distance (MPD) of space-time block codes, and empirical evidence has shown its superiority over STBCs in terms of the error performance under identical channel conditions [20]. This is seen in [20], where optimised labelling maps maximise the MPD of Alamouti STBC codewords, eliminating the need for encoding or bit interleaving, reducing computational complexity (CC), and ensuring efficient bandwidth utilisation. Also, evidence of improving the error performance of MIMO-SM systems is seen in [21], where optimised labelling maps were used in a scheme called labelling diversity (LD) for media-based space-time block coded spatial modulation [21]. The design of optimised labelling maps has been greatly discussed in Xu *et al.* [19] and in Krasicki, [18]. Optimised labelling maps used in this paper were adapted from [19] and are given in Appendix A.1 of Part (IV).

2.1 Motivation

Motivated to improve the error performance of GSM systems like in Part(II) and that of GQSM systems like in Part (III), Part (IV) proposes fusing GSM systems and GQSM systems with optimised labelling maps as they were found to maximise the MPD of STBCs in [20, 22] and in turn, this led to an improved error performance in STBCs [19–21]. Hence, here in Part (IV), two techniques called multiple active antenna generalised spatial modulation with LD (MAA-GSM-LD) and generalised complex quadrature spatial modulation with LD (GCQSM-LD) are proposed. Similarly to Part (II) [23], MAA-GSM-LD builds on C-GSM and optimised labelling maps, by fusing the attributes of C-GSM and those of LD in optimised maps [19]. In Wang *et al.* [11], a MIMO-GSM scheme was proposed and it exhibited improved error performance as compared to C-GSM and C-SM systems. Thus, in [11], it was shown that multiple active transmit antennas increase spatial diversity thereby improving robustness against fading. Hence, in order to improve the error performance of GSM systems, Part (IV) entails the proposal of a scheme that extends MIMO-GSM into transmitting four symbols simultaneously, two from Gray-coded quadrature amplitude modulated (QAM) constellations and two from optimised labelling QAM maps. This MAA-GSM-LD proposed scheme fuses MIMO-GSM with optimised labelling maps because it was shown in [20] and [21], that optimised labelling maps increase the robustness of GSM systems against fading, hence improving the error performance of GSM systems.

Also, to improve on the error performance of MIMO-GQSM schemes like in Part (III) [24], Part (IV), also entails the proposal of extending the MAA-GSM-LD scheme with C-QSM attributes of

expanding the spatial domain into the *I*-phase and *Q* phase dimensions. This proposed scheme is herein named generalised complex quadrature spatial modulation with labelling diversity (GCQSM-LD). This proposed scheme also builds on complex generalised spatial modulation by Mohaisen [16]. Instead of sending two symbols from C-QAM constellations, it draws four symbols, (two from conventional Gray-coded QAM constellations and two from optimised labelling QAM maps). The four symbols are then split into imaginary and real parts of the signal, which are then sent by the *I*-phase and *Q*-phase dimensions, respectively [12, 14]. This further improves the robustness of the proposed schemes as the *I* and *Q* spatial domains are designed to reduce IAS, thereby improving robustness against channel fading.

Thus, the core contributions of this paper are:

1. Proposal of a new GSM scheme called MAA-GSM-LD which incorporates MIMO-GSM and optimised LD maps that maximise the MPD of STBCs, which in turn improves the error performance of the STBCs.
2. Derivation of a union-bound average bit error rate (ABER) expression for the MAA-GSM-LD scheme over independent and identically distributed (i.i.d) Rayleigh frequency-flat fading channels.
3. Validation of the derived analytical bound for the MAA-GSM-LD scheme using Monte Carlo simulation results.
4. Proposal of a scheme called GCQSM-LD that extends the MAA-GSM-LD scheme into the C-QSM domain by using optimised LD maps with GCQSM.
5. Derivation of an upper bound ABER expression for the GCQSM-LD scheme in i.i.d Rayleigh frequency-flat fading channels.
6. Validation of the derived analytical bound for the GCQSM-LD scheme using Monte Carlo simulation results.

Finally, the paper is organised as follows. The introduction of the proposed MAA-GSM-LD scheme is detailed in Section 3. It is presented in the form of a MIMO $N_T \times N_R$ M-QAM system shown in Figures C.1 and C.2. Section 4 presents the second proposed scheme called GCQSM-LD, followed by Section 5, which gives the maximum likelihood detection (MLD) computational complexity (CC) analysis based on real-valued multiplications and additions of the proposed schemes. Then in Section

6, follows the error performance analysis of the proposed MAA-GSM-LD and GCQSM-LD schemes. Section 7, discusses the results of this paper and finally, the paper is concluded in Section 8.

2.2 Notation

In this paper, using mathematical notation, the symbol $(\cdot)^*$ corresponds to the complex conjugate, while $|\ \cdot\ |$ signifies the Euclidean norm operator. Column vectors are indicated using bold lowercase letters, whereas matrices are represented by uppercase letters. Scalar quantities are denoted by regular letters. A set of complex matrices with dimensions $S \times L$ is described by $\mathbb{C}^{S\times L}$. When dealing with complex arguments, $\Re(\cdot)$ and $j(\cdot)$ stand for the real and imaginary components, respectively. The function $Q(\cdot)$ is employed to express the Gaussian Q-function, $E\{\cdot\}$ is used to denote the expectation operator, $\underset{w}{\text{argmin}}\{\cdot\}$ and $\underset{w}{\text{argmax}}\{\cdot\}$ represent finding the argument's minimum or maximum value concerning the variable w, respectively. The operators $[\cdot]^T$ and $(\cdot)^H$ refer to the transpose and Hermitian operators, respectively. The Frobenius norm operator is denoted as $\|\cdot\|_F$. The notation $\lfloor\cdot\rfloor_{2^p}$ signifies the largest integer that is less than or equal to the argument and is a positive integer that is a power of 2 raised to the p. Finally, $\binom{\cdot}{\cdot}$ is used to denote the binomial coefficient of the argument.

3 Proposed MAA-GSM-LD System model

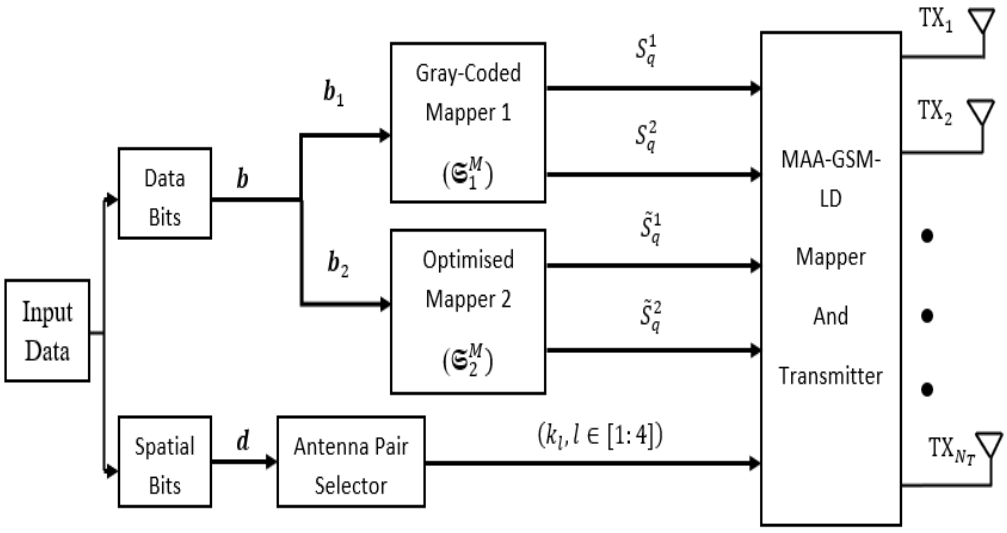

Fig. C.1: Transmitter side of the proposed MAA-GSM-LD system model.

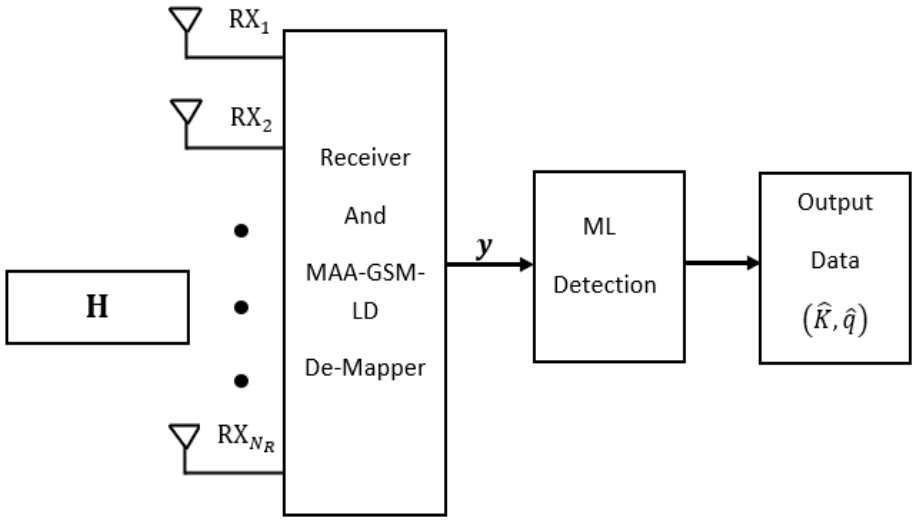

Fig. C.2: Receiver side of the proposed MAA-GSM-LD system model.

The proposed MAA-GSM-LD scheme depicted in Figs. C.1 and C.2, is designed as an $N_R \times N_T$ system. It takes an input data stream, which is categorised into two distinct types: spatial input bits (representing antenna pair indices) and four M-QAM symbol bits. In the first category, spatial information, a set of spatial input bits ($\mathfrak{D} = \log_2 N_c$) is allocated to a specific generalised K^{th} transmit antenna pair, denoted as (k_l for $1 \leq l \leq 4$). These antenna pairs are responsible for transmitting four M-QAM symbols. For example, if we consider a scenario with N_T transmit antennas, there are $n = \binom{N_T}{N_A}$ possible transmit antenna pairs. However, only $N_c = \lfloor \log_2 \binom{N_T}{N_A} \rfloor_{2^p}$ of these pairs are allowed for transmission, where N_c is selected from the range $N_c \leq n$. It is worth noting that the choice of N_A has been addressed in previous work, such as [8], and for the proposed MAA-GSM-LD scheme, the customary value is set to 4 as discussed in [16].

Table C.1 provides an illustrative mapping table that outlines the associations between antenna pairs, their corresponding bit indices, and the rotation angles denoted as θ_k. The purpose of these rotation angles is to minimise the potential interference caused by the overlapping of antenna pairs, as described in [16, 25]. For further details regarding the selection of antenna pairs and the optimal values for θ_k, the discussion can be found in [16, 25].

Table C.1: Transmit antenna pair combinations and mapping ($N_T = 6$ and $N_c = 8$)

Spatial input bits	Antenna pair bit indices	Transmit antenna pairs	Rotation angle
$\boldsymbol{d}$	000	$T_{X1}, T_{X2}, T_{X3}, T_{X4}$	0
$\boldsymbol{d}$	001	$T_{X1}, T_{X2}, T_{X3}, T_{X5}$	0
$\boldsymbol{d}$	010	$T_{X1}, T_{X2}, T_{X3}, T_{X6}$	0
$\boldsymbol{d}$	011	$T_{X1}, T_{X2}, T_{X4}, T_{X5}$	$\frac{\pi}{3}$
$\boldsymbol{d}$	100	$T_{X1}, T_{X2}, T_{X4}, T_{X6}$	$\frac{\pi}{3}$
$\boldsymbol{d}$	101	$T_{X1}, T_{X3}, T_{X4}, T_{X5}$	$\frac{\pi}{3}$
$\boldsymbol{d}$	110	$T_{X1}, T_{X3}, T_{X4}, T_{X6}$	$\frac{2\pi}{3}$
$\boldsymbol{d}$	111	$T_{X1}, T_{X3}, T_{X5}, T_{X6}$	$\frac{2\pi}{3}$

The second category of the input data stream is the message/or symbols bit stream $\boldsymbol{b}$. The message bit stream is partitioned into two bit streams $\boldsymbol{b}_t = \left[b_{t,1} b_{t,2} ... b_{t,r}\right]$, with $t \in [1:2]$ and $r = \log_2 M$. Bit stream $\boldsymbol{b}_1$ is fed into a mapper ($\mathfrak{G}_1$) and bit stream $\boldsymbol{b}_2$ is fed into an optimised labelling mapper ($\mathfrak{G}_2$). Mapper ($\mathfrak{G}_1$) follows the conventional Gray-coded approach, and input bit streams $\boldsymbol{b}_t$, are mapped onto M-QAM signal constellation sets to yield two symbols $S_q^1 = \mathfrak{G}_1^M(\boldsymbol{b}_1)$ and $S_q^2 = \mathfrak{G}_1^M(\boldsymbol{b}_2)$ where $q \in [1:M]$.

In mapper $\mathfrak{G}_2$, the same bit streams ($\boldsymbol{b}_t$), are mapped onto M-QAM signal constellation sets in the Argand plane, yielding symbols $\tilde{S}_q^1 = \mathfrak{G}_2^M(\boldsymbol{b}_1)$ and $\tilde{S}_q^2 = \mathfrak{G}_2^M(\boldsymbol{b}_2)$. It is assumed that the set of all order symbol pairs is contained in set V_{LD}, $E\{|S_q^i|^2\} = 1$ and $E\{|\tilde{S}_q^i|^2\} = 1$, with $i \in [1:2]$. However, the design of mapper $\mathfrak{G}_2$ is different from that of mapper $\mathfrak{G}_1$. The design of mapper $\mathfrak{G}_2$, is the one that ensures LD [17–19], and its design follows that detailed in [18, 19]. For this paper, the used 16-QAM Gray-coded labelling map ($\mathfrak{G}_1^{16}$) and the optimised labelling map ($\mathfrak{G}_2^{16}$) were adopted from [19], whereas the 64-QAM Gray-coded labelling map ($\mathfrak{G}_1^{64}$) and the optimised labelling map ($\mathfrak{G}_2^{64}$) were adopted from [20]. An example of the labelling maps used in this paper is found in Appendix A.1 of Part (IV).

The modulated symbols S_q^1, S_q^2, $\tilde{S}_q^1$, and $\tilde{S}_q^2$, originating from the two mappers, are simultaneously transmitted by four transmit antennas (k_l, where ($1 \leq l \leq 4$) within each time slot. These symbols collectively form an $N_T \times 1$ transmit vector denoted as $\mathbf{x}$, as depicted in Fig.C.3. Consequently, vector $\mathbf{x}$ contains four non-zero elements, and the positions of these four non-zero elements

correspond to the indices of the four chosen active transmit antennas. The SE of the proposed MAA-GSM-LD scheme can be calculated using (C.1).

$$\mathfrak{m} = 2\log_2(M) + \lfloor \log_2 \binom{N_T}{4} \rfloor_{2^p}. \tag{C.1}$$

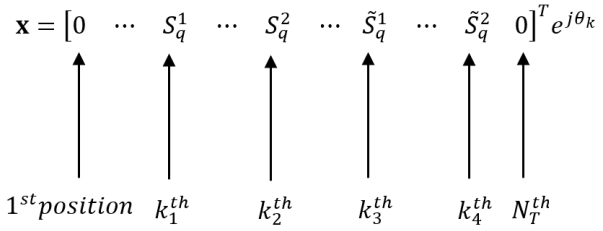

Fig. C.3: Transmitted signal vector $\mathbf{x}$, for the MAA-GSM-LD scheme.

At the receiver, the signal is given by $\mathbf{y} \in \mathbb{C}^{N_R \times 1}$ (C.2), as

$$\begin{aligned}\mathbf{y} &= \sqrt{\frac{\rho}{4}}\mathbf{H}\mathbf{x} + \mathbf{n}, \\ &= \sqrt{\frac{\rho}{4}}\left(\mathbf{h}_{k_1}S_q^1 + \mathbf{h}_{k_2}S_q^2 + \mathbf{h}_{k_3}\tilde{S}_q^1 + \mathbf{h}_{k_4}\tilde{S}_q^2\right)e^{j\theta_k} + \mathbf{n},\end{aligned} \tag{C.2}$$

where the fading channel matrix is denoted as $\mathbf{H} \in \mathbb{C}^{N_R \times N_T}$, and the vector $\mathbf{n} \in \mathbb{C}^{N_R \times 1}$ represents the AWGN. Each $\mathbf{h}_{k_l}$ (for $1 \leq l \leq N_T$) is the lth column vector within the channel gain matrix $\mathbf{H}$, which is defined as $\mathbf{H} = \begin{bmatrix}\mathbf{h}_{k_1} & \mathbf{h}_{k_2} & \mathbf{h}k_3 & ... & \mathbf{h}_{kN_T}\end{bmatrix}$, and each $\mathbf{h}_{k_l}$ itself can be represented as $\mathbf{h}_{k_l} = \begin{bmatrix}h_{1k_l} & h_{2k_l} & h_{3k_l} & ... & h_{N_Rk_l}\end{bmatrix}^T$. It is worth noting that the elements of both the vector $\mathbf{n}$ and the matrix $\mathbf{H}$ are assumed to be i.i.d Gaussian random variables (GRVs) with a distribution of $CN(0,1)$, respectively. Finally, ρ represents the average signal-to-noise ratio (SNR).

The optimal maximum likelihood detection (MLD) procedure for the proposed scheme can be expressed as shown in (C.3). This process involves jointly estimating the indices of the transmission antenna pairs ($\hat{K}$) and the transmitted symbols (S_q^1, S_q^2, $\tilde{S}_q^1$, and $\tilde{S}_q^2$) [13, 16, 26, 27]. The procedure can be described as follows,

$$\left[\hat{K}, S_{\hat{q}}^1, S_{\hat{q}}^2, \tilde{S}_{\hat{q}}^1, \tilde{S}_{\hat{q}}^2\right] = \underset{\substack{\left[S_{\hat{q}}^1, S_{\hat{q}}^2, \tilde{S}_{\hat{q}}^1, \tilde{S}_{\hat{q}}^2\right] \in 1:V_{LD} \\ K \in 1:N_c}}{\operatorname{argmin}} \left\{ \left\| \mathbf{y} - \sqrt{\frac{\rho}{4}}\mathbf{H}\hat{\mathbf{x}} \right\|_F^2 \right\}, \tag{C.3}$$

where $\hat{\mathbf{x}}$ is the estimated received vector shown in Fig. C.4.

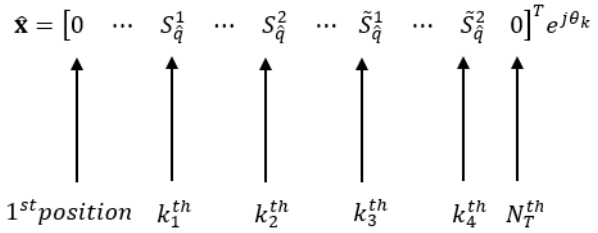

Fig. C.4: Estimated received signal vector for the MAA-GSM-LD scheme.

4 Proposed GCQSM-LD system model

Consider a proposed scheme with dimensions $N_R \times N_T$ similar to the one described in Section 3. This proposed GCQSM-LD scheme utilises the same input data stream as the scheme in Section 3, which is partitioned into two categories: spatial input bits (representing antenna pair indices) and four *M*-QAM symbol bits.

For this proposed system, there are $n = \binom{N_T}{N_A}$ possible transmit antenna pairs, of which only $N_c = \left\lfloor \log_2 \binom{N_T}{N_A} \right\rfloor_{2^p}$ pairs are deemed suitable for transmission, with N_c being less than or equal to n. It is worth noting that the choice of N_A has been addressed in [8], with the commonly adopted value for the proposed GCQSM-LD scheme being 4 [16]. In the first category, spatial information is represented, where spatial input bits ($\mathfrak{D} = \log_2 N_c$) are allocated to a distinct generalised K^{th} antenna pair of transmit antennas (k_l, where $1 \leq l \leq 4$), corresponding to the *I* dimension of the system. The same set of $\mathfrak{D}$ bits is assigned to a separate generalised K^{th} antenna pair of transmit antennas (k_l, where $5 \leq l \leq 8$), designated for the *Q* dimension of the system.

Detailed mapping tables of the grouped bits, covering *I* dimension transmit antenna pairs and *Q* dimension transmit antenna pair combinations, are provided in Tables C.5 and C.6 in Appendix A.1 of Part (IV). Notably, the antenna mappings for the *I* and *Q* dimensions are distinct. This differentiation is essential to prevent ICI or the concurrent transmission of a mixed signal comprising real and imaginary components from the same antenna pair. Such differentiation contributes to enhancing the error performance of the proposed system [12, 16]. The application of rotation angles (θ_k) to various transmit antenna pairs, as discussed in Section 3, further aids in minimising ICI resulting from overlapping antenna pairs [25]. Comprehensive discussions concerning the selection

of antenna pairs and the determination of optimal θ_k are found in Section 3 [16, 25] and [10].

The second category within the input data stream encompasses a message or symbol bit sequence, represented as $\boldsymbol{b}$. The processing of this bit stream $\boldsymbol{b}$ follows the same procedures as detailed in Section 3, leading to the generation of four modulated M-QAM symbols (S_q^1, S_q^2, $\tilde{S}_q^1$, and $\tilde{S}_q^2$). These modulated symbols are further disassembled into their individual real and imaginary components, denoted as ($S_q^{1I} + jS_q^{1Q}$, $S_q^{2I} + jS_q^{2Q}$, $\tilde{S}_q^{1I} + j\tilde{S}_q^{1Q}$, and $\tilde{S}_q^{2I} + j\tilde{S}_q^{2Q}$). Subsequently, the real components of these symbols are transmitted through the I dimension using the in-phase transmit antenna pairs (k_l, where $1 \leq l \leq 4$). On the other hand, the imaginary parts of these symbols are transmitted through the Q dimension using the quadrature antenna pairs (k_l, where $5 \leq l \leq 8$).

As a result, these disassembled symbols are concurrently transmitted using eight transmit antennas within a single time slot. They are encapsulated in the form of an $N_T \times 1$ transmit vector $\mathbf{x}$, as depicted in Fig. C.5. Notably, this vector $\mathbf{x}$ comprises eight non-zero elements, corresponding to the four real parts and the four imaginary parts of the modulated symbols originating from Section 3. The positions of these eight non-zero elements align with the indices of the eight selected active transmit antennas. The SE of the proposed GCQSM-LD scheme is computed in a manner identical to that given by (C.1).

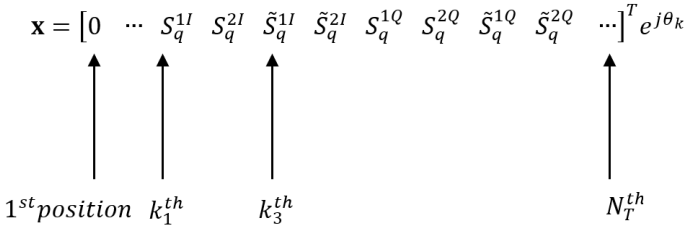

Fig. C.5: Transmitted signal vector $\mathbf{x}$, for the GCQSM-LD scheme.

At the receiver, the signal is given by $\mathbf{y} \in \mathbb{C}^{N_R \times 1}$ (C.4), as

$$\begin{aligned} \mathbf{y} &= \sqrt{\frac{\rho}{8}}\mathbf{H}\mathbf{x} + \mathbf{n}, \\ &= \sqrt{\frac{\rho}{8}}\Big(\mathbf{U} + j\mathbf{W}\Big) + \mathbf{n}, \end{aligned} \tag{C.4}$$

where $\mathbf{U} = \Big(\mathbf{h}_{k_1} S_q^{1I} + \mathbf{h}_{k_2} S_q^{2I} + \mathbf{h}_{k_3} \tilde{S}_q^{1I} + \mathbf{h}_{k_4} \tilde{S}_q^{2I}\Big) e^{j\theta_k}$,

$\mathbf{W} = \left(\mathbf{h}_{k_5} S_q^{1Q} + \mathbf{h}_{k_6} S_q^{2Q} + \mathbf{h}_{k_7} \tilde{S}_q^{1Q} + \mathbf{h}_{k_8} \tilde{S}_q^{2Q}\right) e^{j\theta_k}$, $\mathbf{H} \in \mathbb{C}^{N_R \times N_T}$ and $\mathbf{n} \in \mathbb{C}^{N_R \times 1}$ are similar to those discussed in MAA-GSM-LD Section 3.

The MLD procedure for the proposed scheme is articulated within (C.5). This method encompasses the concurrent estimation of both the indices of the transmission antenna pairs ($\hat{K}$) and the transmitted symbols (Sq^1, Sq^2, $\tilde{S}q^1$, and $\tilde{S}q^2$). This approach has been elaborated on in previous studies, such as [13, 16, 26, 27].

$$\left[\hat{K}, S_{\hat{q}}^1, S_{\hat{q}}^2, \tilde{S}_{\hat{q}}^1, \tilde{S}_{\hat{q}}^2\right] = \underset{\substack{\left[S_{\hat{q}}^1, S_{\hat{q}}^2, \tilde{S}_{\hat{q}}^1, \tilde{S}_{\hat{q}}^2\right] \in 1:V_{LD} \\ K \in 1:N_c}}{\operatorname{argmin}} \left\{ \left\| \mathbf{y} - \sqrt{\frac{\rho}{8}} \mathbf{H}\hat{\mathbf{x}} \right\|_F^2 \right\}, \tag{C.5}$$

where $\hat{\mathbf{x}}$ is the estimated received vector shown in Fig. C.6.

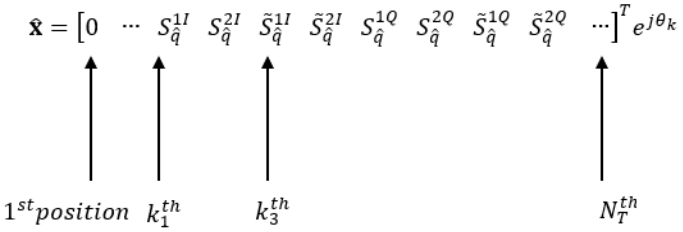

Fig. C.6: Estimated received signal vector for the GCQSM-LD scheme.

5 MLD CCA of the proposed MAA-GSM-LD and GCQSM-LD schemes

The CCA for the MAA-GSM-LD scheme shares similarities with the approach described in previous work, specifically [11]. As for the GCQSM-LD scheme, its CCA is akin to the method outlined in the work by Holoubi *et al.* [28]. Both schemes rely on real-valued multiplications and additions in their complexity analyses. That of MAA-GSM-LD is similar to that given as $N_R M^{N_A}(N_A + 2)N_c$ in [11] and that of GCQSM-LD is similar to that given in [28], as $(20N_R - 1)2^{\mathbf{m}}$. As seen in Table C.2, the MAA-GSM-LD scheme has the highest CC as compared to the GCQSM-LD scheme. Both the proposed schemes have a high CC as compared to that of C-QSM as discussed in Part (III). In Part (III), C-QSM was one of the schemes that had a very high CC, hence this means that the two proposed schemes have the disadvantage of a high complexity ratio. Also, as seen from Fig. C.7, the

CC of the proposed MAA-GSM-LD and GCQSM-LD schemes increase with an increase in the number of receive antennas. Likewise, Fig. C.8 illustrates an increasing CC as the order of quadrature modulation increases for both the proposed schemes (MAA-GSM-LD and GCQSM-LD). It should be noted that the proposed schemes are limited in terms of QAM modulation order (16-QAM and 64-QAM). Thus, Fig. C.8 has other orders of QAM modulation used for clearly illustrating how the CC increases as M increases. The outcome of the CCA discussed in this section, shows that the proposed schemes are ideal for low orders of QAM modulations and a few number of receive antennas. Given the notable high CC exhibited by the proposed scheme, the authors plan to address this limitation in their future work by developing simplified detection algorithms as a solution.

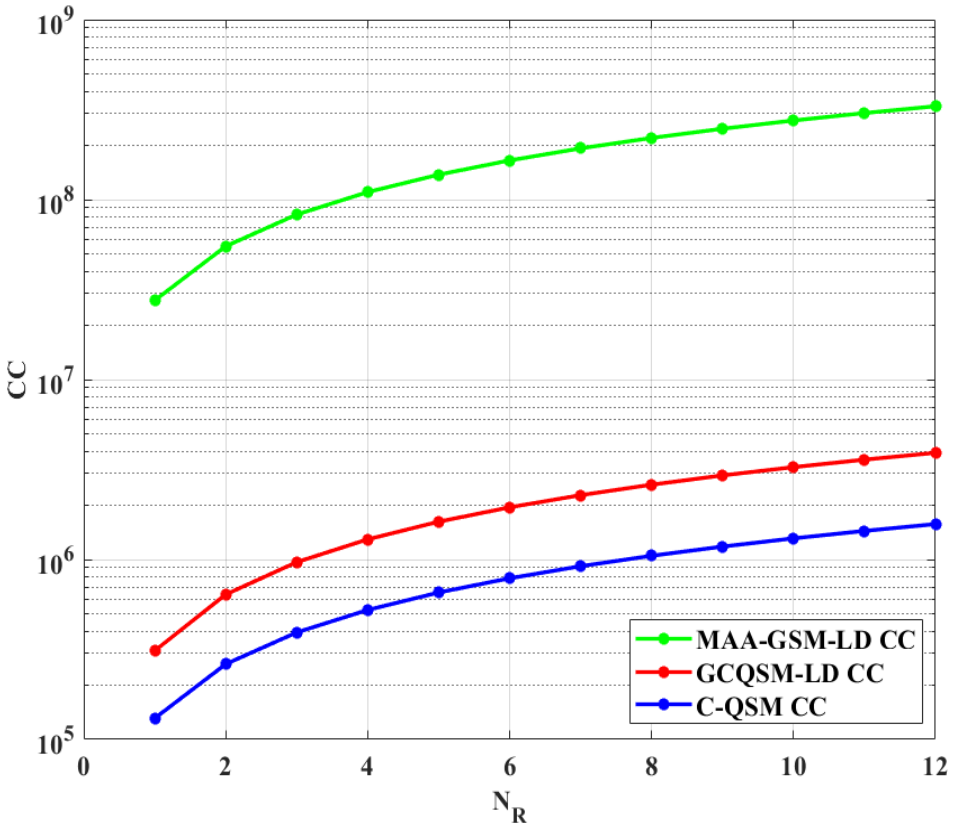

Fig. C.7: CCA of the MAA-GSM-LD, GCQSM-LD and C-QSM with varying N_R but fixed $M = 16, N_A = 4$ and $N_T = 8$.

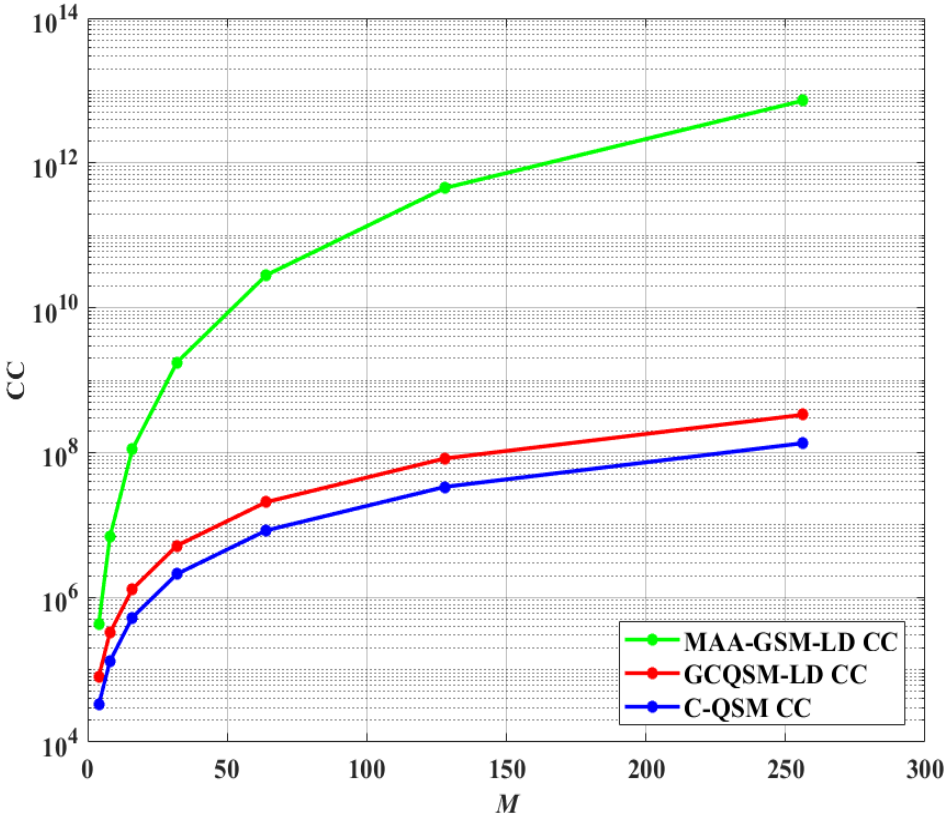

Fig. C.8: CCA of the MAA-GSM-LD, GCQSM-LD and C-QSM with varying M but fixed $N_R = 4, N_A = 4$ and $N_T = 8$.

Table C.2: MLD CCA under the same conditions ($N_T = 8$, $N_R = 4$ and $\mathfrak{m} = 14\ bits/s/Hz$).

Scheme	CCA Formulae	Simulation parameters	CC
GQCSM-LD	$(20N_R - 1)2^{\mathfrak{m}}$	$M = 16$, $N_c = 70$, $N_A = 4$	$1,294,336$
C-QSM	$2^{\mathfrak{m}}(8N_R)$	$M = 32$	$524,288$
MAA-GSM-LD	$N_R M^{N_A}(N_A + 2)N_c$	$M = 16$, $N_c = 70$, $N_A = 4$	$110,100,480$

6 Error performance analysis of MAA-GSM-LD and GCQSM-LD

In this section, the union bound and upper bound are used to derive the theoretical ABEP for the MAA-GSM-LD and GCQSM-LD schemes, respectively, following the approach outlined in [10, 16, 26, 27].

6.1 Error performance analysis of MAA-GSM-LD

The detection process described in Section 3 is a joint detection method. It follows a similar approach as discussed in previous works such as [7, 10, 11], where independent processes for QAM symbols and transmit antenna pair indices are assumed. The detection process in Section 3 involves two types of errors. The first type is related to estimating the average bit error probability (ABEP) of the transmit antenna pair indices (P_a) assuming that the message symbols are detected perfectly, while the second type pertains to the error in estimating the message symbols (P_d) given that the transmit antenna pair index is detected perfectly. As a result, in accordance with the approach presented in [11], the overall ABEP can be bounded by a union of these errors as shown by (C.6).

$$P_e \geq P_c = 1 - (1 - P_a)(1 - P_d). \tag{C.6}$$

It is important to note that assuming independent estimation processes may not be accurate, as the optimal ML detector conducts a joint detection of both the message symbols and the transmit antenna pair index. The assumption of independent estimation processes represents an idealised scenario [7]. Subsequently, sub-subsections 6.1.1 and 6.1.2, entail the derivation of the ABEP for each estimation process separately.

6.1.1 Analytical ABEP of *M*-QAM symbols estimation

This sub-subsection, entails the derivation of the probability of detection (P_d), for estimating the ABEP of *M*-QAM symbols. This estimation assumes perfect detection of transmit antenna pair indices and is based on the system model given in equation (C.2). The formulation presented follows the methodology introduced by Pillay *et al.* [10], along with insights from Naidoo *et al.* [7]. Consequently, by adopting the approach of Pillay *et al.* [10], and considering the presence of four active transmitters, the expression for P_d is found as

$$P_d(\rho) \cong \left(\frac{1}{\log(M^2)}\right)\left(\frac{\alpha}{n}\left[\frac{1}{2}P - \frac{\alpha}{2}R + (1+\alpha)\sum_{i=1}^{n-1} Z + \sum_{i=n}^{n-1} Z\right]\right), \tag{C.7}$$

where $P = \left(\frac{4}{\beta\rho+4}\right)^{N_R}$, $R = \left(\frac{2}{\beta\rho+2}\right)^{N_R}$, $Z = \left(\frac{4\sin^2\Theta_\omega}{\beta\rho+4\sin^2\Theta_\omega}\right)$, $\alpha = \left(1 - \frac{1}{\sqrt{M}}\right)$, $\beta = \frac{3}{M-1}$ and $\Theta = \frac{i\pi}{4n}$. The constant $n \geq 10$ is necessary to ensure convergence between the Gaussian Q-function and its trapezoidal approximation.

6.1.2 Analytical ABEP of transmit antenna pair index estimation

The formulation of the ABEP related to the identification of transmit antenna pair indices, denoted as P_a, aligns with the methodology presented in [10] and [7]. It is worth noting that, in contrast to the C-SM and C-GSM schemes, the MAA-GSM-LD system incorporates four active transmit antennas during each transmission interval. Consequently, by following the approach established by Naidoo *et al.* [7], and Pillay *et al.* [10], the expression for P_a can be derived as

$$P_a \leq \sum_{K=1}^{N_T}\sum_{q=1}^{M^2}\sum_{\hat{K}=1}^{N_T} \frac{N(K,\hat{K})\mu_\alpha^{N_R}\sum_{\omega=0}^{N_R-1}\binom{N_R-1+\omega}{\omega}\left(1-\mu_\alpha\right)^\omega}{M^2 N_T} \tag{C.8}$$

where $N(k,\hat{k})$ is the number of bits in error between the transmit antenna pair index K and the estimated transmit antenna pair index $\hat{K}$. $\mu_\alpha = \frac{1}{2}\left(1 - \sqrt{\frac{\sigma_{\alpha^2}}{1+\sigma_{\alpha^2}}}\right)$ and $\sigma_{\alpha^2} = \frac{\rho}{8}|S_q^1|^2$ as described in [10] and [7].

6.2 Error performance analysis of GCQSM-LD

From [13, 16, 24, 26–28], the ABEP of GCQSM-LD can be derived following the well-known bounding techniques. Thus, following the same approach as [16, 26, 27], the ABEP of GCQSM-LD is defined as

$$P_e \leq \frac{1}{\mathfrak{m}2^{\mathfrak{m}}} \sum_{q=1}^{2^{\mathfrak{m}}} \sum_{\hat{q}=1}^{2^{\mathfrak{m}}} N\left(q, \hat{q}\right) P(\mathbf{x} \rightarrow \hat{\mathbf{x}}), \tag{C.9}$$

where $N_{(q,\hat{q})}$, represents the count of erroneous bits linked to the pairwise error probability (PEP) event denoted as $P(\mathbf{x} \rightarrow \hat{\mathbf{x}}|\mathbf{H})$. This PEP event pertains to the comparison between the transmitted vector $\mathbf{x}$ and the received vector $\hat{\mathbf{x}}$. The formulation for the conditional PEP is expressed as follows:

$$P(\mathbf{x} \rightarrow \hat{\mathbf{x}}) = \left(\frac{1}{2n}\right) \left[\left(\frac{1}{2}\right) \left(1 + \frac{\rho \left(\sum_{l=1}^{8} (D_l)^2\right)}{32}\right)^{-N_R} + \sum_{v=1}^{n-1} \left(1 + \frac{\rho \left(\sum_{l=1}^{8} (D_l)^2\right)}{16\mu_v}\right)^{-N_R} \right], \tag{C.10}$$

where $\mu_v = 2\sin^2\left(\frac{v\pi}{2n}\right)$, $n \geq 6$ is the number of summations for convergence, $d_i = \left[\left(S_q^{iI} - S_{\hat{q}}^{iI}\right) e^{j\theta_k}\right]$, $d_{i+2} = \left[\left(\tilde{S}_q^{iI} - \tilde{S}_{\hat{q}}^{iI}\right) e^{j\theta_k}\right]$, $d_{(i+4)} = \left[\left(S_q^{iQ} - S_{\hat{q}}^{iQ}\right) e^{j\theta_k}\right]$, $d_{i+6} = \left[\left(\tilde{S}_q^{iQ} - \tilde{S}_{\hat{q}}^{iQ}\right) e^{j\theta_k}\right]$ and $i \in [1:2]$. $D_l = |d_l|$ and $l \in [1:8]$. The derivation of the conditional PEP is found in Appendix A.2 of Part (IV).

6.3 Diversity analysis of the GCQSM-LD scheme

It follows on the simplification of (C.10) that,

$$P(\mathbf{x} \rightarrow \hat{\mathbf{x}}) = \left(\frac{1}{2n}\right) \left[\left(\frac{1}{2}\right) \left(1 + \frac{\rho D_u}{32}\right)^{-N_R} + \sum_{v=1}^{n-1} \left(1 + \frac{\rho D_u}{16\mu_v}\right)^{-N_R} \right], \tag{C.11}$$

where $D_u = \sum_{l=1}^{8} (D_l)^2$. At high SNRs, $\left(\frac{\rho D_u}{32} >> 1\right)$ and $\left(\frac{\rho D_u}{16\mu_v} >> 1\right)$. Hence, $P(\mathbf{x} \rightarrow \hat{\mathbf{x}})$ can be approximated at high SNRs as

$$P(\mathbf{x} \rightarrow \hat{\mathbf{x}}) \cong \left(\frac{1}{2n}\right) \left[\left(\frac{1}{2}\right) \left(\frac{\rho D_u}{32}\right)^{-N_R} + \sum_{v=1}^{n-1} \left(\frac{\rho D_u}{16\mu_v}\right)^{-N_R} \right]. \tag{C.12}$$

Further simplification leads (C.12) into (C.13),

$$P(\mathbf{x} \to \hat{\mathbf{x}}) \cong \left(\frac{1}{2n}\right)\left[\left(\frac{1}{2}\right) + \sum_{v=1}^{n-1}\left(\frac{2}{\mu_v}\right)^{-N_R}\right]\left(\frac{D_u}{32}\right)^{-N_R}\rho^{-N_R}. \tag{C.13}$$

The overall diversity gain (G_c) attained by a MIMO-SM scheme has been defined in [29], as

$$-G_c = \lim_{SNR\to\infty}\left\{\frac{\log\left(P_b(SNR)\right)}{\log(SNR)}\right\}, \tag{C.14}$$

where P_b denotes the overall probability of error as a function of SNR. Hence given $P_b(SNR) = P(\mathbf{x} \to \hat{\mathbf{x}})$ as given in (C.13), then (C.14) becomes

$$-G_c = \lim_{\rho\to\infty}\left\{\frac{\log\left(P(\mathbf{x} \to \hat{\mathbf{x}})\right)}{\log(\rho)}\right\}. \tag{C.15}$$

Hence substituting (C.13) into (C.15), leads to (C.16).

$$-G_c = \lim_{\rho\to\infty}\left\{\frac{\log\left(\beta\rho^{-N_R}\right)}{\log(\rho)}\right\}, \tag{C.16}$$

where $\beta = \left(\frac{1}{2n}\right)\left[\left(\frac{1}{2}\right) + \sum_{v=1}^{n-1}\left(\frac{2}{\mu_v}\right)^{-N_R}\right]\left(\frac{D_u}{32}\right)^{-N_R}$.

Since $\lim_{\rho\to\infty}\left(\frac{\log(\beta)}{\log(\rho)}\right) = 0$, therefore $G_c = N_R$. Hence the diversity gain of the proposed system is N_R.

7 Simulation and numerical results analysis

This section presents simulation results for the proposed MAA-GSM-LD and GCQSM-LD systems with varying numbers of transmit antennas. This section also entails the comparison of these schemes with a selection of the best-performing schemes from Part (II) and Part (III). The schemes chosen for comparison include GCQSM, MIMO-GSM, Golden codeword-based GSM (GCW-GSM), and GQSM-AG.

To evaluate the ABEP for the GCW-GSM scheme in the comparisons, equation $(A.4)$ from Part (II) was used. For MIMO-GSM, equation (16) from Wang *et al.* [11] was used, and for GQSM-AG,

equation (9) from [13] was utilised.

The goal of this section is to validate the theoretical performance bounds that were derived in subsections 6.1 and 6.2. The BER of the proposed schemes was assessed using Monte Carlo simulations conducted over i.i.d Rayleigh frequency-flat fading channels with AWGN. Specifically, the BER performance of MAA-GSM-LD was evaluated at different SEs ($\mathfrak{m} = 11\ bits/s/Hz$ and $\mathfrak{m} = 15\ bits/s/Hz$), and the BER performance of GCQSM-LD was evaluated at $\mathfrak{m} = 14\ bits/s/Hz$ and $\mathfrak{m} = 18\ bits/s/Hz$ as functions of the average SNR. The results for these four SEs are depicted in Figs. C.9-C.12. All comparisons were made under consistent conditions, including $N_R = 4$ antennas in all scenarios, the same SE, optimal MLD method, and at a BER of 1×10^{-5} for reference.

To begin, Figs. C.9 and C.11 illustrate the BER performance of the MAA-GSM-LD and GCQSM-LD schemes, respectively, with varying numbers of transmit antennas, specifically $N_T = 6$ and $N_T = 8$. In these figures (C.9 and C.11), the analytical results for both MAA-GSM-LD and GCQSM-LD are validated through simulations, and it is evident that the agreement between the simulations and the analytical derivations tightens as the SNR values increase. This tight correspondence at high SNR levels can be attributed to the predominant influence of the probability of detection (P_d) in MAA-GSM-LD and the upper-bound ABER performance in the GCQSM-LD scheme.

Moving on, Fig. C.10 and Table C.3 provide insight into the error performance gains of the proposed 6×4 MAA-GSM-LD scheme when compared to other 6×4 schemes with the same SE of $\mathfrak{m} = 11$ $bits/s/Hz$. As indicated in Fig. C.10 and Table C.3, the proposed MAA-GSM-LD scheme demonstrates a performance gain of $1.0\ dB$ over the 6×4 GCQSM-C-16-QAM scheme, $4.3\ dB$ over the 6×4 GCW-GSM-C-64-QAM scheme, and $1.2\ dB$ over the 6×4 MIMO-GSM-C-16-QAM scheme. Wang *et al.* [11], discussed MIMO-GSM, highlighting its superior performance over C-SM and C-GSM schemes with similar SEs. Additionally, in Part (III), it was observed that GCQSM schemes outperformed MIMO-GSM schemes. Consequently, the proposed MAA-GSM-LD scheme exhibits performance gains over all the schemes in this study, surpassing GCQSM and the best-performing schemes from Part (III) and the existing literature [11, 25]. This improvement can likely be attributed to the use of optimised labelling maps with multiple active antennas, which enhances spatial diversity and, consequently, the error performance.

Figs. C.12 and Table C.4 provide a performance comparison for the proposed GCQSM-LD scheme at an SE of $\mathfrak{m} = 14\ bits/s/Hz$, with $N_R = 4$ antennas and varying numbers of transmit antennas. In Fig. C.12, the 8×4 GCQSM-LD-C-16-QAM scheme is compared with two of the best 4×4 schemes from Parts (II) and (III), all operating at an SE of $\mathfrak{m} = 14\ bits/s/Hz$. As depicted in Fig. C.12 and Table C.4, the proposed 8×6 GCQSM-LD-C-16-QAM scheme outperforms the 4×4 GQSM-AG-C-32-QAM scheme by $3.6\ dB$ and the 4×4 GCQSM-C-64-QAM scheme by $4.7\ dB$. This demonstrates that the proposed GCQSM-LD scheme surpasses all the schemes from Parts (II) and (III), outperforming GQSM-AG, which was one of the best schemes discussed in the literature [11, 13, 25] and the results from Part (II). This performance can likely be attributed to the use of optimised labelling maps, multiple active antennas, and QSM attributes, all of which enhance spatial diversity and, in turn, improve the error performance of the proposed GCQSM-LD scheme.

Finally, it should be noted that the proposed schemes are limited in terms of the order of modulation (M) (LD with 16-QAM and 64-QAM only), which determines the SE ($\mathfrak{m}$) and the number of receive antennas as discussed in the CCA of Section 5. MAA-GSM-LD is limited to 11 and 15 $bits/s/Hz$, whereas, GCQSM-LD is limited to 14 and 18 $bits/s/Hz$. Anything above the speculated number of SEs results in a much worse MLD complexity that inhibits the systems. Hence it should be noted that due to the aforementioned limitations, the proposed schemes could not be compared against each other and other various schemes of different SE ($\mathfrak{m}$) as they would be incompatible.

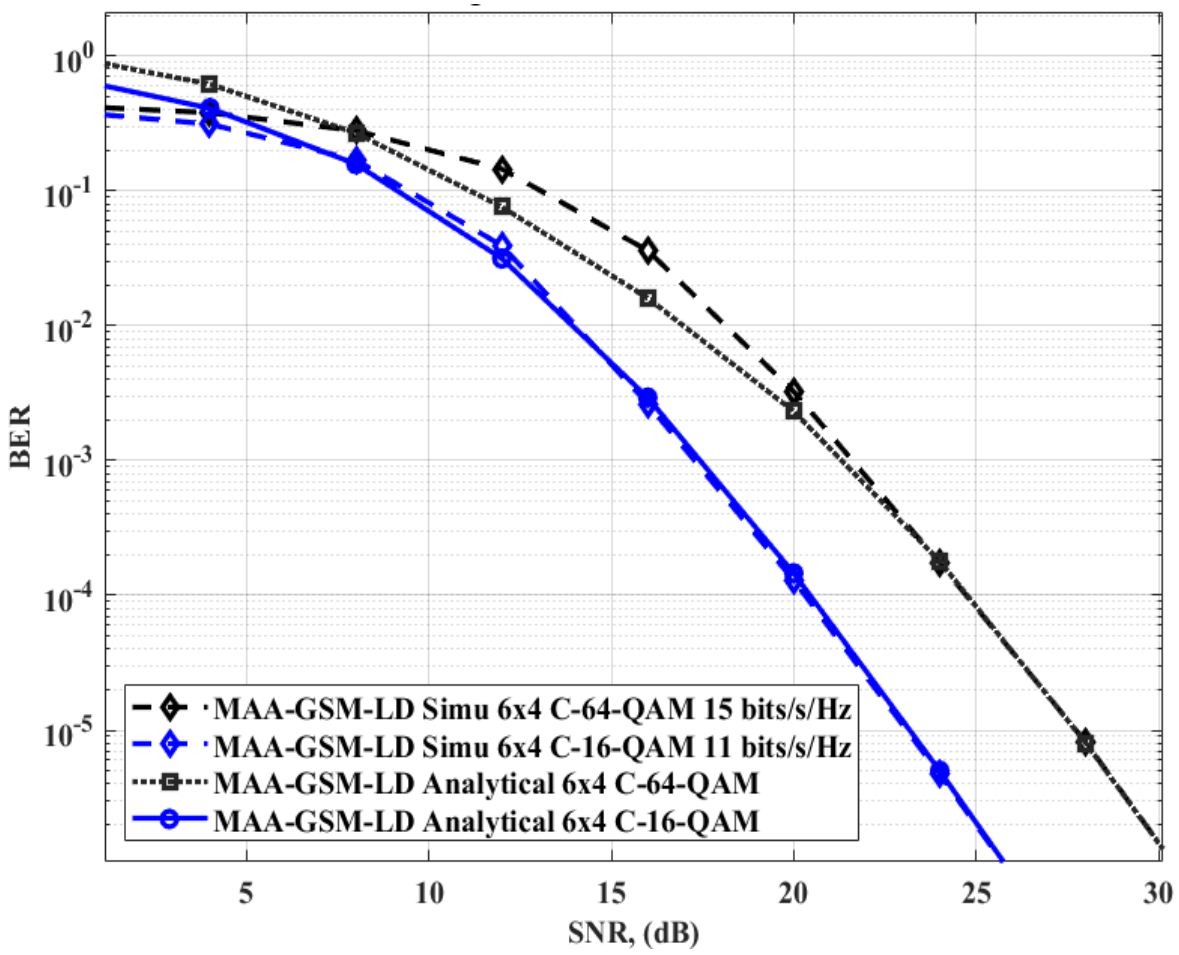

Fig. C.9: 6×4 MAA-GSM-LD 16-QAM and 64-QAM analytical and simulation results.

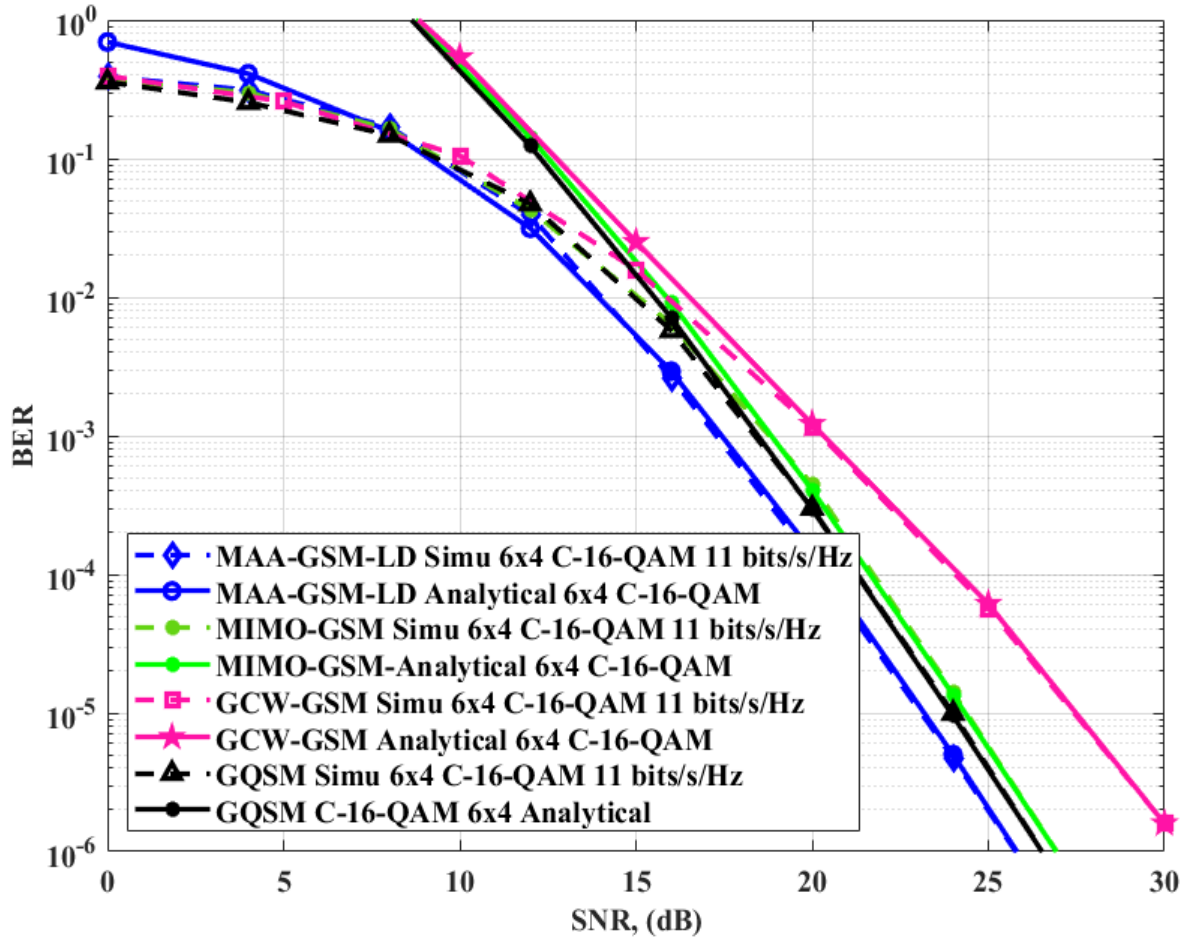

Fig. C.10: Comparison of 4×6 MAA-GSM-LD 16-QAM with various schemes of the same *SE* (11 $bits/s/Hz$), same $N_T = 6$ and $N_R = 4$.

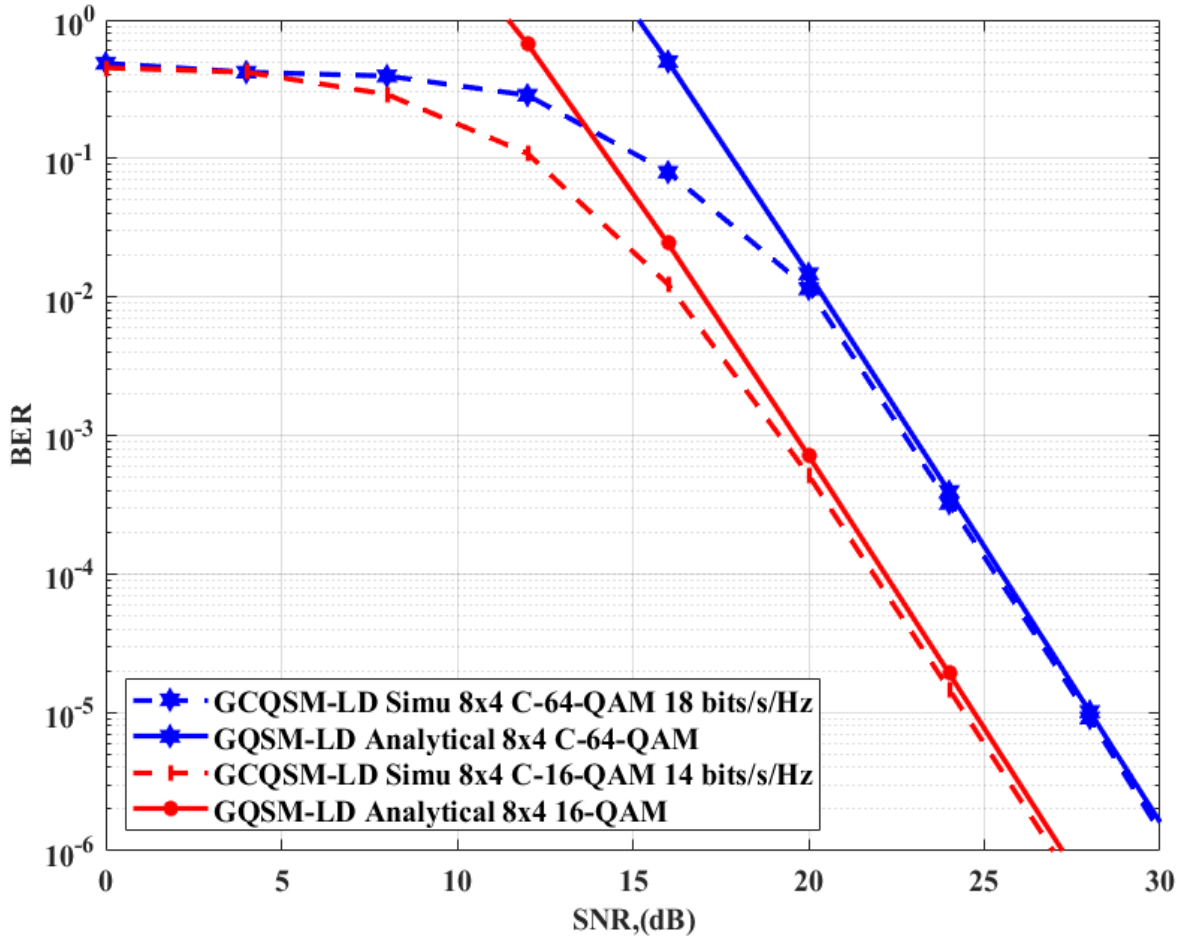

Fig. C.11: 8×4 GCQSM-LD 16-QAM and 64-QAM analytical and simulation results.

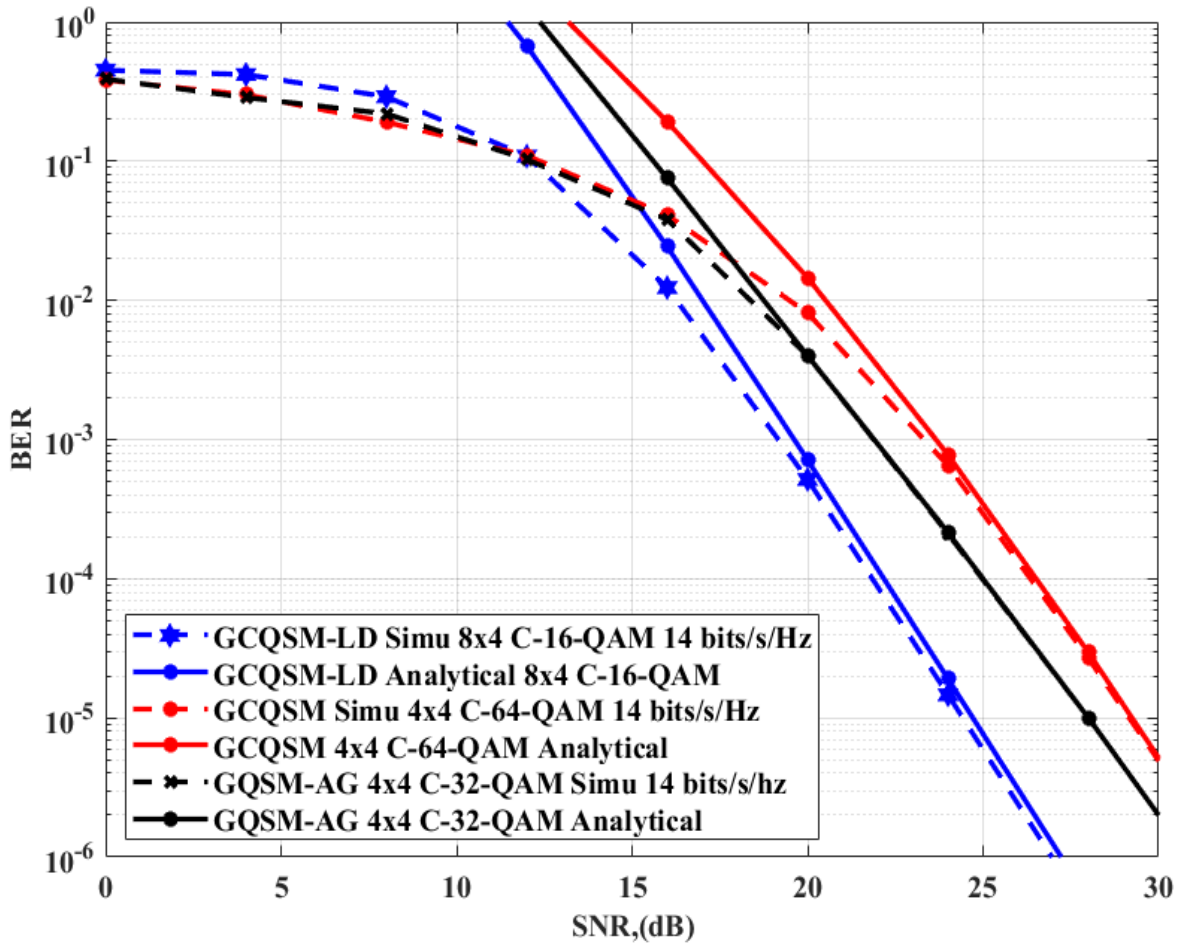

Fig. C.12: Comparison of GCQSM-LD with various schemes of the same *SE* and N_R.

Table C.3: 6×4 MAA-GSM-LD 16-QAM error performance gains over 6×4 various schemes of the same $N_R = 4$, $\mathfrak{m} = 11$ $bits/s/Hz$ and at a BER of 10^{-5}.

Scheme	MAA-GSM-LD 16-QAM proposed scheme (dB) gain
6×4 GQSM-C-16-QAM	1.00
6×4 GCW-GSM-16QAM	4.30
6×4 MIMO-GSM-C-16-QAM	1.20

Table C.4: 8×4 GCQSM-LD 16-QAM error performance gains over various schemes of the same $N_R = 4$, $\mathfrak{m} = 14\ bits/s/Hz$ and at a BER of 10^{-5}.

Scheme	GCQSM-LD 16-QAM proposed scheme (dB) gain
4×4 GQSM-AG-C-32-QAM	3.60
4×4 GCQSM-C-64-QAM	4.70

8 Conclusion

This study, introduced the proposed MAA-GSM-LD and GCQSM-LD schemes as enhancements to improve the error performance of existing GSM and GQSM schemes, much in the same way as presented in Parts (II) and (III), respectively. These schemes represent an evolution of GSM and GQSM by integrating optimised labelling maps and multiple active antennas into the GSM and GQSM systems. Additionally, this research derived analytical formulas for union and upper-bound error performance for the proposed schemes, focusing on i.i.d Rayleigh frequency-flat fading channels. The derived analytical bounds were validated through the use of Monte Carlo simulations, demonstrating their increasingly accurate alignment with observed results as SNR values rose. The outcomes of the investigation revealed that the proposed MAA-GSM-LD and GCQSM-LD schemes outperformed the most prominent schemes in the literature, including GCQSM, GQSM-AG, and MIMO-GSM. Consequently, it can be concluded that MAA-GSM-LD and GCQSM-LD offer viable solutions for enhancing the error performance of MIMO-SM schemes. However, it is essential to acknowledge that the proposed schemes have a high-complexity MLD process. As part of future research, the author aims to explore and develop low-complexity detection methods for these proposed schemes. Furthermore, the author intends to extend the work by exploring the incorporation of Golden codewords to the MAA-GSM-LD and GCQSM-LD schemes, with the aim to further enhance the SE of MIMO-SM systems.

References

[1] C. K. Agubor, F. K. Opara, and G. N. Eze, "A Review of Diversity Techniques for Wireless Communications," *Academic Research International (ARInt.)*, vol. 4, no. 2, pp. 157–167, Mar. 2013.

[2] M. Liu, M. Helard, J. F. Helard, and M. Crussiere, "A fast decodable full-rate STBC with high coding gain for 4× 2 MIMO systems," in *2013 IEEE 24th Annual International Symposium on Personal, Indoor, and Mobile Radio Communications (PIMRC)*. IEEE, Sep. 2013, pp. 677–681.

[3] D. J. Love and R. W. Heath, "Equal gain transmission in multiple-input multiple-output wireless systems," *IEEE Transactions on Communications*, vol. 51, no. 7, pp. 1102–1110, Jul. 2003.

[4] M. K. Simon and M. S. Alouini, *Digital communication over generalized fading channels: a unified approach to performance analysis*. New York: Wiley-Interscience Publication, 2000.

[5] R. Y. Mesleh, H. Haas, S. Sinanovic, C. W. Ahn, and S. Yun, "Spatial modulation," *IEEE Transactions on Vehicular Technology*, vol. 57, no. 4, pp. 2228–2241, Jul. 2008.

[6] J. Jeganathan, A. Ghrayeb, and L. Szczecinski, "Spatial modulation: Optimal detection and performance analysis," *IEEE Communications Letters*, vol. 12, no. 8, pp. 545–547, Aug. 2008.

[7] N. R. Naidoo, H. Xu, and T. A. Quazi, "Spatial modulation: optimal detector asymptotic performance and multiple-stage detection," *IET communications*, vol. 5, no. 10, pp. 1368–1376, Jul. 2011.

[8] A. Younis, N. Serafimovski, R. Mesleh, and H. Haas, "Generalised spatial modulation," in *2010 conference record of the forty fourth Asilomar conference on signals, systems and computers*. IEEE, Nov. 2010, pp. 1498–1502.

[9] S. Afridi and S. A. Hassan, "Spectrally efficient adaptive generalized spatial modulation MIMO systems," in *2017 14th IEEE Annual Consumer Communications & Networking Conference (CCNC)*. IEEE, Jan. 2017, pp. 260–263.

[10] R. Pillay, N. Pillay, and H. Xu, "Improved error performance for generalised spatial modulation with enhanced spectral efficiency," *International Journal of Communication Systems*, vol. 33, no. 2, p. e4176, Jan. 2020.

[11] J. Wang, S. Jia, and J. Song, "Generalised spatial modulation system with multiple active transmit antennas and low complexity detection scheme," *IEEE Transactions on Wireless Communications*, vol. 11, no. 4, pp. 1605–1615, Mar. 2012.

[12] R. Y. Mesleh, S. S. Ikki, and H. M. Aggoune, "Quadrature spatial modulation," *IEEE Transactions on Vehicular Technology*, vol. 64, no. 6, pp. 2738–2742, Jul. 2014.

[13] F. Castillo-Soria, J. Cortez-González, R. Ramirez-Gutierrez, M. M.-B. Fermín, and L. Soriano-Equigua, "Generalized quadrature spatial modulation scheme using antenna grouping," *ETRI Journal*, vol. 39, no. 5, pp. 707–717, Oct. 2017.

[14] S. Oladoyinbo, N. Pillay, and H. Xu, "Adaptive quadrature spatial modulation," *IETE Technical Review*, vol. 37, no. 6, pp. 579–590, Nov. 2020.

[15] S. Kim, "Antenna selection schemes in quadrature spatial modulation systems," *ETRI Journal*, vol. 38, no. 4, pp. 606–611, Aug. 2016.

[16] M. Mohaisen, "Generalised complex quadrature spatial modulation," *Wireless Communications and Mobile Computing*, vol. 2019, no. 1, p. 3137927, Apr. 2019.

[17] M. Krasicki, "Improved labelling diversity for iteratively-decoded multi-antenna systems," in *2011 7th International Wireless Communications and Mobile Computing Conference*. IEEE, Aug. 2011, pp. 359–364.

[18] ——, "Essence of 16-qam labelling diversity," *Electronics letters*, vol. 49, no. 8, pp. 567–569, Apr. 2013.

[19] H. Xu, K. Govindasamy, and N. Pillay, "Uncoded space-time labeling diversity," *IEEE Communications Letters*, vol. 20, no. 8, pp. 1511–1514, Aug. 2016.

[20] K. Govindasamy, H. Xu, and N. Pillay, "Space-time block coded spatial modulation with labelling diversity," *International Journal of Communication Systems*, vol. 31, no. 1, p. e3395, Jan. 2018.

[21] B. S. Adejumobi and T. Shongwe, "Labeling diversity for media-based space-time block coded spatial modulation," *IEEE Access*, vol. 8, no. 1, pp. 99 870–99 879, May. 2020.

[22] S. E. Krouk, *Modulation and Coding Techniques in Wireless Communications*. New Jersey: John Wiley & Sons Ltd,, 2011.

[23] N. Sibanda, H. Xu, and N. Pillay, "Golden codeword-based generalized spatial modulation," *International Journal of Communication Systems*, vol. 39, no. 10, p. e5144, Mar. 2022.

[24] ——, "Error performance analysis of generalized quadrature spatial modulation using h-8qam," *Scientific Reports*, vol. 12, no. 1, pp. 1–13, Nov. 2022.

[25] N. R. Naidoo, "Enhanced performance and efficiency schemes for generalised spatial modulation," Ph.D. dissertation, University of KwaZulu-Natal, 2017.

[26] L. Xiao, Y. Xiao, C. Xu, X. Lei, P. Yang, S. Li, and L. Hanzo, "Compressed-sensing assisted spatial multiplexing aided spatial modulation," *IEEE Transactions on Wireless Communications*, vol. 17, no. 2, pp. 794–807, Feb. 2018.

[27] L. Xiao, P. Xiao, Y. Xiao, H. Haas, A. Mohamed, and L. Hanzo, "Compressive sensing assisted generalized quadrature spatial modulation for massive mimo systems," *IEEE Transactions on Communications*, vol. 67, no. 7, pp. 4795–4810, Jul. 2019.

[28] T. Holoubi, S. Murtala, N. Muchena, and M. Mohaisen, "On the performance of improved quadrature spatial modulation," *ETRI Journal*, vol. 42, no. 4, pp. 562–574, Aug. 2020.

[29] L. Zheng and D. Tse, "Diversity and multiplexing: A fundamental tradeoff in multiple-antenna channels," *IEEE Transactions on information theory,*, vol. 49, no. 5, pp. 1073–1096, May. 2003.

[30] F. Cogen and E. Aydin, "Hexagonal quadrature amplitude modulation aided spatial modulation," in *2019 11th International Conference on Electrical and Electronics Engineering (ELECO)*. IEEE, Nov. 2017, pp. 730–733.

[31] ——, "Performance analysis of hexagonal qam constellations on quadrature spatial modulation with perfect and imperfect channel estimation," *Physical Communication*, vol. 47, no. 1, p. 101379, May. 2021.

[32] A. Koc, I. Altunbas, and E. Basar, "Full-duplex spatial modulation systems under imperfect channel state information," in *2017 24th International Conference on Telecommunications (ICT)*. IEEE, May. 2017, pp. 1–5.

[33] H. Xu, "Symbol Error probability for Generalised Selection Combining reception of M-QAM," *SAIEE Africa Research Journal*, vol. 100, no. 3, pp. 68–71, Sep. 2009.

A Appendix C

A.1 Gray-coded maps and optimised labelling maps

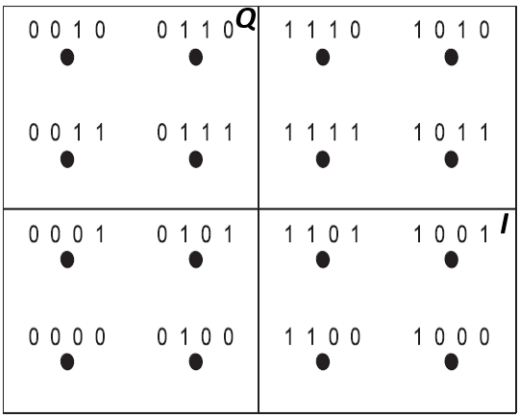

Fig. C.13: 16-QAM Gray-coded labelling map $\mathfrak{G}_1^{16}$ [19]

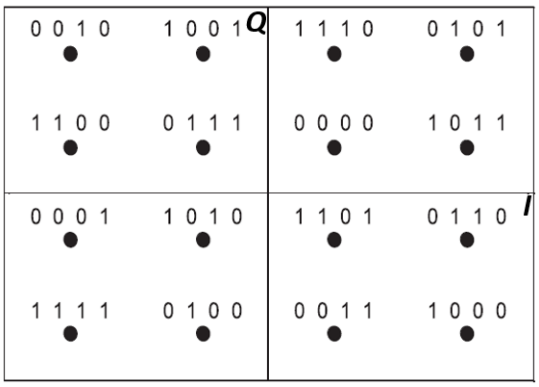

Fig. C.14: Optimised 16-QAM labelling map $\mathfrak{G}_2^{16}$ [19]

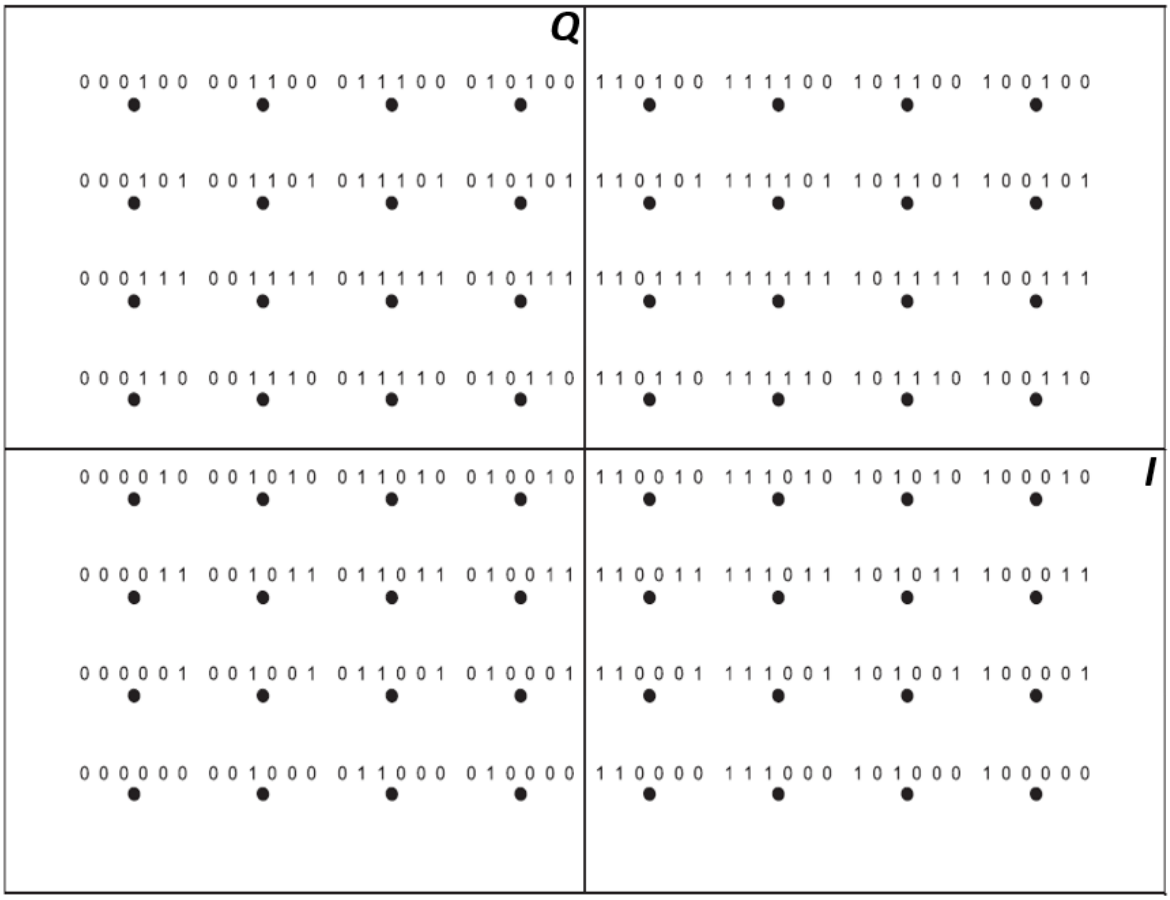

Fig. C.15: 64-QAM Gray-coded labelling map $\mathfrak{G}_1^{64}$ [20]

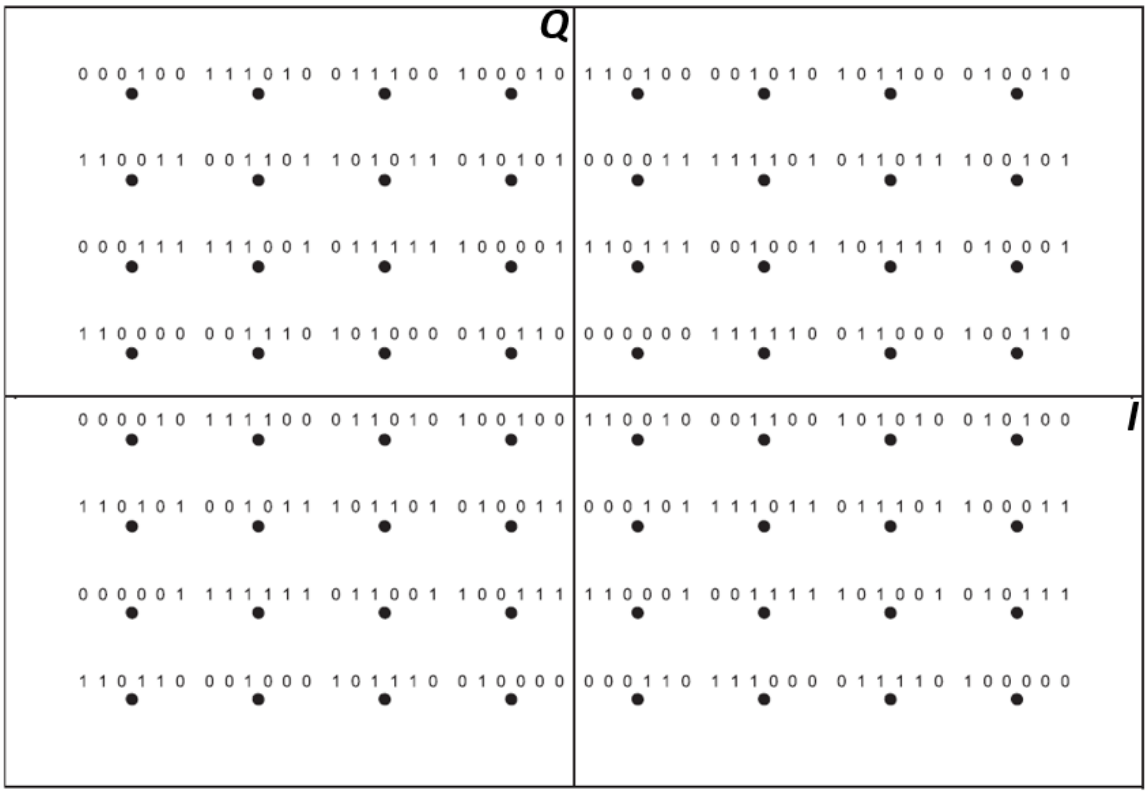

Fig. C.16: Optimised 64-QAM labelling map $\mathfrak{G}_2^{64}$ [20]

Table C.5: I and Q dimension antenna combinations and mapping ($N_T = 8$ and $N_c = 64$) [25, 30, 31]

Spatial input bits	Antenna pair bit indices	I-dimension antenna pairs	Q-dimension antenna pairs	Rotation angle
$\boldsymbol{d}$	000000	T_{X1}, T_{X2}	T_{X5}, T_{X6}	0
$\boldsymbol{d}$	000001	T_{X1}, T_{X3}	T_{X4}, T_{X6}	0
$\boldsymbol{d}$	000010	T_{X1}, T_{X4}	T_{X3}, T_{X6}	0
$\boldsymbol{d}$	000011	T_{X1}, T_{X5}	T_{X2}, T_{X6}	$\frac{\pi}{3}$
$\boldsymbol{d}$	000100	T_{X1}, T_{X6}	T_{X4}, T_{X5}	$\frac{\pi}{3}$
$\boldsymbol{d}$	000101	T_{X2}, T_{X3}	T_{X1}, T_{X4}	$\frac{\pi}{3}$
$\boldsymbol{d}$	000110	T_{X2}, T_{X4}	T_{X1}, T_{X3}	$\frac{2\pi}{3}$
$\boldsymbol{d}$	000111	T_{X2}, T_{X5}	T_{X3}, T_{X4}	$\frac{2\pi}{3}$
$\boldsymbol{d}$	001000	T_{X1}, T_{X2}	T_{X5}, T_{X6}	0
$\boldsymbol{d}$	001001	T_{X1}, T_{X3}	T_{X4}, T_{X6}	0
$\boldsymbol{d}$	001010	T_{X1}, T_{X4}	T_{X3}, T_{X6}	0
$\boldsymbol{d}$	001011	T_{X1}, T_{X5}	T_{X2}, T_{X6}	$\frac{\pi}{3}$
$\boldsymbol{d}$	001100	T_{X1}, T_{X6}	T_{X4}, T_{X5}	$\frac{\pi}{3}$
$\boldsymbol{d}$	001101	T_{X2}, T_{X3}	T_{X1}, T_{X4}	$\frac{\pi}{3}$
$\boldsymbol{d}$	001110	T_{X2}, T_{X4}	T_{X1}, T_{X3}	$\frac{2\pi}{3}$
$\boldsymbol{d}$	001111	T_{X2}, T_{X5}	T_{X3}, T_{X4}	$\frac{2\pi}{3}$
$\boldsymbol{d}$	010000	T_{X1}, T_{X2}	T_{X5}, T_{X6}	0
$\boldsymbol{d}$	010001	T_{X1}, T_{X3}	T_{X4}, T_{X6}	0
$\boldsymbol{d}$	010010	T_{X1}, T_{X4}	T_{X3}, T_{X6}	0
$\boldsymbol{d}$	010011	T_{X1}, T_{X5}	T_{X2}, T_{X6}	$\frac{\pi}{3}$
$\boldsymbol{d}$	010100	T_{X1}, T_{X6}	T_{X4}, T_{X5}	$\frac{\pi}{3}$
$\boldsymbol{d}$	010101	T_{X2}, T_{X3}	T_{X1}, T_{X4}	$\frac{\pi}{3}$

Table C.6: Continuation of *I* and *Q* dimension antenna combinations and mapping ($N_T = 8$ and $N_c = 64$)

Spatial input bits	Antenna pair bit indices	I-dimension antenna pairs	Q-dimension antenna pairs	Rotation angle
$\boldsymbol{d}$	010110	T_{X2}, T_{X4}	T_{X1}, T_{X3}	$\frac{2\pi}{3}$
$\boldsymbol{d}$	010111	T_{X2}, T_{X5}	T_{X3}, T_{X4}	$\frac{2\pi}{3}$
$\boldsymbol{d}$	011000	T_{X1}, T_{X2}	T_{X5}, T_{X6}	0
$\boldsymbol{d}$	011001	T_{X1}, T_{X3}	T_{X4}, T_{X6}	0
$\boldsymbol{d}$	011010	T_{X1}, T_{X4}	T_{X3}, T_{X6}	0
$\boldsymbol{d}$	011011	T_{X1}, T_{X5}	T_{X2}, T_{X6}	$\frac{\pi}{3}$
$\boldsymbol{d}$	011100	T_{X1}, T_{X6}	T_{X4}, T_{X5}	$\frac{\pi}{3}$
$\boldsymbol{d}$	011101	T_{X2}, T_{X3}	T_{X1}, T_{X4}	$\frac{\pi}{3}$
$\boldsymbol{d}$	011110	T_{X2}, T_{X4}	T_{X1}, T_{X3}	$\frac{2\pi}{3}$
$\boldsymbol{d}$	011111	T_{X2}, T_{X5}	T_{X3}, T_{X4}	$\frac{2\pi}{3}$
$\boldsymbol{d}$	100000	T_{X1}, T_{X2}	T_{X5}, T_{X6}	0
$\boldsymbol{d}$	100001	T_{X1}, T_{X3}	T_{X4}, T_{X6}	0
$\boldsymbol{d}$	100010	T_{X1}, T_{X4}	T_{X3}, T_{X6}	0
$\boldsymbol{d}$	100011	T_{X1}, T_{X5}	T_{X2}, T_{X6}	$\frac{\pi}{3}$
$\boldsymbol{d}$	100100	T_{X1}, T_{X6}	T_{X4}, T_{X5}	$\frac{\pi}{3}$
$\boldsymbol{d}$	100101	T_{X2}, T_{X3}	T_{X1}, T_{X4}	$\frac{\pi}{3}$
$\boldsymbol{d}$	100110	T_{X2}, T_{X4}	T_{X1}, T_{X3}	$\frac{2\pi}{3}$
$\boldsymbol{d}$	100101	T_{X2}, T_{X3}	T_{X1}, T_{X4}	$\frac{\pi}{3}$
$\boldsymbol{d}$	100110	T_{X2}, T_{X4}	T_{X1}, T_{X3}	$\frac{2\pi}{3}$

Table C.7: Continuation of *I* and *Q* dimension antenna combinations and mapping ($N_T = 8$ and $N_c = 64$)

Spatial input bits	Antenna pair bit indices	I-dimension antenna pairs	Q-dimension antenna pairs	Rotation angle
$\boldsymbol{d}$	101011	T_{X1}, T_{X5}	T_{X2}, T_{X6}	$\frac{\pi}{3}$
$\boldsymbol{d}$	101000	T_{X1}, T_{X6}	T_{X4}, T_{X5}	$\frac{\pi}{3}$
$\boldsymbol{d}$	101001	T_{X2}, T_{X3}	T_{X1}, T_{X4}	$\frac{\pi}{3}$
$\boldsymbol{d}$	101010	T_{X2}, T_{X4}	T_{X1}, T_{X3}	$\frac{2\pi}{3}$
$\boldsymbol{d}$	101111	T_{X2}, T_{X5}	T_{X3}, T_{X4}	$\frac{2\pi}{3}$
$\boldsymbol{d}$	110000	T_{X1}, T_{X2}	T_{X5}, T_{X6}	0
$\boldsymbol{d}$	110001	T_{X1}, T_{X3}	T_{X4}, T_{X6}	0
$\boldsymbol{d}$	110010	T_{X1}, T_{X4}	T_{X3}, T_{X6}	0
$\boldsymbol{d}$	110011	T_{X1}, T_{X5}	T_{X2}, T_{X6}	$\frac{\pi}{3}$
$\boldsymbol{d}$	110100	T_{X1}, T_{X6}	T_{X4}, T_{X5}	$\frac{\pi}{3}$
$\boldsymbol{d}$	110101	T_{X2}, T_{X3}	T_{X1}, T_{X4}	$\frac{\pi}{3}$
$\boldsymbol{d}$	110110	T_{X2}, T_{X4}	T_{X1}, T_{X3}	$\frac{2\pi}{3}$
$\boldsymbol{d}$	110111	T_{X2}, T_{X5}	T_{X3}, T_{X4}	$\frac{2\pi}{3}$
$\boldsymbol{d}$	111000	T_{X1}, T_{X2}	T_{X5}, T_{X6}	0
$\boldsymbol{d}$	111001	T_{X1}, T_{X3}	T_{X4}, T_{X6}	0
$\boldsymbol{d}$	111010	T_{X1}, T_{X4}	T_{X3}, T_{X6}	0
$\boldsymbol{d}$	111011	T_{X1}, T_{X5}	T_{X2}, T_{X6}	$\frac{\pi}{3}$
$\boldsymbol{d}$	111100	T_{X1}, T_{X6}	T_{X4}, T_{X5}	$\frac{\pi}{3}$
$\boldsymbol{d}$	111101	T_{X2}, T_{X3}	T_{X1}, T_{X4}	$\frac{\pi}{3}$
$\boldsymbol{d}$	111110	T_{X2}, T_{X4}	T_{X1}, T_{X3}	$\frac{2\pi}{3}$
$\boldsymbol{d}$	111111	T_{X2}, T_{X5}	T_{X3}, T_{X4}	$\frac{2\pi}{3}$

A.2 Derivation of the PEP

Based on the equivalent system model in $(C.4)$, the conditional PEP, $P(\mathbf{x} \rightarrow \hat{\mathbf{x}})$ can be formulated as

$$P(\mathbf{x} \rightarrow \hat{\mathbf{x}}|\mathbf{H}) = P\left(\left\|\mathbf{y} - \sqrt{\frac{\rho}{8}}\mathbf{H}\mathbf{x}\right\|_F^2 > \left\|\mathbf{y} - \sqrt{\frac{\rho}{8}}\mathbf{H}\hat{\mathbf{x}}\right\|_F^2\right). \tag{C.17}$$

Substituting $(C.4)$ into $(C.17)$ leads to

$$P(\mathbf{x} \rightarrow \hat{\mathbf{x}}|\mathbf{H}) = P\left(A > B\right), \tag{C.18}$$

where $A = \|\mathbf{n}\|_F^2$, $B = \frac{\rho}{8}\left\|\sum_{l=1}^{8}\mathbf{h}_{k_l}d_l + \mathbf{n}\right\|_F^2$, $d_i = \left[\left(S_q^{iI} - S_{\hat{q}}^{iI}\right)e^{j\theta_k}\right]$, $d_{i+2} = \left[\left(\tilde{S}_q^{iI} - \tilde{S}_{\hat{q}}^{iI}\right)e^{j\theta_k}\right]$, $d_{(i+4)} = \left[\left(S_q^{iQ} - S_{\hat{q}}^{iQ}\right)e^{j\theta_k}\right]$, $d_{i+6} = \left[\left(\tilde{S}_q^{iQ} - \tilde{S}_{\hat{q}}^{iQ}\right)e^{j\theta_k}\right]$ and $i \in [1:2]$.

Equation (C.18) can also be rewritten as;

$$P(\mathbf{x} \rightarrow \hat{\mathbf{x}}|\mathbf{H}) = P\left(A > C + A + D\right), \tag{C.19}$$

where $C = \frac{\rho}{8}\left\|\sum_{l=1}^{8}\mathbf{h}_{k_l}d_l\right\|_F^2$ and $D = 2\Re\{\sqrt{\frac{\rho}{8}}\mathbf{n}^H\left(\sum_{l=1}^{8}\mathbf{h}_{k_l}d_l\right)\}$.

Simplifying Equation (C.19) leads to (C.20).

$$P(\mathbf{x} \rightarrow \hat{\mathbf{x}}|\mathbf{H}) = P\left(\frac{1}{2}D < \frac{1}{2}C\right). \tag{C.20}$$

As $\mathbf{n}^H$ is an element of $\mathbb{C}^{1\times N_R}$, with each entry defined as $\mathbf{n}^H = \begin{bmatrix} n_1^* & n_2^* & n_3^* & \dots & n_{N_R}^* \end{bmatrix}$, and since these entries are Gaussian distributed, it follows that each entry of $\Re\left\{\sqrt{\frac{\rho}{8}}\mathbf{n}^H\mathbf{h}_{k_z}d_z\right\}$, for $z \in [1:8]$, is also a GRV. These entries have a distribution of $N\left(0, \frac{\rho}{8}|d_z|^2\sum_{l=1}^{N_R}|h_{k_z}^l|^2\right)$. Consequently, it implies that our decision variable is likewise Gaussian distributed, and can be represented as $\Re\left\{\sqrt{\frac{\rho}{8}}\mathbf{n}^H\left(\sum_{l=1}^{8}\mathbf{h}_{k_l}d_l\right)\right\} \sim N\left(0, \frac{\rho}{16}\left\|\sum_{l=1}^{8}\mathbf{h}_{k_l}d_l\right\|_F^2\right)$, leading to

$$P(\mathbf{x} \rightarrow \hat{\mathbf{x}}|\mathbf{H}) = Q\left(\frac{\omega_g}{\sqrt{\omega_g}}\right) = Q\left(\sqrt{\omega_g}\right), \tag{C.21}$$

where $\omega_g = \frac{\rho}{16}\left\|\left(\sum_{l=1}^{8}\mathbf{h}_{kl}d_l\right)\right\|_F^2 = \frac{\rho}{16}\left\|\mathbf{H}_k\mathbf{G}_k\right\|_F^2 = \frac{\rho}{16}\left\|\mathbf{H}_k\right\|_F^2\left\|\mathbf{G}_k\right\|_F^2$, with $\mathbf{H}_k = \begin{bmatrix}\mathbf{h}_{k_1} & \mathbf{h}_{k_2} & \cdots & \mathbf{h}_{k_l}\end{bmatrix}$, $\mathbf{G}_k = \begin{bmatrix}d_1 & d_2 & \cdots & d_l\end{bmatrix}^T$, $\{l\} \in [1:8]$. Similarly, based on (11) in Koc *et al.* [32], ω_g are chi-squared RVs with $2N_R$ degrees of freedom defined as $\omega_g = \sum_{t=1}^{2N_R}\alpha_{\omega_g,t}^2$ with $\alpha_{\omega_g,t}^2 \sim N(0,\sigma_{\omega_g}^2)$ and $\sigma_{\omega_g}^2 = \frac{\rho}{16}\left(\sum_{l=1}^{8}(D_l)^2\right)$. $D_l = |d_l|$ and $l \in [1:8]$.

The conditional PEP in (C.21) can then be expressed as

$$P(\mathbf{x}\to\hat{\mathbf{x}}) = \int_0^\infty Q\left(\sqrt{\omega_g}\right) f_{\omega_g}\left(\omega_g\right) d\omega_g, \tag{C.22}$$

where the probability density function of ω_g is given in [4] as

$$f_{\omega_g}\left(\omega_g\right) = \frac{1}{\left(2\sigma_{\omega_g}^2\right)^{N_R}(N_R-1)!}\omega_g^{N_R-1}\exp(-\frac{\omega_g}{2\sigma_{\omega_g}^2}). \tag{C.23}$$

The trapezoidal transformation of the Q-function in [33], is given as

$$Q\left(z\right) \cong \frac{1}{2n}\left(\frac{1}{2}\exp(-\frac{z^2}{2}) + \sum_{i=1}^{n-1}S_v\right), \tag{C.24}$$

where $n \geq 6$ is the number of summations for convergence and $S_v = \exp(-\frac{z^2}{2\sin^2\left(\frac{v\pi}{2n}\right)})$.

Using the trapezoidal transformation (C.24) on (C.21) and then substituting into (C.22) yields

$$P(\mathbf{x}\to\hat{\mathbf{x}}) = \left(\frac{1}{2n}\right)\left[\left(\frac{1}{2}\right)\left(1+\frac{\rho\left(\sum_{l=1}^{8}(D_l)^2\right)}{32}\right)^{-N_R} + \sum_{v=1}^{n-1}\left(1+\frac{\rho\left(\sum_{l=1}^{8}(D_l)^2\right)}{16\mu_v}\right)^{-N_R}\right], \tag{C.25}$$

where $\mu_v = 2\sin^2\left(\frac{v\pi}{2n}\right)$.

Part V

Conclusion and Future work

1 Conclusion

The main contributions and findings outlined in this thesis can be summarised as follows:

Part (I), provided a background study and introduced the transmission model for conventional MIMO schemes, shedding light on their advantages and limitations. This set the stage for the exploration of various innovative MIMO schemes found in the existing literature, designed to address and ameliorate these limitations. The subsequent chapters in this thesis were built upon this foundation.

Part (II), presented Paper A, it introduced the GCW-GSM scheme, which aimed to enhance the BER performance in GSM systems. Monte Carlo simulations demonstrated that, for transmissions operating at a rate of 10 $bits/s/Hz$ and at a BER of 1×10^{-5}, GCW-GSM achieved significant performance gains. Specifically, as shown by Figs. A.5-A.7 and Table A.5, GCW-GSM outperformed C-GSM by 6 dB and C-QSM by 2.9 dB. However, it was outperformed by MIMO-GSM and GQSM-AG by 2 dB and 4 dB, respectively. Additionally, a framework for designing GCW-GSM systems was provided, and an analytical upper bound for the ABER over i.i.d. Rayleigh frequency-flat fading was derived and validated using Monte Carlo simulations.

Part (III), explored the use of H-QAM, particularly H-8QAM, to extend C-GSM into GQSM systems. This extension was aimed at improving the error performance of MIMO-SM systems while maintaining reduced hardware complexity. The resulting GQSM-H-8QAM scheme was investigated over i.i.d. Rayleigh frequency-flat fading channels, with a derived analytical bound for its ABER, which was confirmed by Monte Carlo simulations. As shown in Figs. B.5-B.9 and Tables B.6-B.7, GQSM-H-8QAM demonstrated superior system performance compared to C-QSM, MIMO-GSM, C-GSM, C-SM, and ESE-GSM systems with the same SE. Furthermore, it was observed in Tables B.9 and B.10 that GQSM-H-8QAM required fewer transmit antennas to achieve a specific SE while maintaining a good trade-off between error performance and hardware complexity as compared to QSM, C-GSM, C-SM, and ESE-GSM systems with the same SE and N_R.

In Part IV, sought to further enhance the error performance of GSM systems introduced in Part (II) and GQSM systems from Part (III) through Paper C. In Paper C, proposed the use of multiple active transmit antennas and optimised LD maps, resulting in two schemes termed MAA-GSM-LD and GCQSM-LD. Part (IV) also entails a design framework for these systems and derived analytical bounds for their ABER over i.i.d. Rayleigh frequency-flat fading channels, confirming their accuracy

through Monte Carlo simulations. A comparative analysis between the proposed schemes and various MIMO-SM schemes, all employing equivalent system configurations, yielded significant findings: i) MAA-GSM-LD outperformed GCW-GSM from Part (II) by $4.3\ dB$ and MIMO-GSM by $1.2\ dB$ in terms of error performance. ii) GCQSM-LD, an extension of MAA-GSM-LD, exhibited a $3.6\ dB$ improvement in error performance compared to GQSM-AG, which was identified as one of the best GQSM systems discussed in Part (II) and Part (III). Thus, implying that the GCQSM-LD scheme is a viable solution for enhancing the error performance of MIMO-SM schemes.

2 Future Work

Future research initiatives are envisaged in the following areas:

1. Extension of GCW-GSM scheme to incorporate optimised labelling maps to further improve the error performance and proposal of low-complexity detection methods to make the system more realisable.

2. Further investigation/proposal of low-complexity detection methods for the GQSM-H-8QAM scheme to make it more realisable.

3. Further investigation of the performance of GQSM-H-8QAM and other H-QAM schemes under generalised correlated and uncorrelated fading channel conditions.

4. Proposal of low-complexity detection methods for the MAA-GSM-LD and GCQSM-LD scheme to extend them to higher QAM modulation orders.

5. Extension of the error performance analysis of MAA-GSM-LD and GCQSM-LD schemes under correlated and uncorrelated fading channels.